

Computational Studies on the Effect of Charge and Electric Fields on Systems of Chemical and Biological Interest.

by

Anagh Mukherjee
10CC15J26010

A thesis submitted to the
Academy of Scientific & Innovative Research
for the award of the degree of
DOCTOR OF PHILOSOPHY

in
SCIENCE

Under the supervision of
Dr. Kumar Vanka
and co-supervision of
Dr. Sayam Sengupta (IISER Kolkata)



CSIR- National Chemical Laboratory, Pune



Academy of Scientific and Innovative Research
AcSIR Headquarters, CSIR-HRDC campus
Sector 19, Kamla Nehru Nagar,
Ghaziabad, U.P. – 201 002, India

April 2021

Certificate

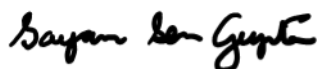
This is to certify that the work incorporated in this Ph.D. thesis entitled, “Computational Studies on the Effect of Charge and Electric Fields on Systems of Chemical and Biological Interest.”, submitted by Anagh Mukherjee to the Academy of Scientific and Innovative Research (AcSIR) in fulfillment of the requirements for the award of the Degree of Doctor of Philosophy In Science, embodies original research work carried-out by the student. We, further certify that this work has not been submitted to any other University or Institution in part or full for the award of any degree or diploma. Research materials obtained from other sources and used in this research work have been duly acknowledged in the thesis. Images, illustrations, figures, tables etc., used in the thesis from other sources, have also been duly cited and acknowledged.



(Signature of Student)

Name: Anagh Mukherjee

Date: 14/04/2021



(Signature of Co-Supervisor)

Name: Dr Sayam Sengupta

Date: 14/04/2021



Signature of Supervisor

Name: Dr Kumar Vanka

Date: 14/04/2021

STATEMENTS OF ACADEMIC INTEGRITY

I, Anagh Mukherjee, a Ph.D. student of the Academy of Scientific and Innovative Research (AcSIR) with Registration No. 10CC15J26010 hereby undertake that, the thesis entitled “Computational Studies on the Effect of Charge and Electric Fields on Systems of Chemical and Biological Interest.” has been prepared by me and that the document reports original work carried out by me and is free of any plagiarism in compliance with the UGC Regulations on “*Promotion of Academic Integrity and Prevention of Plagiarism in Higher Educational Institutions (2018)*” and the CSIR Guidelines for “*Ethics in Research and in Governance (2020)*”.

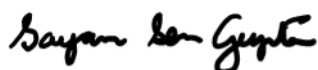


Signature of the Student

Date : 14/04/2021

Place : PUNE

It is hereby certified that the work done by the student, under our supervision, is plagiarism-free in accordance with the UGC Regulations on “*Promotion of Academic Integrity and Prevention of Plagiarism in Higher Educational Institutions (2018)*” and the CSIR Guidelines for “*Ethics in Research and in Governance (2020)*”.




Signature of the Co-supervisor

Name : DR SAYAM SENGUPTA

Date : 14/04/2021

Place : KOLKATA



Signature of the Supervisor

Name : DR KUMAR VANKA

Date : 14/04/2021

Place : PUNE

Dedicated to my Mother

Acknowledgement

The beauty of doing a Ph.D in Sciences is that it makes us logical and reasonable by helping us to attain a rational bent of mind. It is said that life is the best teacher. The journey of my Ph.D has been a time of both transformation and satisfaction.

Firstly, I want to thank *Dr. Kumar Vanka*, my thesis supervisor, for his constant motivation and support. He has been a great inspiration to me for his commitment towards scientific learning and perfection. His stress in thinking out of the box and thrusting importance to monitor every minute details has taught me the intricacies of performing research. I would also like to thank *Dr. Sayam Sengupta*, my thesis co-supervisor, for his insight and contribution to my thesis.

I would take this opportunity to acknowledge my present and past Doctoral Advisory Committee (DAC) members, *Dr. Ashok. P. Giri* (DAC Chairperson), *Dr. Samir Chikkali*, *Dr. Nayana Vaval*, *Dr. Rahul Banerjee* and *Dr. E. Balaraman*, for their insightful suggestions and feedback. I am also grateful to *Dr. Srivari Chandrasekhar*, director, CSIR-NCL, *Dr. Ashwini Nangia*, former director, CSIR-NCL, and *Dr. Sourav Pal*, former director of CSIR-NCL. Moreover, I take the opportunity to thank the present and former heads of the Physical and Materials Chemistry Division for their support and providing all facilities during my Ph.D.

I want to extend my gratitude to all teachers who had taught me during my Ph.D. course work at CSIR-NCL: *Dr. Kumar Vanka*, *Dr. Sakya Sen*, *Dr. E. Balaraman*, *Dr. Benudhar Punji* and *Dr. Rajesh Gonnade*, as well as other scientists in NCL. Let me extend my warm thanks to my research collaborators, *Dr. Gurunath Suryavanshi*, *Dr. Santhosh Babu Sukumaran*, *Dr. Beeran Senthilkumar* and *Dr. Mandeep Singh*. Moreover, I owe many thanks to my college and school teachers for their support and motivation.

I also acknowledge all the non-academic staff of *CSIR-NCL*, and *AcSIR*, for their support and help during my work. Without the funding, this Ph.D. journey would not have been possible; hence I would like to express my gratitude to the *University Grants Commission* (UGC) for the fellowship. Moreover, I want to thank the whole scientific community for being a source of inspiration and motivation.

I have been lucky enough to maintain the company of small group of friends both in and outside my institute. I want to acknowledge the contribution of my friends in NCL like *Sandy*, *Stephyna*, *Saibal*, *Sutanu*, *Jagannath*, *Basudeb*, *Suwendu*, *Himadri*, *Kaushik*, *Sumanda*, *Bikasda*, *Souvikda*, *Saibalda*, *Arjun*, *Tapasda*, *Abhijitda*, *Shantida*, *Anirban*, *Pronoy*, *Pranabda*, *Debu*, *Sibada*, *Rahul*, *Narugopal*, *Arijitda*, *Kaushikda*, *Gabluda*, *Vinitadi*, *Dosda*, *Santanuda*, *Hrideshda*, *Soumenda*, *Shinjini*, *Krishanuda*, *Turbasuda* and *Daku* for making my stay in Pune so memorable. Outside NCL, no words of thanks is enough for my friends, *Dibyendu* and *Nandita*, for standing behind me like a rock whenever I needed them. Moreover, I would like to thank my M.Sc. friends, *Gourab*, *Subhobrata* and *Sneha*, for their support during my Ph.D period. I also thank my school friends gang for their company for lifting my spirits whenever I felt frustrated.

I also extend my thanks to *Tiwariji, Tamalda, and Shailja*, for their help whenever needed during my Ph.D. Also, my special thanks to *Siddarth and Soumya*. Moreover, it is my pleasure to thank my past and present lab mates; *Jugal, Yuvraj, Vipin, Subhrashisda and Ruchi*.

Finally, I want to thank the most important people in my life, my family. No words are sufficient to describe their love, affection, and support. I am highly indebted to my Father (*Dr. Basudeb Mukherjee*) and Mother (*Chayana Mukherjee*) for their unconditional love and the sacrifices they have made for me in their lives. Also, I wish to thank my sister (*Bisakha*) for her continuous support and making my visits to Hyderabad so beautiful. Furthermore, I would like to thank my brother in law (*Pratikda*) for his support and kindness. I consider myself blessed to have such a beautiful family.

Finally, I express my gratitude to the Almighty for the blessings and for providing special challenges.

Anagh Mukherjee

Table of Contents

Abbreviations	i
Physical Constants	ii
Chapter 1: A Brief Introduction to the significance of electric field and charge in Chemistry and Biology	1
Abstract.....	2
1.1 Electric field.....	3
1.2 Electric Charge and its relation to electric field.....	3
1.3 Utility of Electric Field.....	4
1.4 Oriented External Electric Field (OEEF).....	5
1.5 Practical Application of OEEF.....	8
1.6 Local Electric Field (LEF): Impact in Biology.....	10
1.7 Field Effect in Chemistry.....	11
1.8 Objective of the Thesis.....	12
1.9 Organization of the Thesis.....	13
1.10 References.....	14
Chapter 2: Basic Theoretical Introduction to Computational Chemistry	18
Abstract.....	19
2.1 Introduction.....	20
2.2 Basic Tenets of Quantum Mechanics.....	20
2.2.1 Schrodinger Equation.....	20
2.2.2 The Born-Oppenheimer Approximation.....	21
2.2.3 Variation principle.....	21
2.3 Density Functional Theory (DFT).....	22
2.3.1 Functional.....	22
2.3.1.1 Local Density Approximation (LDA).....	22
2.3.1.2 Generalized Gradient Approximation (GGA).....	23
2.3.1.3 Meta-generalized gradient approximation Functionals (MGGA).....	23
2.3.1.4 Hybrid Functional.....	23
2.3.2 Electron Density.....	24
2.3.3 The Hohenberg-Kohn Theorems.....	24

2.3.4 The Kohn-Sham Approach.....	26
2.4 Natural Bond Orbital (NBO) Analysis.....	28
2.5 Non Covalent Interaction (NCI) Plot.....	28
2.6 Ab Initio Molecular Dynamics (AI-MD).....	29
2.7 References.....	30
Chapter 3: What Drives the H-abstraction Reaction in Bio-mimetic Oxoiron-bTAML Complexes? A Computational Investigation.....	32
Abstract.....	33
3.1 Introduction.....	34
3.2 Results and Discussion.....	35
3.2.1 Effect of overall charge in oxoiron biuret-TAML species.....	35
3.2.2 Effect of ligand substitution.....	40
3.3 Computational Details.....	42
3.4 Conclusion.....	43
3.5 References.....	43
Chapter 4: Unraveling the role of counter anions in “Ge(II) inside a Molecular Cage” Systems.....	48
Abstract.....	49
4.1 Introduction.....	50
4.2 Methods.....	52
4.3 Results and Discussion.....	53
4.4 Conclusion.....	66
4.5 References.....	66
Chapter 5: Hidden Role of Counter Anions: Implications in Biology and Surface Science.....	69
Abstract.....	70
5.1 Introduction.....	71
5.2 Methods.....	72
5.3 Results and Discussions.....	72
5.4 Conclusion.....	79

5.5 References.....	79
Chapter 6: Computational Investigation on the Role of External and Local Electric Fields in Macrocyclic Chemical and Biological Systems.....	81
Abstract.....	82
6.1 Introduction.....	83
6.2 Methods.....	84
6.2.1 π -conjugated macrocycles.....	85
6.2.2 Valinomycin macrocycle.....	85
6.3 Results and Discussion.....	85
6.3.1 Oriented External Electric field (OEEF) in π -conjugated macrocycles.....	85
6.3.2 Local Electric field (LEF) in Valinomycin.....	88
6.4 Conclusion.....	93
6.5 References.....	94
Chapter 7: Summary and Future Outlook.....	98
7.1 Theme of the Thesis.....	99
7.2 Computational Methods.....	101
7.3 Future Directions from this Thesis.....	102
7.4 References.....	102
ABSTRACT.....	104
Details of the publications emanating from the thesis work.....	105

List of Figures

Figure 1.1 Illustration of electric field emanating from a positive and negative electric charge. The arrow denotes the direction of the electric field.....	3
Figure 1.2 Illustration of the concept behind a) electrophoresis and b) electrolysis.....	5
Figure 1.3 Illustration of the VBT based theoretical explanation of OEEF in H ₂ molecule as proposed by Shaik and co-workers.....	6
Figure 1.4 a) Energy barriers (in kcal/mol) for the DA reaction between cyclopentadiene and maleic anhydride vs the electric field strength in the Y-direction. ²⁸ b) ΔE (R, S) i.e., the energy difference between the respective barriers associated with the formation of the R and S product in kcal/mol, induced by an F _X field (± 0.75 V/Å) for an array of dienophiles reacting with cyclopentadiene, plotted against the field-free X-dipole moment components (μ_x , in debye units, D) of the dienophiles.....	7
Figure 1.5 External electric field mediated a) Diel's Alder bond forming reaction and b) bond cleavage of alkoxyamine employing STM experimental setup.....	8
Figure 1.6 IEF mediated Rh-porphyrin catalyzed carbene rearrangement reaction whereby the region-selectivity was modulate by varying the voltage.....	9
Figure 1.7 Top: Illustration of a field effect on the carbonyl group induced by a polar group. Below: the two oxoferryl porphyrin complex that differs by charge and exhibits a significant difference in HAT rate.....	11
Figure 1.8 Structural Representation of the applicability of the interplay of the concepts of electric field and charge in relevant chemical and biological systems as described in this thesis.....	13
Figure 2.1 Flowchart illustrating the iteration cycle for calculating the single point electronic energy.....	28
Figure 3.1 Square scheme with associated thermodynamic parameters involved in HAT reactions.....	34
Figure 3.2 Biuret TAML based iron complexes used for this study.....	35
Figure 3.3 Gibb's free energy HAT reactions profile of b-TAML complexes with benzyl alcohol at M06-L/6-311G*/LANL2DZ(Fe)//M06-L/6-311G*/LANL2DZ(Fe),C-PCM (acetonitrile) level of theory.....	37
Figure 3.4 Optimized TS geometries of C-H abstraction in benzyl alcohol employing 1a and 2 at M06-L/6-311G*/LANL2DZ (Fe)/ C-PCM (acetonitrile) level of theory.....	38
Figure 3.5 Schematic diagram of the key MOs (EDO and EAO) at an O-H distance of 2.0 Å in solution phase of the encounter complexes (the left and right side indicate the MOs of 1a and 2 respectively) at BP86/def2-TZVPP, C-PCM (acetonitrile) level of theory.....	38

Figure 4.1 Cryptand and crown ether stabilized Ge(II) with their counter anions, as isolated in the crystal structure.....	51
Figure 4.2 Noncovalent interaction (NCI) plot for Ge(II) complexes (1-4) illustrating the non-covalent electrostatic interaction between the germanium dication and the heteroatoms of the molecular cage.....	54
Figure 4.3 Snapshots depicting the trajectory of ab initio molecular dynamics (AIMD) simulations done for Case 1, where the Ge(II) and the counter anion, [OSO ₂ CF ₃] ⁻ , remain unattached.....	55
Figure 4.4 Snapshots depicting the trajectory of ab initio molecular dynamics (AIMD) simulations done for Cases 2, 3 and 4 where the Ge(II) and their respective counter anion remain unattached.....	56
Figure 4.5 Snapshots depicting the trajectory of AIMD simulations for Case 1, where Ge(II) and the counter anion (OSO ₂ CF ₃) ⁻ remain attached.....	57
Figure 4.6 Snapshots depicting the trajectory of ab initio molecular dynamics (AIMD) simulations done for Cases 2, 3 and 4 where the Ge(II) and their respective counter anion remain attached.....	57
Figure 4.7 Geometries of free and counter anion bound crown ether and cryptand complexes (1 , 2 , 3) of Ge(II), optimized at the M06-2X/ 6-311G (d, p) level of theory.....	58
Figure 4.8 Geometry optimization trajectory of counter anion binding in Case 4	59
Figure 4.9 Snapshots depicting the trajectory of ab initio molecular dynamics (AIMD) simulations done for Cases 1, 2, 3 and 4 where the Ge(II) and their respective counter anion remain attached.....	59
Figure 4.10 Computationally generated ¹⁹ F-NMR spectra for counterion (i) bound and (ii) not bound to the Ge(II) dication center in complex 1	61
Figure 4.11 DFT Optimization trajectory for Case 1 keeping both triflate counterions at the germanium centre.....	62
Figure 4.12 Illustration of cancellation of coulombic interactions between the Ge(II) center and the oxygen heteroatoms in Case 4	66
Figure 5.1 Optimized geometries of free and counter anion bound ionophore complexes of Mg(II) and Ca(II), with Cl ⁻ considered as the counter anion.....	72
Figure 5.2 Noncovalent interaction (NCI) plot for Mg/Ca/Li based ionophore illustrating the non-covalent electrostatic interaction between the Mg/Ca centers and the heteroatoms of the ionophore cage.....	74
Figure 5.3 Illustration of the isoionic phenomenon.....	76

Figure 5.4 Optimized geometries of two Li(I) cations encompassed by Mg-Ionophore VII (the two lithium unfixed and fixed) at the M06-2X/6-31G* level of theory.....	77
Figure 5.5 Optimized geometry of C ₁₈ on an NaCl surface as seen (a) from the top (b) from the side and (c) from the top showing the distances of the two enclosed Na(I) cations from the nearest carbon of the C ₁₈ molecule, at the M06-2X/3-21G* level of theory.....	78
Figure 6.1 a) cyclocarbon b) cycloparaphenylene (CPP) c) cycloparaphenylacetylene (CPPA).....	83
Figure 6.2 Valinomycin ionophore macrocycle.....	84
Figure 6.3 Illustration of the optimized geometries, involving the three molecules from three families (cyclocarbon, CPP and CPPA) transforming to a distorted structure under OEEF....	86
Figure 6.4 Illustration denoting the direction of the net force on Cl ⁻ in the counter anion incorporated K ⁺ /Na ⁺ valinomycin complex and the NaCl/KCl moiety in bulk solution.....	90
Figure 6.5 Potential Energy Surface (PES) for the path of Na ⁺ exiting the valinomycin cage computed via linear transit scan.....	92
Figure 7.1 Pictorial summary of the work presented in this thesis.....	101

List of Tables

Table 3.1 Thermochemical free energy analysis for HAT reactions of 1a and 2 in acetonitrile medium(C-PCM Model) using benzyl alcohol as the substrate.....	36
Table 3.2 Thermochemical analyses of bTAML complexes (1a-1d).....	36
Table 3.3 Thermochemical analyses of bTAML complexes (2).....	37
Table 3.4 The Gibb's free energy activation barrier (ΔG^\ddagger) and free energy change in initial electron transfer ($\Delta G_{E.T}$) or proton transfer ($\Delta G_{P.T}$) for the HAT step, using benzyl alcohol as the substrate for various bTAML complexes that have been investigated at M06-L/6-311G*/LANL2DZ(Fe)//M06-L/6-311G*/LANL2DZ (Fe), C-PCM (acetonitrile) level of theory.....	41
Table 3.5 Relative energies of the EAOs of the reported complexes at BP86/def2-TZVPP,C-PCM (acetonitrile) level of theory.....	41
Table 3.6 Mulliken and Natural Population Analysis (NPA) charges of iron in the bTAML complexes (1a and 1d) in acetonitrile medium (C-PCM) at different levels of theory.....	42
Table 4.1 Different parameters associated with the reported Ge(II) complexes (1-4).....	53
Table 4.2 Thermodynamic parameters of counterion binding of the respective counter anions in solution, at the M06-2X/6-311G (d, p) // M06-2X/6-311G (d, p) level of theory.....	60
Table 4.3 Different parameters comparing the case of [Ge-Br] ⁺ in a bare state with the [Ge-Br] ⁺ encapsulated inside the cage in Case 3 in solution.....	63
Table 4.4 The force at the Ge(II) center for reported Ge(II) complexes (1-4).....	65
Table 5.1 Highest Wiberg Bond Indices (WBI) of the ionophore cation and a heteroatom in the ionophore cage in all the ionophores reported.....	73
Table 6.1 HOMO-LUMO Energy of Original and Distorted Structure for molecule a-c	87
Table 6.2 Binding Energies and WBI Values for Cl ⁻ incorporated K ⁺ and Na ⁺ valinomycin complexes.....	88
Table 6.3 Thermodynamic parameters of Cl ⁻ binding at the PBE/TZVP // PBE/TZVP level of theory.....	89
Table 6.4 Values of the two parameter (Ω and σ) using different charge analysis methods.....	91

Abbreviations

AIMD	ab initio Molecular Dynamics
B3LYP	Becke, 3-parameter, Lee-Yang-Parr
COSMO	Conductor-like Screening Model
DFT	Density Functional Theory
GGA	Generalized Gradient Approximation
KS	Kohn-Sham
LDA	Local Density Approximation
MARIJ	Multipole Accelerated Resolution of Identity
M06	Minnesota 06
NBO	Natural Bond Orbital
NCI	Non-covalent Interactions
PBE	Perdew, Burke and Ernzerhof
PCM	Polarizable Continuum Model
RI	Resolution of Identity
SCF	Self-consistent Field
TZVP	Triple Zeta Valence plus Polarization
TS	Transition state
OEEF	Oriented External Electric Field
LEF	Local Electric Field

Physical Constants

Avogadro's Constant (N_A) = $6.02214129 \times 10^{23} \text{ mol}^{-1}$

Atomic Mass Unit (u) = $1.660538921 \times 10^{-27} \text{ kg}$

Boltzmann's Constant (k) = $1.3806488 \times 10^{-23} \text{ JK}^{-1}$

Bohr Radius (a_0) = $5.291772109 \times 10^{-11} \text{ m}$

Elementary Charge (e) = $1.602176565 \times 10^{-19} \text{ C}$

Gas Constant (R) = $8.3144621 \text{ JK}^{-1}\text{mol}^{-1}$

Mass of Electron (m_e) = $9.10938291 \times 10^{-31} \text{ kg}$

Mass of Proton (m_p) = $1.672621777 \times 10^{-27} \text{ kg}$

Mass of Neutron (m_n) = $1.674927351 \times 10^{-27} \text{ kg}$

Rydberg Constant (R) = $1.097373157 \times 10^5 \text{ cm}^{-1}$

Speed of Light (c) = $2.99792458 \times 10^8 \text{ ms}^{-1}$

Planck's Constant (h) = $6.62606957 \times 10^{-34} \text{ Js}$

Chapter 1: A Brief Introduction to the significance of electric field and charge in Chemistry and Biology.

Chapter 1

A Brief Introduction to the significance of electric field and charge in Chemistry and Biology.

Abstract

Electric field is a phenomenon that encompasses every area of science on account of its sheer importance in every area of scientific research. External field is closely intertwined to charged species and is a useful tool to understand electrostatic interaction in such systems. Understanding the interaction between an electric field and chemical/biological systems of interest is an emerging area of research. In this chapter, we will provide a brief introduction to the concept of electric field, its relation to charge and its widespread applicability in our daily life. Also, we shall shed light on the instances of recent theoretical and experimental studies directed towards unraveling the role of external and internal electric field in relevant systems.

1.1 Electric field

Electric field is a fundamental quantity which is relevant in every avenues of science. It is broadly defined as the physical field encompassing a charged particle and applies a force on every other charge in its vicinity.¹Quantitatively, it is the force exerted on a unipositive charge.²

$$E = F/q \quad (1.1)$$

E = Electric Field Strength, F= force and q= magnitude of the charge.

Electric field is a vector quantity (oriented along a direction in space) and its strength is expressed in Newton per coulomb or Volts per meter.

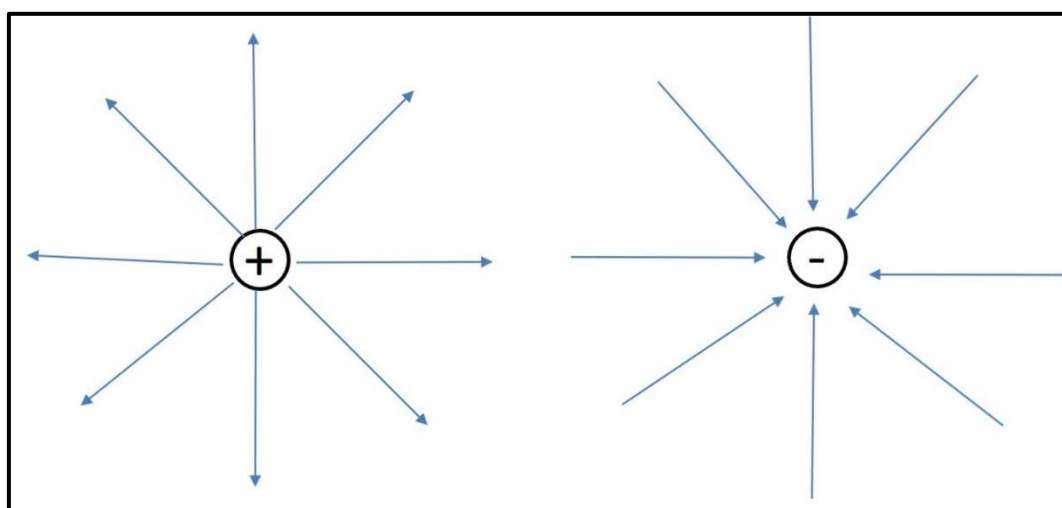


Figure 1.1 Illustration of electric field emanating from a positive and negative electric charge. The arrow denotes the direction of the electric field.

Besides charged bodies,³ electric field is also produced by pulsed magnet field.⁴Study of electric fields arising out of stationary points is called electrostatics. Gauss's theorem and Faraday's law of induction forms the basis behind the concept of electric field. In this thesis, we will observe various dimension of electric field in diverse systems.

1.2 Electric Charge and its relation to electric field

Electric charge is the physical property of a system that causes it to experience a force when it is placed in an electromagnetic field. The SI unit of charge is coulomb. As we already know, electric field is caused by electric charges. The relation between the two physical quantities is shown in equation (1.1). This can be also expanded by introducing Coulomb's law equation in (1.2). This quantitatively connects the electric

field strength on a test charge (q_0) to the distance between the source charge, which creates the electric field, and a test charge.

$$E = 1/4\pi\epsilon (q/r^2) \quad (1.2)$$

where, q is the charge which generates the electric field on a test charge, r is the spatial distance between the source charge and the test charge.

Hence, electric field strength and charge are inalienable from each other. Any change in magnitude of charge produces a corresponding change in the electric field strength. Since electric field is a vector quantity, any change in the orientation of the charge can affect the magnitude and direction of the electric field. In this thesis, we will notice several instances of modulation of electric field via tuning of absolute charges of atoms in molecular systems by various means.

1.3 Utility of Electric Field

Being a fundamental topic of science by not being confined to a single area, electric fields are widely used due to their potential to generate physical and chemical phenomenon and their ability to facilitate changes in both natural and inanimate systems. The field strength can easily be modulated by constant pulsating voltage and alternate voltage of any frequency. Electric field has significant utility in chromatographic, industrial and chemical processes.⁵ Furthermore, if this is applied in conjunction with a magnetic field, the scope of its application gets wider.

Similarly, electric field has varied applications in biology and medicine. Its role in wound healing, embryonic formation and tissue generation has been well established.⁶ It can be exploited for drug delivery⁷ and also genetic engineering by driving DNA into the nucleus.⁸ Electric fields can also affect cellular function.⁹ Pulsed electric fields are used for treatment in bio-based industry.¹⁰ It has also been proved that humans and animals recognize static electric field to a considerable extent.¹¹ It is already known that some classes of ion channels, known as voltage gated ion channels, function by varying the membrane electric potential.¹² The role of external electric field in tuning the transmembrane potential has been illustrated clearly.¹³

Electric field can also have a wide range of utilization in materials science. Dipolar gases, condensed to very low temperature, can exhibit electric field strength as high as 10^8 V/m.¹⁴ Also, electric field has been known for synthesis and consolidation of materials and this technique being known as the plasma sintering method.¹⁵ Electric fields are commonly used to separate charged particles, a practice known as electrophoresis

(**Figure 1.1**).¹⁶This method is utilized for separation of molecules and also for analyzing DNA, RNA and proteins. Also, a similar non-uniform electric field can separate non-charged entities, a phenomenon known as dielectrophoresis.¹⁷This procedure could be exploited for manipulating nanoparticle and nanowire.¹⁸

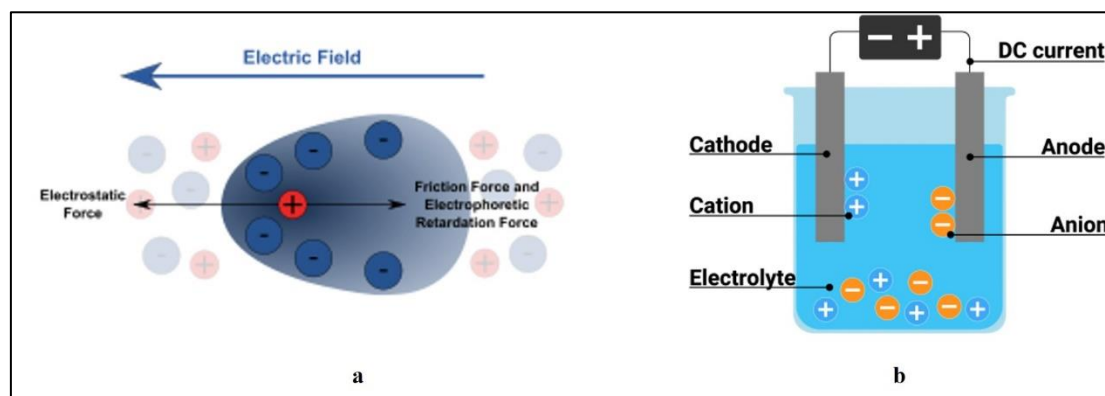


Figure 1.2 Illustration of the concept behind a) electrophoresis¹⁶ and b) electrolysis.¹⁹

One of the commonly used case of applied electric field is the method known as electrolysis (**Figure 1.2**).¹⁹It is technique utilized to drive non-favorable transformations by applying a net current. A common practice is to use low strength electric field as preservatives in the food- processing industry to destroy bacterial cells.²⁰Hence an applied electric field could be exploited for directing useful outcomes in our everyday life. In this thesis, we will illustrate the benefits that a system gains by using an applied or modulating an already existing electric field.

1.4 Oriented External Electric Field (OEEF)

In the earlier section, we discussed the relevance of electric fields in diverse areas of application. For some times, the potential of applying an oriented external electric field (OEEF) on molecular systems.²¹This field was theoretically conceptualized by Shaik and co-workers.²²This involves applying an electric field along a particular bond axis in a molecular systems. OEEF can induce dipole moment inside a no-polar molecule in alignment with the direction of an external electric field.²³The driving force for this polarization is the stabilization interaction between the molecule and an external electric field. OEEF can cause significant changes in both the electronic and geometric property of a molecule. One of the natural fallout is the removal of restriction of the otherwise forbidden mixing between two orbitals and energy states, this phenomenon commonly known as Stark effect.²⁴

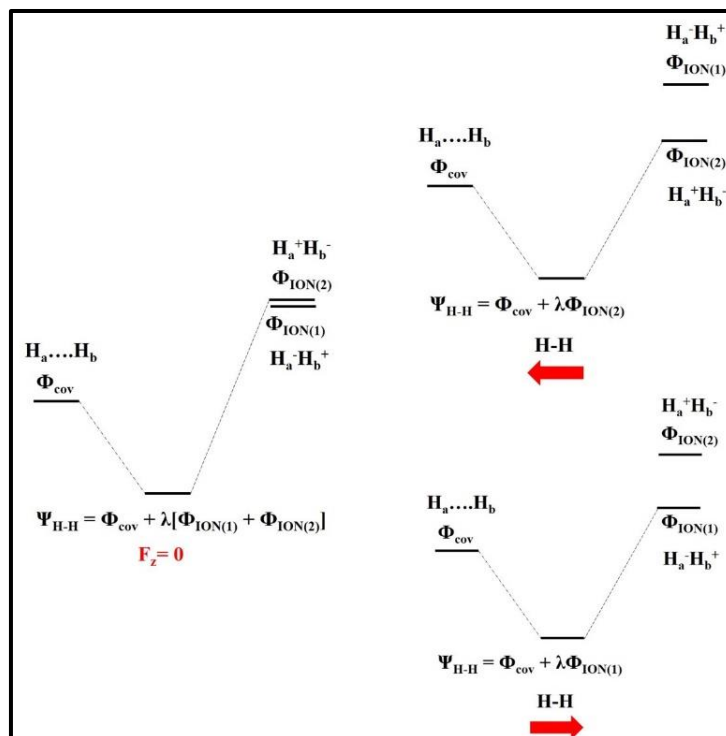


Figure 1.3 Illustration of the VBT based theoretical explanation of OEEF in H₂ molecule as proposed by Shaik and co-workers. The bond-wave function (Ψ_{H-H}) devoid of an electric field (left side) results out of equal overlap of the covalent structure (Φ_{cov}) with the degenerate ionic structures ($\Phi_{ion(1)}$, $\Phi_{ion(2)}$), producing a nonpolarized covalent bond. $F_z < 0$ and $F_z > 0$ (right side) exert selective stabilization of the ionic structure that opposes the field's polarity. The polarized resultant molecular orbital arises out of covalent-ionic orbital mixing.

As mentioned earlier, an electric field induces a polarity and stabilization in a molecule. Shaik and co-workers provided a valence bond theory (VBT) based explanation.²¹ For a H₂ molecule, there is a symmetrical structure without any external electric field due to equal overlap contribution of the two degenerate ionic orbitals (**Figure 1.3**). However in presence of an OEEF, the molecule gets polarized along the applied field due to significant mixing of the ionic orbital with either of the two ionic orbitals which loses its degeneracy on account of the external field (**Figure 1.3**). Hence a certain amount of ionicity is induced in the molecule. It is also that even a moderate external electric field can promote bond cleavage by inducing ionicity into bonds.²⁵ This fact could explain the spurt in reaction rates in presence of an external electric field. Also it is observed that the effect of a field is more profound on a single bond than a double bond.²³

Altogether, OEEFs have been known to be boosting catalysis, inhibition, bond dissociation and regio/stereo-selectivity in important systems of interest.^{26,27} The increase in rates can be attributed to the stabilization of the transition states (TS) when an electric field was applied along the reaction axis. This is due to the enhanced charge transfer and ionicity in the reaction axis of the TS conformation. This field of OEEF assisted chemistry burst into relevance when an theoretically applied OEEF was found to mediate and control the region-selectivity of a Diel's Alder (DA) reaction involving cyclopentadiene and maleic anhydride.²⁸ An increment in the reaction rate was observed when an electric field was applied along the reaction axis while an exo/endo selectivity was observed when an applied along an perpendicular direction to the reaction axis. This path breaking incidence regarding OEEF mediated chemistry increased the interest among researchers to initiate potentially useful transformations exploiting OEEF. A similar OEEF can register region-selectivity in bond activation reaction of cytochrome P-450 like systems.²² Subsequently, it has been found that a theoretically generated OEEF can also foment enantio-selectivity in a DA reaction.²⁹ In this case, the enantiomeric excess increases steadily with increase in the electric field strength in a specific spatial direction. Also, an external electric field can stabilize a certain reaction pathway over another in a fragmentation reaction.³⁰

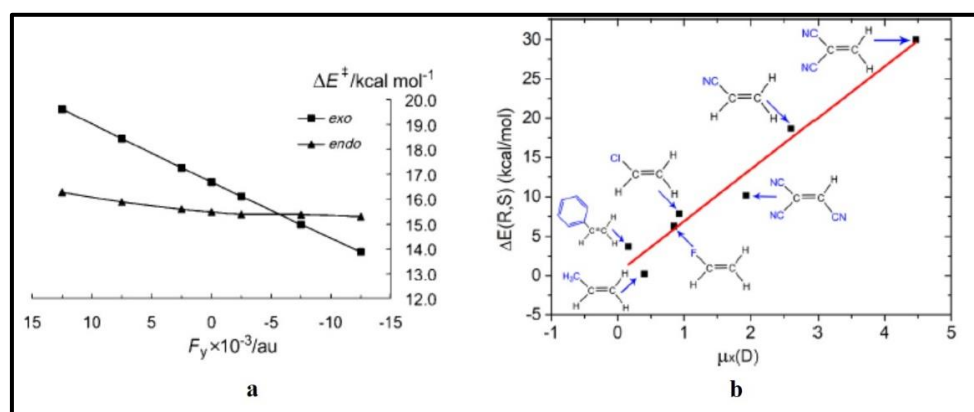


Figure 1.4 a) Energy barriers (in kcal/mol) for the DA reaction between cyclopentadiene and maleic anhydride vs the electric field strength in the Y-direction.²⁸ b) $\Delta E(R,S)$ i.e., the energy difference between the respective barriers associated with the formation of the R and S product in kcal/mol, induced by an F_x field (± 0.75 V/Å) for an array of dienophiles reacting with cyclopentadiene, plotted against the field-free X-dipole moment components (μ_x , in debye units, D) of the dienophiles.²⁹

These examples are just some of the few to illustrate the importance of OEEF and showcases it's potential to change the field of synthetic chemistry as we know. This could be of useful insight for experimental

chemists to design electric field based synthetic procedures and also adjudge the amount of field strength needed to direct the necessary changes.

Also theoretically generated OEEF can force changes in geometry of molecules.^{22,31} External electric field can foment spin flipping in metal complexes which is accompanied by a change in geometry.³² Low strength electric field can affect the structural frameworks of molecular networks,³³ protein folding³⁴ and water cluster.³⁵

1.5 Practical Application of OEEF.

In the earlier section, we have primarily discussed the theoretical concept and applicability of OEEF. But, the real challenge lies with converting the concepts of OEEF, deduced by high level theoretical calculation, into actual practical use. These effective methods would revolutionize synthetic chemistry because of the huge potential possessed by OEEF in chemistry as described in the earlier section. However this is a highly difficult task considering that the microscopic control over molecular alignment is a prerequisite to fully harnessing the OEEF.

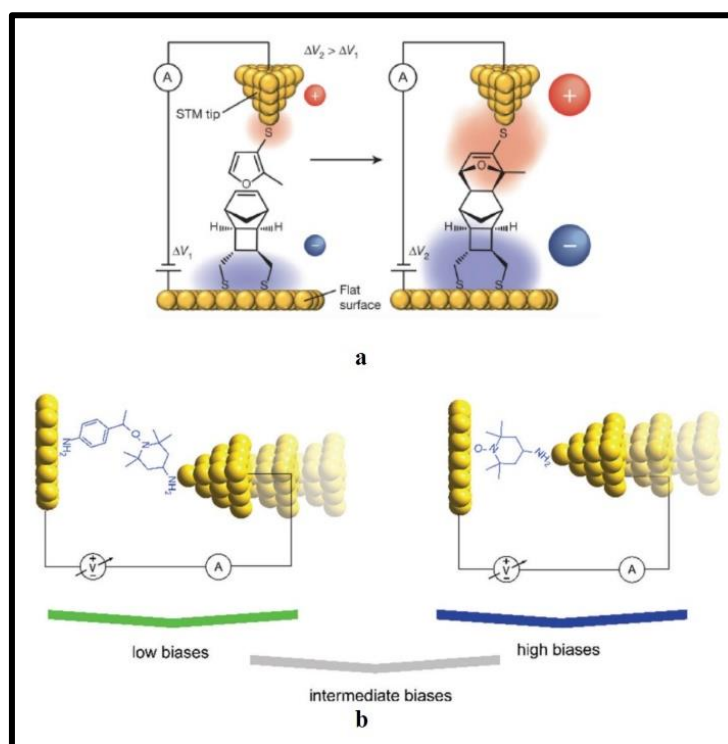


Figure 1.5 External electric field mediated a) Dieckmann condensation³⁶ and b) bond cleavage of alkoxyamine employing STM experimental setup.³⁷

Despite these difficulties, scientists have designed some techniques to exploit the OEEF in chemical systems. In a landmark work that marked the initiation of the endeavor, Coote and co-workers employed a scanning tunneling microscope (STM) experimental set up to perform a bond forming Diels-Alder (DA) reaction under an OEEF whereby the reactants were tethered on a gold surface (**Figure 1.5**).³⁶ A linear relationship between the field strength and the rate of reaction was obtained. Subsequently, a bond cleavage reaction of alkoxyamine was also performed under the influence of an external electric field using a STM setup which prescribes a certain amount of versatility to this method (**Figure 1.5**).³⁷ Though STM produces a relatively high electric field, it has a scalability issue. Nevertheless, a large number of reactions could be attempted in this promising technique as the relation between the reaction rate and the electric field has been fairly well established in this single molecule based method. Also, STM tapping and blinking method can produce results within a very short duration at room temperature employing various solvents.

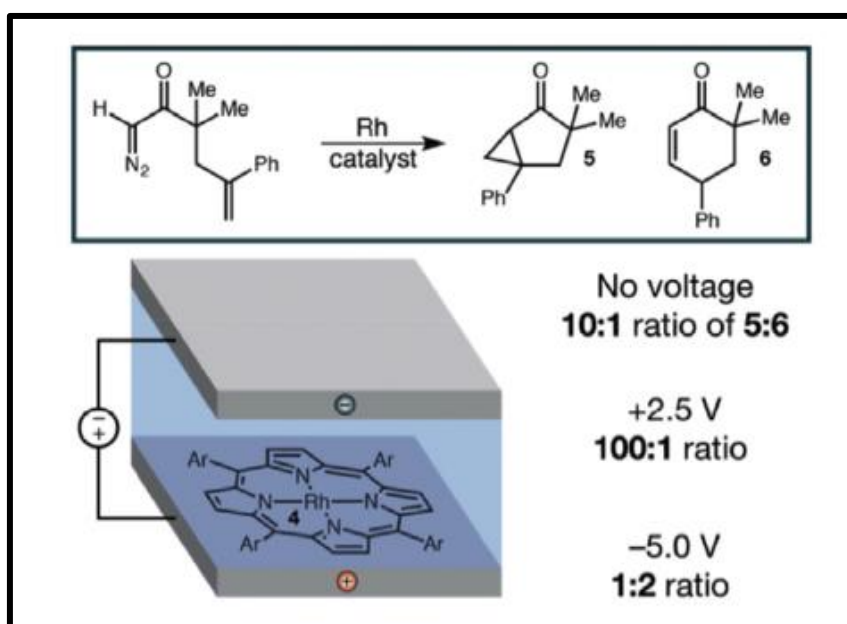


Figure 1.6 IEF mediated Rh-porphyrin catalyzed carbene rearrangement reaction whereby the regioselectivity was modulated by varying the voltage.⁴⁰

However, the scalability issue makes it imperative to design alternate methods that successfully tap an external electric field. One such method would be the use of electrochemical cells used for usual faradaic reactions which is known as interfacial electric field (IEF).³⁸ Whenever a charged electrode is immersed in an electrolyte, a charge double or Debye layer is formed. This bilayer creates an electric field whose strength gradually decreases with distance from the electrode. This arrangement could sometimes be used to generate a directional electric field using surface tethering of reactants. This method was used for modifying the

selectivity of a π -anionic catalyst.³⁹ Also, region-selectivity could be introduced in an Rh-porphyrin catalyzed carbene rearrangement reaction under the influence of an IEF.⁴⁰ Apart from using STM and IEF, more molecular devices could be utilized for applying a directional electric field on molecules. One such technique is using designed-local electric field (D-LEF), which will be discussed in the next section.

1.6 Local Electric Field (LEF): Impact in Biology.

Apart from studying the effects of external electric field, the cases of local electric field (LEF) adds another dimension in this field. These refers to a relatively visible electric field which is already ingrained into a molecular system. This field is introduced into the system on accounts of its polar functional groups which induces a strong electrostatic force. Warshel and co-workers was the first to theoretically propose that the LEF generated by the protein side groups is the reason behind the catalytic activity of biomolecules.^{41,42} This idea has been further corroborated by other groups.^{43,44,45} This has also been experimentally corroborated by Boxer and co-workers on the basis of vibrational Stark effect measurement whereby an extremely high electric field was successfully quantified in a *ketosteroid isomerase* enzyme.⁴⁶ Further experimental evidence was provided by Spackmann and co-workers.⁴⁷ This quantification of the LEF in natural systems is not only important in understanding its key properties but also to designing new systems for mimicking the activity of the biomolecules. Recently, it has been illustrated that an artificial enzymes which reprise the catalytic active of biological enzymes can be created by focusing on modifications that aims to enhance the electric field inside the enzyme framework.⁴⁸

These phenomenon provides important insights into designing systems where a strong directional field could be reproduced. One such example is designed-local electric field (D-LEF). It is the process of applying a field along a bond axis by suitable alignment of a functional group attached to the reactants for a specific transformation.⁴⁹ One method designed was the pH switchable D-LEF whereby the LEF was switched between on-off based on the protonation/deprotonation of a acidic or basic group in the molecular framework. This stimuli based technique was utilized for tuning bond-dissociation energy (BDE),^{50,51} reactivity^{52,53} and mechanism.⁵⁴ It has also been established that D-LEF can influence the outcome of chemical reactions by providing altering electrostatic environment whenever different reactants are applied for a reaction.⁵⁵⁻⁵⁷ It has also been hypothesized that D-LEF plays a role in frustrated Lewis acid-base pair (FLP) assisted dihydrogen activation reaction⁵⁸ and also in zeolite framework based catalysis.⁵⁹ Hence understanding the intricacies of LEF can be exploited to design new systems with a targeted application. Also, D-LEF can be used as a promising technique to apply an OEEF in addition to the STM and IEF method. Various roles of LEFs has been discussed in Chapter 3, 4, 5, 6 of this thesis.

Since electric field is dependent on the distribution of charges, it is imperative that charges play the primary role of modulation of LEFs as will be seen specifically in Chapter 4 and 5 of this thesis.

1.7 Field Effect in Chemistry

As in biological systems, intrinsic electric fields are widespread in chemical systems as well. This is generally referred to the polarization of a molecule by an electric field imposed on it spatially via through a polar group at a distal position (**Figure 1.7**).⁶⁰ This effect has quite a fair amount of consequences. The electric field can either increase or decrease the activation barrier of a reaction depending on the nature of the dipole.⁶¹ Similar as in the case of induction effect, field effects influences the acidity/basicity of a molecule.⁶² This is evident in the variation of the pKa values with electronic properties of different substituents in a series of molecules.^{63,64,65} Subsequently, this field can enhance the hydrogen donor ability for anion sensing method.⁶⁶

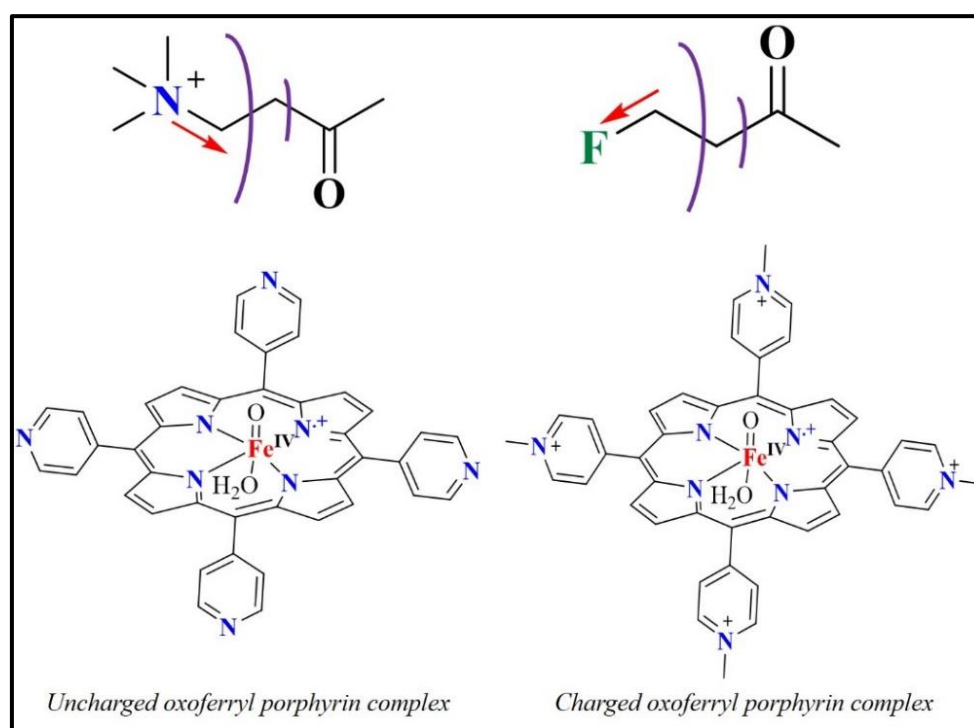


Figure 1.7 Top: Illustration of a field effect on the carbonyl group induced by a polar group. Below: the two oxoferryl porphyrin complex that differs by charge and exhibits a significant difference in HAT rate.

It is interesting to note that electric field already played a key role in modulating the key features of chemical systems with the researchers remaining oblivious of this fact. One such case is the where an extra positive charge on a ligand atom in an oxoferryl porphyrin complex increases the hydrogen abstraction reaction rate

by manifolds compared to the uncharged complex.^{67,68} This has been attributed to the difference in the electric field induced electrostatic environment between the parent complex and its additionally charged analogue. We will illustrate another example of this hidden role of electric field in chemical systems of interest in Chapter 3 of this thesis. Overall, we will investigate the role of this field effect in Chapter 3, 4, 5 and 6 of this thesis.

1.8 Objective of the Thesis

We have summarized the concept of electric field and charge and their subsequent utility in the preceding sections. The judicious use of electric field in smart chemistry is a promising new area of investigation. Computational techniques involving high level quantum chemical calculations can predict the outcome of the applied electric field. This theoretical technique can be best utilized to estimate the intricacies of electric field in natural systems to explain their basic properties. In this thesis, we computationally deduce the role of electric field in chemical and biological systems.

Firstly, we explored this field effect in high-valent intermediates in non-heme biomimetic systems. We selected the iron complexed biuret based tetra-amido macrocyclic ligand (bTAML) and illustrated the role of an extra positive charge on the iron center in enhancing the HAT rate by several folds over the former. DFT calculations have been exploited to deduce the effect of this LEF on the frontier molecular orbitals which leads to the stabilization of the TS. Hence our investigation explains the reactivity of an important bio-mimic on the basis of the variation of electric field.

This study provides a seed for understanding actual physical observations in entities where the electric field is induced by the systems itself. As we know, charge modulation can lead to change in the electric field. One of way to alter charged species is to bind more charged species to it. Hence we explored of role of counter anions in the intriguing group of Ge(II)-crown ether/cryptand complexes. By performing an ab initio molecular dynamics (AIMD) simulations and DFT calculations, we deduced the exact function of the corresponding counter anion in solution. The implications of this result is felt in biological ionophore systems involving dications whereby similar observations involving counter-anions are recorded. We proposed a new concept of “isoionicity” based upon our findings which further explains biological phenomenon. This idea was further applied in an important system of surface science. This exhibits the function of a charged species (counter-anions) in modifying the charge and subsequently the local electric field and its ramifications in chemistry and biology.

Similarly, the electronic and geometric effect of an electric field along a certain direction of space in unique macromolecular systems has also been computationally studied. Furthermore, we emphasized the importance of LEFs in biological macrocycle of valinomycin which can regulate its primary functions.

Our thesis thus adds significantly new insights to an already booming research area. We have successfully showcased the applicability of the intertwining concept of electric field and charge on important chemical and biological systems via computational techniques.

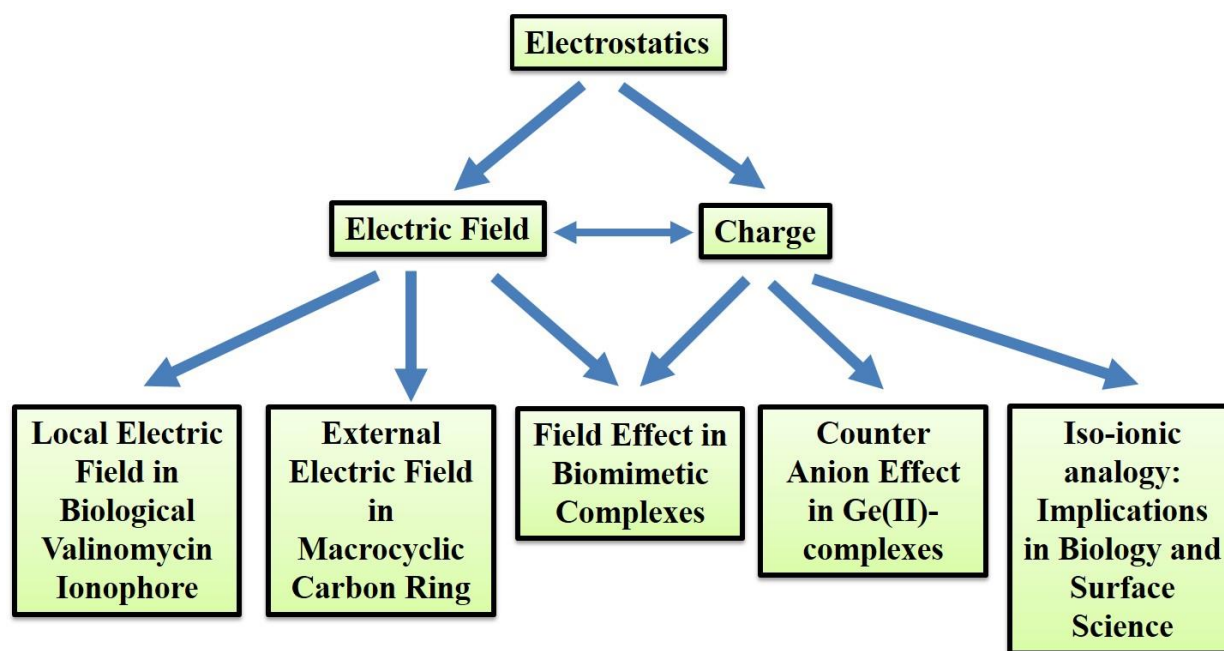


Figure 1.8 Structural Representation of the applicability of the interplay of the concepts of electric field and charge in relevant chemical and biological systems as described in this thesis.

1.9 Organization of the Thesis

The thesis has been divided into 7 chapters

Chapter 1: A Brief Introduction to the significance of electric field and charge in Chemistry and Biology.

This chapter introduces the concept of electric field and charge. It also discusses its prevalence in natural systems and its utility. Also, its role in smart chemistry and biological systems has also been discussed.

Chapter 2: Basic Theoretical Introduction to Computational Chemistry

In this chapter, we will discuss the theory behind the different computational methods we have exploited in this thesis.

Chapter 3: What Drives the H-abstraction Reaction in Bio-mimetic Oxiron-bTAML Complexes? A Computational Investigation

In this chapter, we will discuss the effect of variation charge in a bio-mimetic iron macrocyclic complex. Our calculations will exhibit the role of charge in modulating the hydrogen abstraction reaction rate.

Chapter 4: Unraveling the role of counter anions in “Ge(II) inside a Molecular Cage” Systems

In this chapter, we deduced the exact role of counter anions in Ge(II)-crown ether/cryptand by high level quantum chemical theory.

Chapter 5: Hidden Role of Counter Anions: Implications in Biology and Surface Science

In this chapter, we extended our theoretically deduced concept regarding involvement of counter anions to biological ionophore systems. We proposed a new analogy of “isoionicity”. Furthermore, we extended our proposal to surface science.

Chapter 6: Computational Investigation on the Role of External and Local Electric Fields in Macrocyclic Chemical and Biological Systems

In this chapter, we observed the outcome of applying a theoretically generated oriented external electric field (OEEF) on novel macromolecular systems. We also illustrated the significance of local electric field (LEF) in naturally occurring valinomycin macrocycle which provides an explanation for one of its key function.

Chapter 7: Summary and Future Outlook

In this chapter, we briefly summarize the key outcomes of the work presented in the thesis and also provide a logical futuristic plan based upon our findings.

1.10 References

1. E. M. Purcell, D. J. Morin, *Electricity and Magnetism (3rd ed.)*. New York: Cambridge University Press.2013, 14.

2. a) R. Feynman, *The Feynman Lectures on Physics Vol II. Addison Wesley Longman*. 1970, 1; b) E. M. Purcell, D. J. Morin, *Electricity and Magnetism (3rd ed.)*. New York: Cambridge University Press. **2013**, 15.
3. R. Chabay, B. Sherwood, *Matter and interactions (4th ed.)*. Wiley. **2015**, 867.
4. E. M. Purcell, *Faraday's Law of Induction*, 356.
5. T. Tsuda, *Electric Field Applications in Chromatography, Industrial and Chemical Processes*. **1995**, ISBN 3-527-28687-X.
6. a) C. E. Pullar, *The Physiology of Bioelectricity in Development, Tissue Regeneration, and Cancer*. Boca Raton, FL: CRC Press. **2011**, 342; b) C. D. McCaig, A. M. Rajnicek, B. Song, M. Zhao, *Physiological Reviews*. **2005**, 85, 943; c) K. R. Robinson, M. A. Messerli, *BioEssays*. **2003**, 25, 759.
7. M. L. Yarmush, A. Golberg, G. Sersa, T. Kotnik, D. Miklavic. *Annual Review of Biomedical Engineering*. **2014**, 16, 295.
8. C. Rosazza, S. H. Meglic, A. Zumbusch, M. P. Rols, D. Miklavcic, *Current Gene Therapy*. **2016**, 16, 98.
9. T. Taghian, D. A. Narmoneva, A. B.Kogan, *J. R. Soc. Interface*. **2015**, 12, 0153.
10. L. Buchmann, A. Mathys, *Front. Bioeng. Biotechnol.* **2019**, 7, 265.
11. A. K. Petri, K. Schmiedchen, D. Stunder, D. Dechent, T. Kraus, W. H. Bailey, S. Driessen, *Environmental Health*. **2017**, 16, 41.
12. D. Purves, G. J. Augustine, D. Fitzpatrick, *Neuroscience*. 2nd edition. Sunderland (MA): Sinauer Associates; **2001**. Voltage-Gated Ion Channels.
13. W. Guan, M. A. Reed, *Nano Lett.* **2012**, 12, 6441.
14. O. Plekan, A. Cassidy, R. Balog, N. C. Jones, J. Dunger, *International Reviews in Physical Chemistry*. **2013**, 32, 345.
15. Z.A. Munir, U. Anselmi-Tamburini, M. Ohyanagi, *J Mater Sci*. **2006**, 41, 763.
16. J. L. Anderson, *Ann. Rev. Fluid Mech.* **1989**, 21, 69.
17. H. A. Pohl, *Dielectrophoresis: The Behavior of Neutral Matter in Nonuniform Electric Fields*. **1978**. Cambridge University Press. ISBN 978-0521216579.
18. a) M. P. Hughes, *Nanotechnology*. **2000**, 11, 2; b) M. Constantinou, G. P. Rigas, F. A. Castro, V. Stolojan, K. F. Hoettges, M. P. Hughes, E. Adkins, B. A. Korge, M. Shkunov, *ACS Nano*. **2016**, 10, 4384.
19. E. Fabri, T. J. Schimdt, *ACS Catal.* **2018**, 8, 9765.

20. L. Barsotti, J. C. Cheftel, *Food Rev Int.* **1999**, *15*, 181.
21. S. Shaik, D. Mandal, R. Ramanan, *Nat. Chem.* **2016**, *8*, 1091.
22. S. Shaik, R. Ramanan, D. Danovich, D. Mandal, *Chem. Soc. Rev.* **2018**, *47*, 5125.
23. C. Wang, D. Danovich, H. Chen, S. Shaik, *J. Am. Chem. Soc.* **2019**, *141*, 7122.
24. J. Stark, *Nature.* **1913**, *92*, 401.
25. a) K. Bhattacharyya, S. Karmakar, A. Datta, *Phys. Chem. Chem. Phys.* **2017**, *19*, 22482; b) G. Gryn'ova, M. L. Coote, *J. Am. Chem. Soc.* **2013**, *135*, 15392.
26. S. Shaik, T. Stuyver, J. Joy, Z. Wang, *J. Am. Chem. Soc.* **2020**, *142*, 12551.
27. T. Stuyver, D. Danovich, J. Joy, S. Shaik, *WIREs Comput Mol Sci.* **2019**, e1438.
28. R. Meir, H. Chen, W. Lai, S. Shaik, *ChemPhysChem.* **2010**, *11*, 301.
29. Z. Wang, D. Danovich, R. Ramanan, S. Shaik, *J. Am. Chem. Soc.* **2018**, *140*, 13350.
30. C. J. Laconsay, K. Y. Tsui, D. J. Tantillo, *Chem. Sci.* **2020**, *11*, 2231.
31. P. M. De Biase, D. A. Paggi, F. Doctorovich, *J. Am. Chem. Soc.* **2009**, *131*, 16248.
32. G. D. Harzmann, R. Frisenda, H. S. van der Zant, *Angew Chem Int Ed.* **2015**, *54*, 13425.
33. a) G. Velpula, J. Teyssandier, S. De Feyter, K. S. Mali, *ACS Nano.* **2017**; *11*, 10903; b) A. K. Jissy, A. Datta. *ChemPhysChem.* **2012**, *13*, 4163; c) M. Novak, C. Foroutan-Nejad, R. Marek. *J Chem Theor Comput.* **2016**, *12*, 3788.
34. N. J. English, D. A. Mooney, *J Chem Phys.* **2007**, *126*, 1105.
35. a) S. Vaitheeswaran, J. C. Rasaiah, G. Hummer. *J Chem Phys.* **2004**, *121*, 7955; b) S. Vaitheeswaran, H. Yin, J. C. Rasaiah. *J Phys Chem B.* **2005**, *109*, 6629.
36. A. C. Aragonés, N. L. Haworth, N. Darwish, *Nature.* **2016**, *531*, 88.
37. L. Zhang, E. Laborda, N. Darwish, B. B. Noble, J. Tyrell, S. Pluczyk, A. P. L. Brun, G. G. Wallace, J. Gonzalez, M. L. Coote, S. Ciampi, *J. Am. Chem. Soc.*, **2018**, *140*, 766.
38. E. Gileadi, *Electrode kinetics for chemists, chemical engineers and materials scientists.* New York, NY: Wiley-VCH Verlag GmbH, **1993**.
39. M. Akamatsu, N. Sakai, S. Matile, *J. Am. Chem. Soc.* **2017**, *139*, 6558.
40. C. F. Gorin, E. S. Beh, Q. M. Bui, G. R. Dick, M. W. Kanan. *J. Am. Chem. Soc.* **2013**, *135*, 11257.
41. A. Warshel, *Acc. Chem. Res.* **1981**, *14*, 284.
42. A. Warshel, P. K. Sharma, M. Kato, Y. Xiang, H. Liu, M. H. M. Olsson, *Chem. Rev.* **2006**, *106*, 3210.
43. P. A. Kollman, B. Kuhn, O. Donini, M. Perakyla, R. Stanton, D. Bakowies, *Acc. Chem. Res.* **2001**, *34*, 72.

44. S. Martí, M. Roca, J. Andrés, V. Moliner, E. Silla, I. Tuñón, J. Bertrán, *Chem. Soc. Rev.* **2004**, *33*, 98.
45. B. Szefczyk, A. J. Mulholland, K. E. Ranaghan, W. Sokalski, *J. Am. Chem. Soc.* **2004**, *126*, 16148.
46. S. D. Fried, S. Bagchi, S. G Boxer, *Science.* **2014**, *346*, 1510.
47. M. W. Shi, S. P. Thomas, V. R. Hathwar, *J. Am. Chem. Soc.* **2019**, *141*, 3965.
48. V. Vaissier Welborn, T. Head-Gordon, *Chem. Rev.* **2019**, *119*, 6613.
49. D. L. Marshall, G. Gryn'ova, B. L. Poad, *Int. J. Mass. Spectr.* **2019**, *435*, 195.
50. M. Klinska, L. M. Smith, G. Gryn'ova, M. G. Banwell, M. L. Coote, *Chem Sci.* **2015**, *6*, 5623.
51. G. Gryn'ova, M. L. Coote, *Aust. J. Chem.* **2017**, *70*, 367.
52. N. S. Hill, M. L. Coote, *J. Am. Chem. Soc.* **2018**, *140*, 17800.
53. M. T. Blyth, M. L. Coote, *J Org Chem.* **2019**, *84*, 517.
54. Y. Li-Juan, M. L. Coote, *J Phys Chem A.* **2018**, *123*, 582.
55. C. Geng, J. Li, T. Weiske, M. Schlangen, S. Shaik, H. Schwarz, *J. Am. Chem. Soc.* **2017**, *139*, 1684.
56. L. Yue, J. Li, S. Zhou, *Angew. Chem. Int. Ed.* **2017**, *56*, 10219.
57. C. Geng, J. Li, M. Schlangen, *Dalton Trans.* **2018**, *47*, 15271.
58. S. Grimme, H. Kruse, L. Goerigk, G. Erker, *Angew. Chem. Int. Ed.* **2010**, *49*, 1402.
59. N. Liu, R. Zhang, Y. Li, B. Chen. *J Phys Chem C.* **2014**, *118*, 10944.
60. S. E. Wheeler, K. N. Houk, *J. Chem. Theory Comput.* **2009**, *5*, 2301.
61. E. V. Anslyn, D.A. Dougherty, *Modern physical organic chemistry.* Sausalito, CA: University Science. **2006**, ISBN 9781891389313.
62. S. Parveen, A. K. Chandra, T. Zeegers-Huyskens, *J. Phys. Chem. A.* **2009**, *113*, 6182.
63. C. Hansch, A. Leo, R. W. Taft, *Chem. Rev.* **1991**, *91*, 165.
64. M. J. S. Dewar, P. J. Grisdale, *J. Am. Chem. Soc.* **1962**, *84*, 3548.
65. E. J. Grubbs, R. Fitzgerald, R. E. Philips, R. Petty, *Tetrahedron.* **1971**, *27*, 935.
66. B. W. Tresca, R. J. Hansen, C. V. Chau, B. P. Hay, L. N. Zakharov, M. M. Haley, D. W. Johnson, *J. Am. Chem. Soc.* **2015**, *137*, 14959.
67. S. R. Bell, J. T. Groves, *J. Am. Chem. Soc.* **2009**, *131*, 9640.
68. H. Gao, J. T. Groves, *J. Am. Chem. Soc.* **2017**, *139*, 3938.

**Chapter 2: Basic Theoretical Introduction to Computational
Chemistry**

Chapter 2

Basic Theoretical Introduction to Computational Chemistry

Abstract

In this chapter, we have discussed the theoretical background for the various computational techniques applied in this thesis. Density Functional Theory (DFT) is a powerful tool based on quantum mechanics to map the static energetics (thermodynamics and kinetics) of various processes. Herein, we have discussed the foundations of different quantum mechanical methods leading to the conceptualization of DFT. Apart from DFT, we have mapped the dynamics of various processes utilizing ab initio molecular dynamics (AIMD). The basic principle behind AIMD has also been discussed in this thesis. Additionally, we have illustrated the theory behind different critical modules described in this thesis.

2.1 Introduction

It has been established that kinetics and thermodynamics plays an important role in all observable transformations. This provides necessary understanding regarding the pathway of the transformation and the energy associated with it. This can be chalked out by both theoretical and experimental methods. The calculation of potential energy surface (PES) by invoking the laws of quantum mechanics (QM) gives a significant understand a large number chemical and biological processes described in this thesis. Hence ab initio methods like configuration interaction¹ (C.I) and coupled cluster² (CCSD) can solve the Schrodinger equation exactly. However these process is computationally expensive and hence faces difficulty in implementation. Over the years, Density Functional Theory (DFT) has emerged as one of the most commonly techniques to be implemented for quick and a relatively accurate calculation.³We have applied the DFT methodology extensively in our thesis. In this chapter, we will discuss about the founding concepts of the quantum theory and delve into its various facets to understand its utility in finding solutions to the problem of many body systems. We will also illustrate the concepts behind different computational methods described in this thesis.

2.2 Basic Tenets of Quantum Mechanics.

2.2.1 Schrodinger Equation

One of the key targets of quantum mechanics is to calculate the energy of the system under consideration. In 1926, Erwin Rudolf Josef Alexander Schrödinger forwarded the time dependent Schrodinger equation to solve the electronic energies of systems. However, the relevance of time dependent Schrodinger equation is negligible in chemistry and biology. The time independent Schrodinger equation for n number electrons with m number of nuclei is given by:

$$\hat{H}\Psi(x_1x_2,x_3,\dots,x_n, r_1r_2,\dots,r_m) = E\Psi(x_1x_2x_3,\dots,x_n, r_1r_2,\dots,r_m) \quad (2.2.1)$$

Where, E (the eigen value) is the total energy of the system, $\Psi(x_n, r_m)$ (eigen function) is the wave function for the system and \hat{H} is the hamiltonian. The wave function contains every possible information about the particle associated with it. The Hamiltonian \hat{H} is expressed as:

$$\hat{H} = \frac{-\hbar}{2} \sum_{a=1}^m \frac{1}{m_a} \nabla_a^2 - \frac{\hbar}{2m_e} \sum_{i=1}^n \nabla_i^2 + \sum_a \sum_{a>b} \frac{Z_a Z_b e^2}{r_{ab}} + \sum_a \sum_i \frac{Z_a e^2}{r_{ia}} + \sum_{ji} \sum_{i>j} \frac{e^2}{r_{ij}} \quad (2.2.2)$$

The first two terms specifies the kinetic energy of the nuclei and electrons. The other three terms specifies the nuclear-nuclear repulsion, nuclear-electron attraction, and electron-electron repulsion respectively, $\hbar = h/2\pi$ and h is the Planck's constant, m_a and m_e represents the masses of the nuclei and electrons respectively, Z_a and Z_b are the charges of nuclei, r_{ab} is the distance between the nuclei a and b , r_{ia} represents the distance between the i^{th} electron and the a^{th} nuclei and r_{ij} is the distance between the i^{th} and the j^{th} electron.

The $|\Psi(x_n, r_m)|^2$ value provides the probability density of the particle x_n . An ideal case involves the presence of a single electron.

The probability of finding n electrons in the entire space is always equal to unity.

For solving real systems, we need to solve this equation for a multi-electronic system involving many particles. Hence, approximate methods have been devised to minimize the difficulty in solving multi-electron Schrodinger equation. In the upcoming sections, we shall discuss the different approximate approaches.

2.2.2 The Born-Oppenheimer Approximation.

One of the commonly used approximations used in theoretical calculations is the Born- Oppenheimer (BA) Approximation. The nuclei's position are approximated to be fixed during an electronic transition as the nucleus are considered to be heavier than electrons. Hence the nuclear kinetic energy becomes nil and the corresponding potential energy becomes fixed. Hence the equation (2.2.2) reduces to the electronic Hamiltonian \hat{H}_e .

$$\hat{H}_e = -\frac{\hbar}{2m_e} \sum_{i=1}^n \nabla_i^2 + \sum_a \sum_i \frac{Z_a e^2}{r_{ia}} + \sum_{ji} \sum_{i>j} \frac{e^2}{r_{ij}} \quad (2.2.3)$$

Hence the electronic energy of a system can be calculated by solving the Schrodinger equation using the \hat{H}_e operator.

$$\hat{H}_e \Psi_e = E_e \Psi_e \quad (2.2.4)$$

2.2.3 Variation principle

As seen from the equation 2.2.4, the strategy for elucidating the electronic energy of a real system is cumbersome and painstaking. One has to first establish a Hamiltonian for a particular system and then estimate the eigen function of that particular Hamiltonian. Hence, to sidetrack this laborious process, a trial

wave function could be used to get an accurate electronic energy value. The variation principle thus states that the energy (E) obtained by utilizing a trial wave function (φ) is always equal or higher than the ground state energy (E_0).

$$E(\varphi) = \frac{\langle \varphi | \hat{H} | \varphi \rangle}{\langle \varphi | \varphi \rangle} > E_0 \quad (2.2.5)$$

This variation method of trial and error has been applied in most of the approximate methods used for calculating the total electronic energy of the system specified in this thesis.

2.3 Density Functional Theory (DFT)

The calculation of energy based on wave functions is a very expensive one. Hence to reduce the complexities of using this approach, alternate accurate and speedy methods need to be conceived. Density functional theory (DFT) is the most suitable alternative method that could be implemented for estimating the total electronic energy of a multi-electronic system. This is because, unlike wave functions, DFT utilizes electron density to adjudicate the critical molecular properties. This cuts the cost of computation as compared to the wave function based method. In this thesis, we have mostly employed this particular method for computing various important insights of a wide range of systems. DFT is widely used in chemistry and biology to study its important components over the recent years. This is because this method improves the scope of its applicability. In the upcoming sections, we will discuss the rudimentary elements of the DFT method.

2.3.1 Functional

A functional is generally referred to as a function of a function. For an example, the variation integral $F(\varphi) = \langle \varphi | \hat{H} | \varphi \rangle$ is a function of the trial wave function φ . We can also estimate the derivative of a functional just like a general function. Functionals can be classified as i) local-density (LDA), ii) generalized gradient (GGA), iii) meta-generalized gradient and iv) hybrid approximation functional.

2.3.1.1 Local Density Approximation (LDA)

This approximation can be only considered for a homogenous gaseous medium where there is lesser variation in electron density [$\rho(\vec{r})$]. Hence, there is very less fluctuation in electron density in this approximate density. At every position in this model, the exchange-correlation factor is the same. The exchange-correlation factor can be expressed as

$$E_{XC}^{LDA}[\rho] = \int \rho(\vec{r}) \epsilon_{xc}[\rho(\vec{r})] d\vec{r} \quad (2.3.1.1)$$

where ϵ_{xc} is the exchange-correlation energy /particle of a homogeneous electron gas of electron density ρ . The exchange-correlation energy can be expressed as the total of the addition of exchange [$\epsilon_x(\rho)$] and correlation term [$\epsilon_c(\rho)$].

$$\epsilon_{xc}(\rho) = \epsilon_x(\rho) + \epsilon_c(\rho) \quad (2.3.1.2)$$

LDA approximations could be applied to both closed shell and open shell (radical) systems.

2.3.1.2 Generalized Gradient Approximation (GGA)

LDA functionals cannot be applied in systems where the electron density changes in different positions. Hence the gradient of electron density [$\nabla(\rho)$] should be included into consideration. $E_{XC}^{GGA}(\rho)$ can be expressed as

$$E_{XC}^{GGA}(\rho) = E_{XC}^{GGA} + E_X^{GGA} \quad (2.3.1.3)$$

Several GGA functionals like Perdew functionals (P86, Pc86, PW91, PWc91, PBE) and Becke functional (B88, Bx88) could be used to expedite the ease of calculations and deduce authentic results.

2.3.1.3 Meta-generalized gradient approximation Functionals (MGGA)

Meta-generalized gradient Functionals can be described as another form of GGA function as it considers the second derivative of the electron density. The MGGA can be expressed as

$$E_{XC}^{MGGA}[\rho^\alpha, \rho^\beta] = \int f(\rho^\alpha, \rho^\beta, \nabla \rho^\alpha, \nabla \rho^\beta, \nabla^2 \rho^\alpha, \nabla^2 \rho^\beta, \tau^\alpha, \tau^\beta) d\vec{r} \quad (2.3.1.4)$$

where, τ^α, τ^β are the independent kinetic energy density that can be defined as

$$\tau^\alpha = \frac{1}{2} \sum_i |\nabla \theta_{i\alpha}^{KS}(r)|^2 \text{ where, the } \theta_{i\alpha}^{KS}(r) \text{ are the Kohn-Sham orbitals for the electrons that have } \alpha \text{ spin.}$$

This functional like M06-L and TPSS provides more accurate results than a GGA functional but is more expensive than it.

2.3.1.4 Hybrid Functional

Most of functional employed recently are the hybrid functionals. This functional includes an exact exchange term from the Hartree Fock (HF) theory along with an exchange-correlation term from an ab-initio or empirical source. The exact exchange term is expressed as

$$E_X^{\text{HF}} = -\sum_{i=1}^n \sum_{j=1}^n \left\langle \varphi_i^{\text{KS}}(1) \varphi_j^{\text{KS}}(2) \left| \frac{1}{r_{ij}} \right| \varphi_i^{\text{KS}}(2) \varphi_j^{\text{KS}}(1) \right\rangle \quad (2.3.1.5)$$

One of the commonly used hybrid functional is B3LYP.

2.3.2 Electron Density

One the intrinsic property of DFT is the presence of an electron density. Electron density can be defined as the probability of finding an electron in a specific volume. This can be specified as

$$\rho(\vec{r}) = N \int |\varphi(\vec{x}_1 \dots \vec{x}_n)|^2 ds d\vec{x}_2 \dots \dots \dots d\vec{x}_n$$

where, $\vec{x} = r^{\vec{s}}$ and $\rho(\vec{r})$ state the probability of finding the N electrons with any spin state in the volume $d\vec{r}_1$. Unlike wave functions, electron density can be experimentally measured by x-ray diffraction, electron diffraction, and scanning tunneling microscope (STM) which provides DFT with an extra advantage. The electron density is always a positive number and its first derivative provides the gradient and its distribution in the system under consideration. The second derivatives also provides critical extra information about the electron density distribution.

Though DFT has used electron density as a basis for its approximation, it is not the first instance of its use to develop a theoretical model. This model, known as Thomas-Fermi model, utilizes electron density instead of wave function. This model conceptualizes an electron gas model consisting of uniform electron density. However, this model suffers predictably from various discrepancies. It doesn't considers the exchange-correlation interaction and considers the electron as constant in all points which is far removed from reality.

2.3.3 The Hohenberg-Kohn Theorems

The idea behind DFT was first put forward by Kohn and Hohenberg in a landmark work in 1964.⁴This idea was based on two proven theorems.

Theorem 1:

“The external potential $\widehat{V}_{ext}(\vec{r})$ is (to within a constant) a distinctive functional of $\rho(\vec{r})$; since, in turn $\widehat{V}_{ext}(\vec{r})$ remain constant we observe that the multi-particle ground state is a sole functional of $\rho(r)$.”

Proof:

If we consider two external potentials \widehat{V}_{ext} and \widehat{V}'_{ext} (these two quantities varies from each other by more than a constant value), resulting in identical ground-state electron density $\rho(\vec{r})$. These two distinct external potentials will definitely concur to the two individual electronic Hamiltonian operators \widehat{H} and \widehat{H}' respectively, and \widehat{H} and \widehat{H}' will belong to two different ground state wave functions φ , and φ' respectively. E_0 and E_0' are the ground state energies of the two wave functions φ , and φ' respectively.

$$E_0 = \langle \varphi | \widehat{H} | \varphi \rangle \quad E_0' = \langle \varphi' | \widehat{H}' | \varphi' \rangle \quad \text{where, } E_0 \neq E_0' \quad (2.3.1)$$

$$\widehat{H} = \widehat{T} + \widehat{V}_{ee} + \widehat{V}_{ex}$$

$$\widehat{H}' = \widehat{T}' + \widehat{V}'_{ee} + \widehat{V}'_{ex}$$

Since both the wave functions results in the same electron density, it can be expressed as

$$\widehat{V}_{ex} \rightarrow \widehat{H} \rightarrow \varphi \rightarrow \rho(\vec{r}) \leftarrow \varphi' \leftarrow \widehat{H}' \leftarrow \widehat{V}'_{ex}$$

Now, by applying the variation principle by using a trial wave function φ' for the \widehat{H}' Hamiltonian.

$$E_0 < \langle \varphi_0 | \widehat{H} | \varphi_0 \rangle = \langle \varphi_0 | \widehat{H}' | \varphi_0 \rangle - \langle \varphi_0 | \widehat{H} - \widehat{H}' | \varphi_0 \rangle \quad (2.3.2)$$

By inserting the values of \widehat{H} and \widehat{H}' ,

$$E_0 < E_0' + \langle \varphi_0 | \widehat{T} + \widehat{V}_{ee} + \widehat{V}_{ex} - \widehat{T}' - \widehat{V}'_{ee} - \widehat{V}'_{ex} | \varphi_0 \rangle = E_0 < E_0' + \int \rho(\vec{r}) \{ \widehat{V}_{ex} - \widehat{V}'_{ex} \} \quad (2.3.3)$$

The R.H.S of the above equation (2.3.3) can also be written as

$$E_0' < E_0 + \int \rho(\vec{r}) \{ \widehat{V}_{ex} - \widehat{V}'_{ex} \}$$

Adding equation (2.3.2) and (2.3.3)

$$E_0 + E_0' < E_0' + E_0 \text{ or } 0 < 0$$

So, it is proved that there can only exist a unique value of V_{ex} that produces the same ground state energy.

Hence the ground state energy can be represented as

$$E_v[\rho_0] = T[\rho_0] + V_{ne}[\rho_0] + V_{ee}[\rho_0] \quad (2.3.4)$$

$$E_v[\rho_0] = \int \rho_0(\vec{r})v(\vec{r}) d\vec{r} + T[\rho_0] + V_{ee}[\rho_0] \quad (2.3.5)$$

In equation 2.3.5 the earlier part, $\int \rho_0(\vec{r})v(\vec{r}) d\vec{r}$ is the time independent part and latter part, $T[\rho_0] + V_{ee}[\rho_0]$ is the Hohenberg-Kohn functional $F_{HK}[\rho_0]$.

$$F_{HK}[\rho_0] = T[\rho_0] + V_{ee}[\rho_0] \quad (2.3.6)$$

The $F_{HK}[\rho_0]$ value is not dependent on the external potential (V_{ex}).

Theorem 2

“The functional that generates the ground state energy of the system, $F_{HK}[\rho_0]$, delivers the lowest energy only if the input density represents the true ground state density, ρ_0 .”

Proof:

We considered a guess density that will have its distinct Hamiltonian H' and wave function φ . This wave function can be implemented as a guess wave function for the Hamiltonian, which is created from the external potential V_{ext} . Hence,

$$\langle \varphi | \hat{H} | \varphi \rangle = T[\rho'] + V_{ee}[\rho'] + \int \rho(\vec{r}) \overline{V_{ex}}(\vec{r}) d\vec{r} = E[\rho'] \geq E_0[\rho_0] = \langle \varphi_0 | \hat{H} | \varphi_0 \rangle \quad (2.3.7)$$

2.3.4 The Kohn-Sham Approach

The Hohenberg-Kohn theorems are applied to calculate the ground state energy of a multi-electronic system. The ground state energy calculated from the Hohenberg-Kohn theorems can be expressed as:

$$E_0 = \min_{\rho \rightarrow N} (F_{HK}[\rho] + \int \rho(\vec{r}) \overline{V_{Ne}}(\vec{r}) d\vec{r}) \quad (2.3.8)$$

where, $F_{HK}[\rho]$ is a universal functional; it includes the kinetic energy $T[\rho(\vec{r})]$, the classical Coulomb $J[\rho(\vec{r})]$, and the non-classical contribution $E_{ncl}[\rho(\vec{r})]$.

$$F[\rho(\vec{r})] = T[\rho(\vec{r})] + J[\rho(\vec{r})] + E_{ncl}[\rho(\vec{r})] \quad (2.3.9)$$

In the above expression, the kinetic energy term is unknown according to Hohenberg-Kohn theorems. Hence Kohn and Sham devised an approach to derive the ground state energy of molecular systems wherein a non-interacting reference system of electrons has been assumed.⁵Hence,

$$T_s = -\frac{1}{2} \sum_i^N \langle \varphi_i | \nabla^2 | \varphi_i \rangle \text{ and } \rho_s(\vec{r}) = \sum_i^N \sum_s |\varphi_i(\vec{r}, s)|^2 = \rho(\vec{r}) \quad (2.3.10)$$

where, T_s is the kinetic energy, and Ψ_i refers to the wave function of the reference system. It is to be noted that T and T_s are never equal. A substantial part of the $T[\rho(\vec{r})]$ has been reintroduced through the T_s term. Hence, to override this problem, Kohn-Sham suggested a partitioned universal functional where the exchange-correlation energy, $E_{XC}[\rho]$, has been added.

$$F[\rho] = T_s[\rho] + J[\rho] + E_{XC}[\rho] \quad (2.3.11)$$

$$\text{where, } E_{XC}[\rho] = (T[\rho] - T_s[\rho]) + E_{ec}[\rho] - J[\rho] \quad (2.3.12)$$

The corresponding component of the $E_{XC}[\rho]$ term are difficult to be estimated. The next task was to calculate the value for the non-interacting reference system which has a similar electron density as the interacting system.

$$E[\rho] = T_s[\rho] + J[\rho] + E_{EX}[\rho] + E_{Ne}[\rho] \quad (2.3.13)$$

So expanding the term in equation (2.3.11)

$$E[\rho] = T_s[\rho] + \frac{1}{2} \frac{\int \int \rho(\vec{r}_1) \rho(\vec{r}_2)}{r_{12}} d\vec{r}_1 d\vec{r}_2 + E_{ex}[\rho] + \int V_{Ne} \rho(\vec{r}) d\vec{r} \quad (2.3.14)$$

$$= -\frac{1}{2} \sum_i^N \langle \varphi_i | \nabla^2 | \varphi_i \rangle + \frac{1}{2} \sum_i^N \sum_j^N \int \int |\varphi_i(\vec{r}_1)|^2 \frac{1}{r_{12}} |\varphi_j(\vec{r}_1)|^2 d\vec{r}_1 d\vec{r}_2 + E_{EX}[\rho] - \sum_i^N \int \sum_A^M \frac{Z_A}{r_{1A}} |\varphi_j(\vec{r}_1)|^2 d\vec{r}_1 \quad (2.3.15)$$

The only unknown term is $E_{XC}[\rho]$ and the minimization of the energy via the variation principle results in the Kohn-Sham equation.

$$-\frac{1}{2} \nabla^2 + \left[\int \frac{\rho(\vec{r}_2)}{r_{12}} d\vec{r}_2 + V_{XC}(r_1) - \sum_A^M \frac{Z_A}{r_{1A}} \right] \varphi_i = \epsilon_i \varphi_i \quad (2.3.16)$$

$$V_{XC}(\vec{r}) = \frac{dE_{XC}[\rho(\vec{r})]}{d\rho(\vec{r})} \quad (2.3.17)$$

The self-consistency can be estimated from the $V_{\text{eff}}(\vec{r})$ value which is calculated from the above equations. The mapping of the interaction between the kinetic energy and the electron density can be plotted by using Ψ_i s. It is to be noted here that Ψ_i s does not signifies the real orbitals and the Kohn-Sham method is a single determinant module.

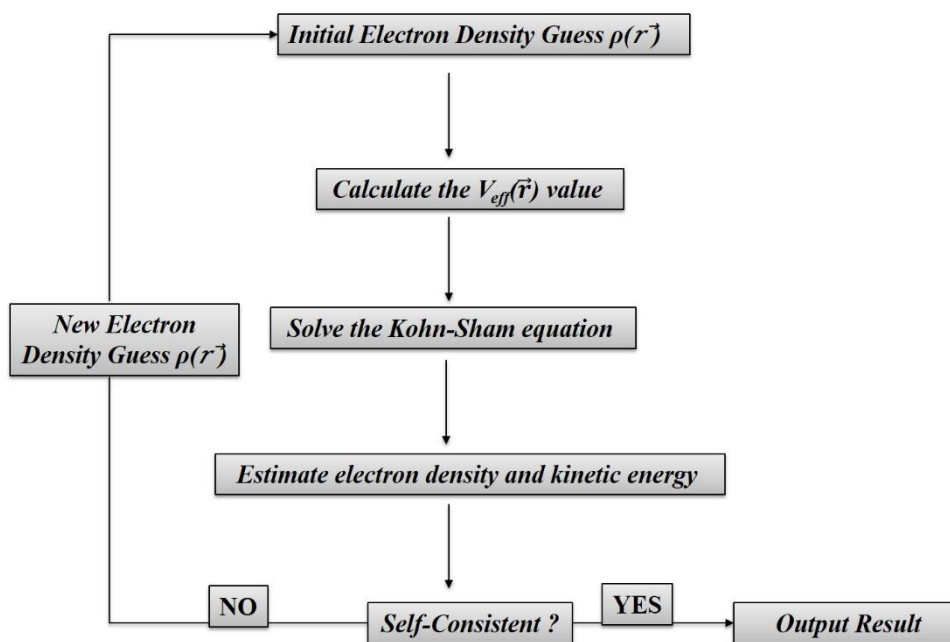


Figure 2.1 Flowchart illustrating the iteration cycle for calculating the single point electronic energy.

2.4 Natural Bond Orbital (NBO) Analysis.

NBO is a class of natural localized orbital set and is a method for mapping electron density and charge density in molecular systems where the distinct set of orthonormal 1-electron functions, intrinsic to the n -electron wave function $Y(1,2,\dots,n)$, that can change a specified wave function, φ , into a localized form consisting of lone pairs and bonds akin to a Lewis structure of a molecule.⁶NBO is a second-order perturbation theory method that takes into account every interactions between donor NBOs and acceptor NBOs. The donor-acceptor interaction energy $E(2)$ can be expressed as;

$$E(2) = \nabla E_{ij} = q_i \frac{F(i,j)^2}{E_i - E_j} \quad (2.4.1)$$

where q_i is the donor orbital occupancy and $F(i,j)$ is the NBO Fock matrix element. We have this methods and various modules originating from this theory for understanding the nature of the bonding in different molecular systems investigated in this thesis.

2.5 Non Covalent Interaction (NCI) Plot

This method was developed by Yang et al for visualizing non-covalent interactions in molecules.⁷This method is based on electron density gradient estimation in the molecular framework. We have used this method in Chapter 4 and 5 of our thesis.

2.6 Ab Initio Molecular Dynamics (AI-MD)

Molecular Dynamics is a widely used form of computer based simulation whereby the dynamic evolution of molecules are mapped. The pathway of the atoms in the molecule is elucidated via solving the Newton's law of motion. The forces acting on each atoms or particles of the system under simulation study is provided by the classical mechanical force field. However, the force can also be calculated from the laws of quantum mechanics, like density functional theory (DFT) to obtain an accurate electronic behavior of the simulated systems. This simulation approach is known as Ab Initio Molecular Dynamics (AI-MD). This is a computationally costly method and hence is applied on smaller molecules.

In this respect, DFT based molecular simulations could be done by introducing the method of steepest descent to the laws of Newtonian motion to obtain an authentic idea about the electronic structure of the system. This class of simulation was first proposed by Car & Parrinello (CP) in 1985. Car & Parrinello (CP) proposed a classical Lagrangian for a system where the coefficients corresponding to the basis functions are considered to be dynamic variables.

$$L_{CP} = \sum_i \frac{1}{2} \mu_i \langle \varphi_i | \dot{\varphi}_i \rangle + \frac{1}{2} \sum_I M_I R_I^2 - \langle \varphi_o | H | \varphi_o \rangle + \text{constraints} \quad (2.6.1)$$

$$E = \langle \varphi_o | H | \varphi_o \rangle = \int V_{ext}(\vec{r}) \rho(\vec{r}) d\vec{r} + \langle \varphi_o | \hat{T} + \hat{V}_{ee} | \varphi_o \rangle \quad (2.6.2)$$

where the total wave function $|\varphi_o\rangle$; M_I is the nuclear mass and μ_i is the theoretical electron mass. T is the kinetic energy of mutually non-interacting electrons and V_{ee} is the electron exchange and correlation potential.

Also,

$$\text{Constraints} = \sum_{ij} \Delta_{ij} (\varphi_i^* \varphi_j d^3\vec{r} - \delta_{ij}) \quad (2.6.3)$$

Where δ_{ij} is the Lagrangian multipliers. Now,

$$\begin{aligned} E = \langle \varphi_o | H | \varphi_o \rangle &= \int V_{ext}(\vec{r}) \rho(\vec{r}) d\vec{r} + \langle \varphi_o | \hat{T} + \hat{V}_{ee} | \varphi_o \rangle \\ &= \int V_{ext}(\vec{r}) \rho(\vec{r}) d\vec{r} + F[\rho(\vec{r})] \end{aligned} \quad (2.6.4)$$

The $F[\rho(\vec{r})]$ value cannot be calculated as is a distinct property of every system. This can only be estimated by a functional. Euler-Lagrange equations could be utilized to solve the Newton's law of motion.

$$\frac{d}{dt} \left(\frac{dL_{CP}}{dR_I} \right) = \frac{dL_{CP}}{dR_I}$$

$$\frac{d}{dt} \left(\frac{dL_{CP}}{d\varphi_i^*} \right) = \frac{dL_{CP}}{d\varphi_i^*}$$

For the coupled electron-ion molecular dynamics, the CP equations of motions becomes,

$$L_{CP} = \sum_i \frac{1}{2} \mu_i \langle \varphi_i | \varphi_i \rangle + \frac{1}{2} \sum_I M_I R_I^2 - E(\varphi_o, \vec{R}) + \text{constraints} \quad (2.6.5)$$

The atomic and electron degree of freedom could be exploited to calculate the classical forces.

$$M_I R_I(t) = -\frac{d}{dR_I} \langle \varphi_o | H | \varphi_o \rangle + \frac{d}{dR_I} (\text{constraints}) \quad (2.6.6)$$

$$\mu_i R_I(t) = -\frac{d}{d\varphi_i^*} \langle \varphi_o | H | \varphi_o \rangle + \frac{d}{d\varphi_i^*} (\text{constraints}) \quad (2.6.7)$$

As mentioned earlier, the steepest descent and other similar methods could be of advantage to calculate the ground state electronic energy of a system for a fixed nuclear position.

$$\varphi_i(t) = -\frac{1}{2} \frac{\delta E}{\delta \varphi} + \sum_J \Delta_{ij} \varphi(t) = -\frac{1}{2} H \varphi_i(t) + \sum_J \Delta_{ij} \varphi(t) \quad (2.6.8)$$

The dynamical property of a system can be estimated after determining the ground state electronic energy using equation (2.6.8)

2.7 References

1. a) C. J. Cramer, Chichester: John Wiley & Sons, Ltd. **2002**, 191; b) C. D. Sherrill, H. F. Schaefer III, The Configuration Interaction Method: Advances in Highly Correlated Approaches, San Diego: Academic Press, **1999**, 143.
2. a) H. G. Kmmel, *Int. J. Mod. Phys. B*, **2003**, *17*, 5311; b) R. F. In Bishop, T. Brandes, K. A. Gernoth, N. R. Walet, Y. Xian, H. Kmmel, in Proceedings of the 11th International Conference on Recent Progress in many-body theories, Singapore: World Scientific Publishing, **2002**, 334; b) I. Shavitt, R. J. Bartlett, Many-Body Methods in Chemistry and Physics: MBPT and Coupled-Cluster Theory, Cambridge University Press. **2009**.
3. a) M. H. N. Assadi, D. A. H. Hanao, *J. Appl. Phys*, **2013**, *113*, 233913; b) M. D. Segall, P. J. D. Lindan, M. J. Probert, C. J. Pickard, P. J. Hasnip, S. J. Clark, M. C. Payne, *J. Phys: Condens. Matter*,

-
- 2002**, **14**, 2717; b) F. R. Somayeh, H. Soleymanabadi, *J. Mol. Model.*, **2014**, **20**, 2439; c) F. R. Somayeh, H. Soleymanabadi, *J Mol Model* , **2013**, **19**, 3733; d) D. Music, R. W. Geyer, J. M. Schneider, *Surface & Coatings Technology*, **2016**, **286**, 178.
4. P. Hohenberg, W. Kohn, *Physical review*, **1964**, **136**, B864.
 5. W. Kohn, L. J. Sham, *Physical review*, **1965**, **140**, A1133.
 6. a) F. Weinhold, C. R. Landis,. *Chem. Edu. Res. Pract.* **2001**, **2**, 91; b) *Physics Rev.* **1955**, **97**, 1474.
 7. a) E. R. Johnson, S. Keinan, P. M. Sanchez, J. C. Garcia, A. J. Cohen, W. Yang, *J. Am. Chem. Soc.* **2010**, **132**, 6498. b) J. C. Garcia, E. R. Johnson, S. Keinan, R. Chaudret, J. P. Piquemal, D. N. Beratan, W. Yang, *J. Chem. Theory Comput.* **2011**, **7**, 625.
 8. R. Car, M. Parrinello, *Phys. Rev. Lett.* **1985**, **55**, 2471.

**Chapter 3: What Drives the H-abstraction Reaction in Bio-mimetic
Oxoiron-bTAML Complexes? A Computational Investigation**

Chapter 3

What Drives the H-abstraction Reaction in Bio-mimetic Oxoiron-bTAML Complexes? A Computational Investigation

Abstract

Monomeric Iron-oxo units have been confirmed as intermediates involved in the C-H bond activation in various metallo-enzymes. Biomimetic oxoiron complexes of the biuret modified tetra-amido macro cyclic ligand (bTAML) have been demonstrated to oxidize a wide variety of unactivated C-H bonds. In the current work, density functional theory (DFT) has been employed to investigate the hydrogen abstraction (HAT) reactivity differences across a series of bTAML complexes. The cause for the differences in the HAT energy barriers has been found to be the relative changes in the energy of the frontier molecular orbitals (FMOs), induced by electronic perturbation.

3.1 Introduction

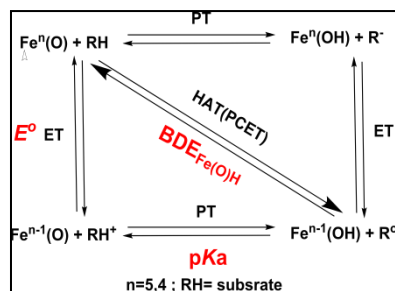


Figure 3.1 Square scheme with associated thermodynamic parameters involved in HAT reactions.

Numerous model complexes and functional mimics have been studied for the purpose of understanding the chemical reactions taking place in heme and nonheme based enzyme systems. One important question in this regard is with respect to the H-atom transfer (HAT) reactivity difference during C-H abstraction in such systems. The existence of the reactive intermediates, oxoiron(V) and oxoiron(IV) species, have been confirmed experimentally during the mechanistic elucidation of HAT, oxygen activation and oxygen-atom transfer (OAT) reactions.¹⁻¹⁵ A plethora of theoretical models and functional mimics have been employed to study and explain the sluggish C-H abstraction reactivity of Cpd II (Compound II, oxoiron(IV) porphyrins) with respect to Cpd I (Compound I; oxoiron(IV) porphyrin π -cation radicals), with theoretical calculations yielding a 2.0-5.0 kcal/mol higher H-abstraction barrier for Cpd II mimics in comparison to the mimics of Cpd I.¹⁶⁻²² Theoretical insight into the HAT reactivity of a proposed nonheme oxoiron(V) and its one electron reduced intermediate indicates higher reactivity of the former but the inherent reason elucidating the reactivity difference was not provided.¹⁴ However, a related comparison between a pure monomeric Fe^V(O) and Fe^{IV}(O), experimentally isolated with high purity, has not been reported in the literature until recently. In a recent study, our group has compared the spectroscopy and H-atom abstraction activity of nonheme oxoiron (V) and oxoiron (IV) complexes of the biuret based tetra-amido macro cyclic ligand (bTAML) system (**1a** and **2**), which are isoelectronic to Cpd I and Cpd II respectively (**Figure 3.2**).²³⁻²⁴ **1a** showed a 2500 fold increase in reactivity in comparison to **2** when benzyl alcohol was employed as the substrate. However, the stability of both the oxo-iron complexes is pH dependent: while **1a** is stable below pH 10, **2** can only be synthesized above pH 11. Hence, it was not possible to experimentally study the reactivity of both complexes at a common pH. Though HAT was found to be the principal rate influencing step for both the complexes (**1a** and **2**), a certain amount of quantum chemical tunnelling was also observed during the H-abstraction in **1a**.²³ Hence, the exact reason for the reactivity difference was not illustrated clearly in our earlier report. This provides the impetus for the current work. We have employed

density functional theory (DFT) based calculations to evaluate the thermodynamics and kinetics that guide the HAT reactions involving the above mentioned complexes. This is significant, as a computational approach with a suitable solvent model yields an ideal common ground for a comparative study that was not possible in the experimental case, due to the pH related complexity mentioned earlier. For high valent metal-oxo moieties, the counteracting roles of the redox potential of the oxo species (E^0) and the basicity of the terminal oxo species, expressed in terms of the pK_a of the protonated oxo moiety (Fe-OH), affects the reactivity involving C-H abstraction reactions.²⁵⁻³¹ These two factors, steering the formation of the H-abstraction transition state (TS), are expressed in terms of the thermodynamic parameter of bond dissociation energy (BDE). These two effects have been further illustrated through the use of the thermodynamic square scheme shown in **Figure 3.1**.

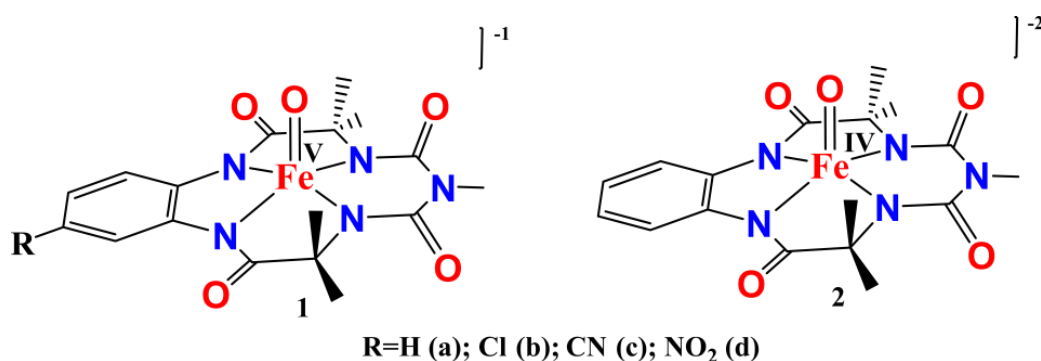


Figure 3.2 Biuret TAML based iron complexes used for this study.

$$\text{BDE}_{\text{Fe}(\text{O})\text{H}} = 1.37 \text{ p}K_a + 23.06 E^0 + C$$

E^0 = $1e^-$ reduction potential of the high valent iron-oxo species and pK_a mentioned here refers to pK_a of the $1e^-$ reduced Fe(O)H species. C is a constant dependent on the solvent.

3.2 Results and Discussion

3.2.1 Effect of overall charge in oxoiron biuret-TAML species

Neese and co-workers have associated the differential HAT reactivity for a series of hypothetical iron oxo and iron nitride complexes (exhibiting varying oxidation states on iron) to the unequal compensation of the mutually opposing electron and proton affinities.³² Also, for explaining the reactivity difference between the oxoiron (V) and oxoiron (IV) biuret-TAML species, it is important to know the pK_a of both Fe^{IV}(OH) and Fe^{III}(OH). Although the Fe^{IV}(OH) pK_a can be experimentally measured (~ 10), it is not possible to experimentally measure the pK_a of Fe^{III}(OH).²³ A significantly high Fe^{III}(OH) pK_a value could well offset the reported higher reactivity of **1a** over

2. Keeping in mind that both the E° and pK_a values are very important constituents in the overall thermodynamics governing a HAT process, we have performed calculations utilizing different density functionals, including the quantitative calculation of the pK_a of Fe^{III} -OH. Thermodynamic calculations suggest a favourable hydrogen abstraction process for **1a** over **2** (Table 3.1).

Table 3.1 Thermochemical free energy analysis for HAT reactions of **1a** and **2** in acetonitrile medium(C-PCM Model) using benzyl alcohol as the substrate. All energies are reported in kcal/mol.

Level of Theory	1a	2
ΔG_{HAT} BP86/TZVP, LANL2DZ (Fe)	0.4	14.1
ΔG_{HAT} PBE/6-31G*, LANL2DZ (Fe)	1.1	16.4
ΔG_{HAT} M06-L/6-31G*, LANL2DZ (Fe)	-3.3	7.9

Calculations confirm that the basicity of $Fe^{III}(O)$ (calculated $pK_a=54.35$, Table 3.3) is indeed not sufficient to compensate for the large redox potential difference between **1a** and **2** ($\Delta E^\circ_{exp}= 0.75$ V, $\Delta E^\circ_{cal}= 1.68$ V) which contributes to a more conducive HAT reaction for **1a**.

Table 3.2 Thermochemical analyses of bTAML complexes (**1a-1d**). Energies are reported in kcal/mol. E° are reported in Volts (V).

Catalyst	E° ($Fe^{V/I}$ V) calc	pK_a (Fe^{IV} - OH) calc	ΔG_{HAT} (BP86/TZVP/LAN L2DZ-Fe)	ΔG_{HAT} (M06-L/6- 31G*/LANL2DZ-Fe)	ΔG_{HAT} (PBE/631G*/LANL2D Z-Fe)
1a	-1.72	18.62	0.41	-3.3	1.07
1b	-1.68	17.83	0.21	-4.4	1.32
1c	-1.60	17.11	0.26	-4.6	2.06
1d	-1.58	16.49	0.41	-4.9	2.09

Table 3.3 Thermochemical analyses of bTAML complexes (**2**). Energies are reported in kcal/mol. E° are reported in Volts (V).

Catalyst	E° (Fe ^{III/I} V) calc	pKa (Fe ^{III} - OH) calc	ΔG_{HAT} (BP86/TZVP/LA NL2DZ-Fe)	ΔG_{HAT} (M06-L/6- 31G*/LANL2DZ-Fe)	ΔG_{HAT} (PBE/6- 31G*/LANL2DZ-Fe)
2	-3.40	54.35	14.1	8.0	16.4

Subsequently, a ~ 7.0 kcal/mol lowering of the HAT activation free energy barrier for **1a** in comparison to **2** (**Table 3.4**) was observed. Computed HAT activation barrier for **1a** (13.9 kcal/mol) without tunnelling correction indicates a minimal tunnelling influence on the HAT reactivity when it was compared to the experimental activation barrier ($\sim 15 \pm 1$ kcal/mol). Apart from this, the higher reactivity of the Cpd I mimics over Cpd II counterparts has also been attributed to the spin state crossover phenomenon.²² Calculated free energy profile shows no spin state crossing en route to the TS for both **1a** and **2** (**Figure 3.3**). This has also been illustrated previously while performing toluene oxidation for **1a**.³³ For **2**, the large triplet-quintet energy gap confines the HAT reaction pathway to a single spin state.²³

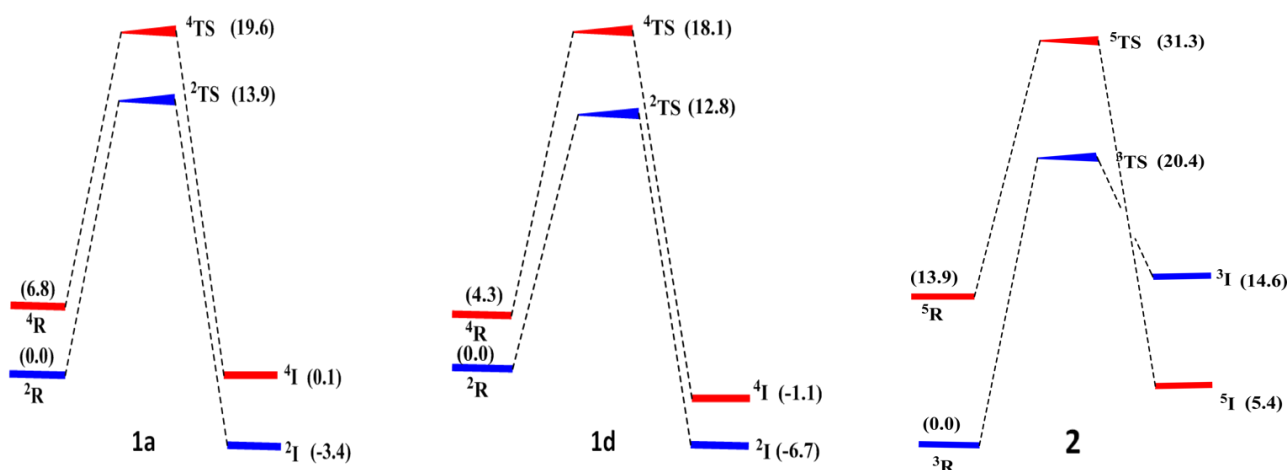


Figure 3.3 Gibb's free energy HAT reactions profile of b-TAML complexes with benzyl alcohol at M06-L/6-311G*/LANL2DZ(Fe)//M06-L/6-311G*/LANL2DZ(Fe),C-PCM (acetonitrile) level of theory.

A closer look into the optimized transition state geometries reveals substantial differences in the bond lengths of the C–H bond in benzyl alcohol, the O–H bond in Fe–OH and the Fe–O bond (**Figure 3.4**). Our calculations suggest significant scission of the C–H bond (1.45 Å) for Fe^{IV}(O), signifying a late transition

state, since the BDE of $\text{Fe}^{\text{III}}\text{O-H}$ and benzyl alcohol is similar. The high basicity of O in $\text{Fe}^{\text{III}}(\text{O})$ in comparison to $\text{Fe}^{\text{IV}}(\text{O})$, as suggested by the weaker and longer $\text{Fe}^{\text{III}}(\text{O})$ bond relative to $\text{Fe}^{\text{IV}}(\text{O})$, leads to significant weakening of the C–H bond in the transition state.

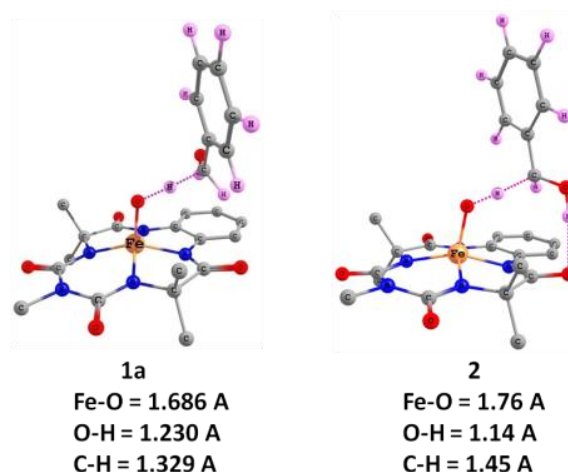


Figure 3.4 Optimized TS geometries of C-H abstraction in benzyl alcohol employing **1a** and **2** at M06-L/6-311G*/LANL2DZ (Fe)/ C-PCM (acetonitrile) level of theory.

Apart from the thermodynamic stabilization of **1a** over **2**, we have also explained their HAT reactivity on the basis of frontier molecular orbital (FMO) theory. Subsequently, the effect of the overall charge of the complex was also investigated. A positive charge is supposed to generate an electrostatic field that would reduce the energies of both the electron acceptor orbital (EAO) and the electron donor orbital (EDO).³⁴⁻³⁷ Additionally, it has been outlined that even slight changes in the EAO-EDO energy gap value can modulate the activation barrier and subsequently alter the HAT reaction rates.³⁸

If in the close structural proximity of the catalyst and the substrate, the overall charge modulates the energies of frontier molecular orbitals (FMOs), i.e., reduces the energy gap between the EDO based on the substrate (benzyl alcohol) and the $\pi^*(d_{xz}^*, d_{yz}^*)$ metal centred EAO, the HAT barrier is lowered. Recently, in order to explain the reactivity difference between Cpd I and Cpd II, the overall effect of the relative charge differences in its mimicking system, $[(4\text{-TMPyP})^+\text{Fe}^{\text{IV}}\text{O}]^{5+}\{4\text{-TMPyP}=5,10,15,20\text{-tetrakis}(\text{N-methyl-4-pyridinium})\text{ porphyrinate}\}$ complex and its one electron reduced analogue has been investigated.¹⁸ The extra positive charge in the porphyrin ligand periphery stabilized both the metal based and the substrate orbitals and thus modulated the EDO-

EAO energy gap. This observation explained the higher HAT reactivity of the poly-cationic Cpd I mimic over its Cpd II counterpart. Therefore, in order to observe analogous charge effects in the purely metal centred high valent oxoiron-bTAML systems (**1a** and **2**), differing only by a net single overall charge (-1 and -2 respectively), we have analyzed the electronic structure of the encounter complex of both **1a** and **2**. The encounter structures analyzed was taken to be such that there would be negligible chance of mixing between EAO and EDO, giving us a reliable model to study charge induced orbital stabilization (**Figure 3.5**). The results show that an extra positive charge on **1a** has a more pronounced effect on the EAOs than EDOs due to the relative differences in proximity from the charge and shielding from the solvent.^{3c} A higher downhill shift of EAO in **1a** lowers the energy gap between EAO and EDO ($\Delta E=1.0$ eV) to a larger extent than in **2** ($\Delta E=1.9$ eV) and hence explains the lowering of the HAT barrier height in **1a**.

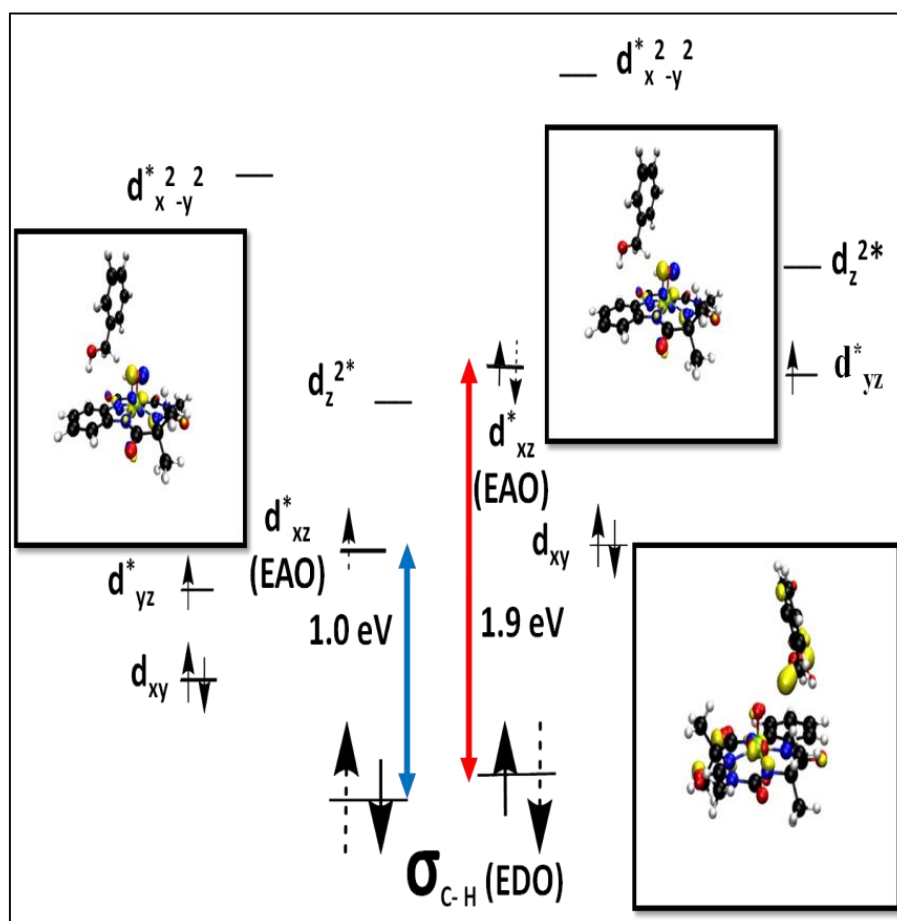


Figure 3.5 Schematic diagram of the key MOs (EDO and EAO) at an O-H distance of 2.0 Å in solution phase of the encounter complexes (the left and right side indicate the MOs of **1a** and **2** respectively) at

BP86/def2-TZVPP, C-PCM (acetonitrile) level of theory. The dotted arrow indicates the trajectory of the electron transfers (π pathway). The MOs of the EAOs and the EDO are provided in the inset.

3.2.2 Effect of ligand substitution

The role of axially substituted donating groups in regulating the pKa value of the high valent iron species in different heme proteins has been studied for various heme containing proteins.^{39,40} Therefore, as in the case with variable oxidation states, looking into ligand structural variation effects on the counter balancing electron and proton transfer processes that regulate the HAT, and the subsequent effect on the overall reaction, is of utmost importance. Previously, experimental analysis in this direction has been performed on a metal hydride species.⁴¹ A ligand promoted electronic perturbation on a copper hydroxide unit has also been reported.⁴² Recently, a similar thermodynamic analysis on the hydrogen abstraction thermodynamics for a superoxo-dicopper complex has also been performed.⁴³ Ligand fields can be tuned to provide an ideal environment for C-H activation.⁴⁴ Recently Ghosh *et.al* has developed a mechanism guided nitro substituted analogue (**1d**) of the previously reported **1a** complex for highly selective C-H bond activation.⁴⁵ Experiment (KIE) has suggested the HAT as the rate determining step. We have, therefore, analysed the four equatorially located phenyl ring substituted bTAML sets that were supposed to perturb the overall electronics on the high valent iron centres in **1(a-d)**, thereby affecting the overall HAT reaction. To this end, we have calculated the thermodynamics facilitating the HAT reactions of the four substituted complexes of the sets of oxoiron (V) complexes using benzyl alcohol as the substrate, by employing different density functionals. This included the theoretical estimation of the pKa and E values (**Table 3.2**), in order to understand the relative displacement of these two aspects that would result out of structural alteration. Theoretical calculations can be a reliable alternative for quantitative estimation of the electrochemical reduction potential (E°) and pKa values; as a means to mitigate various possible inaccuracies in the experimental evaluations.^{46,47} Our calculations show a minimal change in the overall energetics of the HAT reactions across the ligand series, implying a “see-saw” equal and opposite compensation of an unfavourable factor with a favourable one and vice-versa. A ligand with lower electron donating characteristics (like $-\text{NO}_2$) does not stabilize the high valent oxo species well enough, leading to a lower pKa value, but this penalty is equally compensated for by a feasible electrochemical reduction potential (E°). Quantitative calculation of pKa and E° does not exactly coincide with the corresponding

experimental values.²³ However, our approach sheds considerable light upon the underlying principles of the internal processes of HAT.

Table 3.4 The Gibb's free energy activation barrier (ΔG^\ddagger) and free energy change in initial electron transfer ($\Delta G_{E.T}$) or proton transfer ($\Delta G_{P.T}$) for the HAT step, using benzyl alcohol as the substrate for various bTAML complexes that have been investigated at M06-L/6-311G*/LANL2DZ(Fe)//M06-L/6-311G*/LANL2DZ (Fe), C-PCM (acetonitrile) level of theory. All energies are reported in kcal/mol.

Catalyst	ΔG^\ddagger	$\Delta G_{E.T}$	$\Delta G_{P.T}$
1a	13.9	51.5	58.9
1d	12.8	44.5	62.3
2	20.4	117.6	36.0

Despite this internal compensation, the calculated difference in reaction rates across the electronically variable ligand series arises due to the subtle change in the relative barrier heights of the H-abstraction reaction. A thorough thermo-chemical analysis has already shown minimal energy changes on moving across variant substituent (**1a-1d**). However, **1d** exhibits a higher turn-over number (TON) over **1a** in their corresponding HAT reactions.⁴⁵ Calculations reveal a lower hydrogen atom abstraction barrier height for the nitro substituted catalysts (**Table 3.4**) in comparison to the unsubstituted catalysts.

Table 3.5 Relative energies of the EAOs of the reported complexes at BP86/def2-TZVPP,C-PCM (acetonitrile) level of theory. All energies are reported in kcal/mol.

Catalyst	1
a	0.0
b	-1.3
c	-2.9
d	-4.1

Very similar to the case pertaining to **1a** and **2**, axial and equatorial ligand mediated reactivity differences have also been adjudged to be due to the interaction between the EDO and EAO, which therefore also contributes significantly to the driving force of the reaction.⁴⁸⁻⁵⁴ An analysis of the electronic structures of

the **1d** shows relative stabilization of the anti-bonding π^* EAO by almost 4.0 kcal/mol in its free structure, compared to that in **1a** (Table 3.5). The strongly donating tetra-amido framework induces a strong equatorial ligand field, as shown by Mulliken and Natural Population Analysis (NPA) charge estimation (Table 3.6). It reveals that substitution of the phenyl ring by an electron- withdrawing group somewhat reduces electron donation to the iron centre. This, in fact, directly leads to minimization of the anti-bonding interaction between the metal and ligand orbitals and indirectly reduces the electronic charge density on the metal centre, leading to a relative stabilization of the EAO, as a result of the charge effect.

Table 3.6 Mulliken and Natural Population Analysis (NPA) charges of iron in the bTAML complexes (**1a** and **1d**) in acetonitrile medium (C-PCM) at different levels of theory.

Catalyst	Mulliken			NPA	
	M06-L/6-31G*/LANL2DZ-Fe	BP86/TZVP/LANL2DZ-Fe	PBE/6-31G*/LANL2DZ-Fe	M06-L/6-31G*/LANL2DZ-Fe	PBE/6-31G*/LANL2DZ-Fe
1a	0.948	0.613	0.621	0.403	0.243
1d	0.967	0.621	0.639	0.409	0.245

This effectively reduces the energy gap between EDO and EAO. Thus, this fine-tuning of frontier orbital energy induced due to variable electronic environments plays a critical role in reducing the barrier height and thereby explains the decrease in the HAT activation barrier, going from **1a** to **1d**. Furthermore, in all the HAT cases that we have analysed, the question of a stepwise electron transfer/proton transfer (PT/ET) mechanism does not arise. Our calculations indicate a concerted HAT, as the free energy for initial electron or proton transfer ($\Delta G_{E,T}$ and $\Delta G_{P,T}$) is considerably higher than the free energy of activation for hydrogen abstraction in the reported HAT processes (Table 3.4). Thus, the concerted mechanism is a constant phenomenon in all our cases, irrespective of any electronic perturbation.

3.3 Computational Details

All the calculations were done using *Gaussian09* suite of quantum chemical programs.⁵⁵ All the transition states were optimized at the (DFT)-M06-L/6-311G*-LANL2DZ (Fe) level of theory.⁵⁶⁻⁵⁸ M06-L density

functional accounts for the medium-range electron correlation effects⁵⁶ and has proven robust for the modeling of redox non-innocent ligands⁵⁹ and iron spin-state splitting energies,^{60,61} Also, it has been used for the quantum chemical analysis of the mechanism of water oxidation using structurally similar iron-based TAML catalyst.⁶² The zero point vibrational energy corrections and thermal corrections were applied to the “bottom-of-the-well” values to obtain values for the Gibbs free energy at 298.15 K. Solvent effects were added using conductor-like polarizable continuum model (C-PCM) using a dielectric continuum of acetonitrile ($\epsilon=37.6$).^{63,64} M06-L, PBE⁶⁵ and BP86⁶⁶ levels of theory were employed for evaluating the thermo-chemistry involving the HAT reactions. Furthermore, all the pK_a and E^o values were calculated at B3LYP/6-31G*-LANL2DZ (Fe) // B3LYP/6-31G*-LANL2DZ (Fe) level of theory using a dielectric continuum of water ($\epsilon=80.1$) employed via C-PCM solvation model.⁶⁷ For analyzing the electronic structures of our reported complexes, the BP86/def2-TZVPP level of theory was used. This is because this particular functional and basis set combination produces a better spin state ordering and electron distribution, as has been demonstrated by Nam *et al.* before.⁶⁸ Mulliken and natural-population analysis (NPA) atomic partial charges were calculated for mentioned the bTAML catalysts to understand the intramolecular charge distribution. Mulliken charge analysis was done at three different levels of theory in combination of three basis sets to get a better viewpoint. MO images were created from the Gaussian outputs using the VMD software.⁶⁹

3.4 Conclusion

In summary, we have extended the beneficial effect of an extra positive charge on the observed HAT reactivity involving heme based systems to a pair of non-isoelectronic nonheme system. Also, looking at the effect of ligand modulation across a set of bTAML complexes (**1a-1d**), there is negligible change in hydrogen atom transfer (HAT) energetics, due to internal balancing between the pK_a and E^o values. The difference in the HAT activation barriers arises due to modulation of frontier molecular orbitals (FMOs), because of differential electronic environments of the ligand systems. Calculations suggest that FMO energies are more affected by the charge on the system than by ligand modulation. The current work therefore provides a comprehensive, theoretical analysis of the HAT process, and it is expected that the insights gained will aid in the rational design of efficient biomimetic nonheme complexes for C-H abstraction.

3.5 References

1. G. Denisov, T. M. Makris, S. G. Sligar, I. Schlichting, *Chem. Rev.* **2005**, *105*, 2253.

2. L. Que, W. B. Tolman, *Nature*. **2008**, *455*, 333.
3. J. Rittle, M. T. Green, *Science*. **2010**, *330*, 933.
4. J. T. Groves, In *Cytochrome P450: Structure, Mechanism, and Biochemistry*, 3rd ed.; Ortiz de Montellano, P.R., Ed.; *Kluwer-Academic/Plenum: New York*, **2005**, 183.
5. P. R. O de Montellano, *Chem. Rev.* **2010**, *110*, 932.
6. M. Sono, M. P. Roach, E. D. Coulter, J. H. Dawson, *Chem. Rev.* **1996**, *96*, 2841.
7. W. Nam, *Acc. Chem. Res.* **2007**, *40*, 522.
8. J. Hohenberger, K. Ray, K. Meyer, *Nat. Commun.* **2012**, *3*, 720.
9. M. Costas, M. P. Mehn, M. P. Jensen, L. Que, *Chem. Rev.* **2004**, *104*, 939.
10. H. Fujii, *Coord. Chem. Rev.* **2002**, *226*, 51.
11. H.P. Hersleth, U. Ryde, P. Rydberg, C. H. Gorbitz, K. K. J. Andersson, *Inorg. Biochem.* **2006**, *100*, 460.
12. M. Puri, L. Que, *Bull. Jpn. Soc. Coord. Chem.* **2016**, *67*, 10.
13. W. N Oloo, L. Que, *Acc. Chem. Res.* **2015**, *48*, 2612.
14. P. Comba, M. Maurer, P. Vadivelu, *J. Phys. Chem. A.* **2008**, *112*, 13028.
15. W. N. Oloo, R. Banerjee, J. D. Lipscomb, L. Que, *J. Am. Chem. Soc.* **2017**, *139*, 17313.
16. A. Altun, S. Shaik, W. Thiel, *J. Am. Chem. Soc.*, **2007**, *129*, 8978.
17. L. Tahsini, M. Bagherzadeh, W. Nam, S. P de Visser, *Inorg. Chem.* **2009**, *48*, 6661.
18. G. Ricciardi, E. J Baerends, A. Rosa, *ACS Catal.* **2016**, *6*, 568.
19. J.F. Berry, S.D. George, F. Neese, *Phys. Chem. Chem. Phys.* **2008**, *10*, 4361.
20. O. Y. Lyakin, K. P. Bryliakov, E. Talsi, *Inorg. Chem.* **2011**, *50*, 5526.
21. W. N. Oloo, Y. Feng, S. Iyer, S. Parmelee, G. Xue, L. Que, *New J. Chem.* **2013**, *37*, 3411.
22. S. R Bell, J. T. Groves, *J. Am. Chem. Soc.* **2009**, *131*, 9640.
23. S. Pattanayak, A. Jasniowski, A. Rana, A. Draksharapu, K.K. Singh, A. Weitz, M. Hendrich, L. Que, A. Dey, S. Sen Gupta, *Inorg. Chem.* **2017**, *56*, 6352.
24. M. Ghosh, K. K. Singh, C. Panda, A. Weitz, M. P. Hendrich, T. J. Collins, B. B. Dhar, S. Sen Gupta, *J. Am. Chem. Soc.* **2014**, *136*, 9524.
25. A. S. Borovik, *Chem. Soc. Rev.* **2011**, *40*, 1870.
26. J. J. Warren, T. A. Tronic, J. M. Mayer, *Chem. Rev.* **2010**, *110*, 6961.
27. D. Dhar, W. B. Tolman, *J. Am. Chem. Soc.* **2015**, *137*, 1322.
28. J. M. Mayer, I. J. Rhile, *Biochim. Biophys. Acta, Bioenerg.* **2004**, *1655*, 51.
29. J. M. Mayer, *Annu. Rev. Phys. Chem.* **2004**, *55*, 363.

30. F. G. Bordwell, J. P. Cheng, J. A. Jr Harrelson, *J. Am. Chem. Soc.* **1988**, *110*, 1229.
31. J. M. Mayer, *Acc. Chem. Res.* **2011**, *44*, 36.
32. C. Geng, S. Ye, F. Neese, *Dalton Trans.* **2014**, *43*, 6079.
33. K. K. Singh, M. K. Tiwari, B. B. Dhar, M. Ghosh, C. Panda, A. Weitz, M. P. Hendrich, B. B. Dhar, K. Vanka, S. Sen Gupta, *Inorg. Chem.* **2015**, *54*, 1535.
34. L. Bernasconi, E. J. Baerends, *Eur. J. Inorg. Chem.* **2008**, *10*, 1672.
35. L. Bernasconi, E. J. Baerends, *J. Am. Chem. Soc.* **2013**, *135*, 8857.
36. A. Kazaryan, E. J. Baerends, *ACS Catal.* **2015**, *5*, 1475.
37. P. C. Andrikopoulos, C. Michel, S. Chouzier, P. Sautet, *ACS Catal.* **2015**, *5*, 2490.
38. S. Ye, C.Y. Geng, S. Shaik, F. Neese, *Phys. Chem. Chem. Phys.* **2013**, *15*, 8017.
39. T. H. Yosca, J. Rittle, C. M. Krest, E. L. Onderko, A. Silakov, J. C. Calixto, R. K. Behan, M. T. Green, *Science.* **2013**, *342*, 825.
40. T.H. Yosca, R.K. Behan, C.M. Krest, E. L. Onderko, M. C. Langston, M.T. Green, *J. Am. Chem. Soc.* **2014**, *136*, 9124.
41. Tilset. M. In: *Electron Transfer in Chemistry*; Balzani. V; editor. WILEY-VCH Verlag GmbH: Weinheim, Germany, 2001; 677.
42. D. Dhar , G.M. Yee, A. D. Spaeth, D.W. Boyce, H. Zhang, B. Dereli, C. J. Cramer, W. B. Tolman, *J. Am. Chem. Soc.* **2016**, *138*, 356.
43. N. Kindermann, C.J. Gunes, S. Dechert, F. Meyer, *J. Am. Chem. Soc.* **2017**, *139*, 9831.
44. L. Bernasconi, M. J. Louwarse, E. J. Baerends, *Eur. J. Inorg. Chem.* **2007**, *19*, 3023.
45. M. Ghosh, S. Pattanayak, B. B. Dhar, K. K. Singh, C. Panda, S. Sen Gupta, *Inorg. Chem.* **2017**, *56*, 10852.
46. A.V. Marenich, J. Ho, M. L. Coote, C. J. Cramer, D. G. Truhlar, *Phys. Chem. Chem. Phys.* **2014**, *16*, 15068.
47. B. Thapa, H. B. Schlegel, *J. Phys. Chem. A.* **2016**, *120*, 5726.
48. S. Shaik, W. Lai, H. Chen, Y. Wang, *Acc. Chem. Res.* **2010**, *43*, 1154.
49. W. Lai, C. Li, H. Chen, S. Shaik, *Angew. Chem. Int. Ed.*, **2012**, *51*, 5556.
50. J. C. Schoneboom, S. Cohen, H. Lin, S. Shaik, W. Thiel, *J. Am. Chem. Soc.*, **2004**, *126*, 4017.
51. R. Latifi, M. Bagherzadeh, S. P. de Visser, *Chem. Eur. J.* **2009**, *15*, 6651.
52. L. W. Chung, X. Li, H. Hirao, K. Morokuma, *J. Am. Chem. Soc.* 2011, **133**, 20076.
53. P. K. Das, S. Chatterjee, S. Samanta, A. Dey, *Inorg. Chem.* 2012, **51**, 10704.
54. C.Y. Geng, S. Ye, F. Neese, *Angew. Chem. Int. Ed.* **2010**, *49*, 5717.

55. M. J. Frisch, G. W. Trucks, H. B. Schlegel, G. E. Scuseria, M. A. Robb, J. R. Cheeseman, G. Scalmani, V. Barone, B. Mennucci, G. A. Petersson, H. Nakatsuji, M. Caricato, X. Li, H. P. Hratchian, A. F. Izmaylov, J. Bloino, G. Zheng, J. L. Sonnenberg, M. Hada, M. Ehara, K. Toyota, R. Fukuda, J. Hasegawa, M. Ishida, T. Nakajima, Y. Honda, O. Kitao, H. Nakai, T. Vreven, J. A., Jr. Montgomery, J. E. Peralta, F. Ogliaro, M. Bearpark, J. J. Heyd, E. Brothers, K. N. Kudin, V. N. Staroverov, R. Kobayashi, J. Normand, K. Raghavachari, A. Rendell, J. C. Burant, S. S. Iyengar, J. Tomasi, M. Cossi, N. Rega, J. M. Millam, M. Klene, J. E. Knox, J. B. Cross, V. Bakken, C. Adamo, J. Jaramillo, R. Gomperts, R. E. Stratmann, O. Yazyev, A. J. Austin, R. Cammi, C. Pomelli, J. W. Ochterski, R. L. Martin, K. Morokuma, V. G. Zakrzewski, G. A. Voth, P. Salvador, J. J. Dannenberg, S. Dapprich, A. D. Daniels, Ö. Farkas, J. B. Foresman, J. V. Ortiz, J. Cioslowski, D. J. Fox, *Gaussian 09*, revision B.01; Gaussian, Inc.: Wallingford, CT, **2009**.
56. Y. Zhao, D. G. Truhlar, *J. Chem. Phys.* **2006**, *125*, 194101.
57. Y. Zhao, D. G. Truhlar, *Acc. Chem. Res.* **2008**, *41*, 157.
58. Y. Zhao, D. G. Truhlar, *Theor. Chem. Acc.* **2007**, *120*, 215.
59. P. Milko, M.A. Iron, *J. Chem, Theory. Comput.* **2014**, *10*, 220.
60. a) K. R. Delle. Chiaie, A. B. Biernesser, M. A. Ortuno, B. Dereli, D. Iovon, M. J. T. Wilding, B. Li, C. J. Cramer, J. A. Byers. *Dalton. Trans.*, **2017**, *46*, 12971; b) M. A. Ortuno, B. Dereli, Delle.Chiaie, A, B Biernesser, M. Qi, J. A. Byers, C. J. Cramer, *Inorg. Chem.* **2018**, *57*, 2064.
61. a) M. Swat, *Chem. Phys. Lett.* **2013**, *580*, 166. b) T. R. Rensen, J. R. Nitschke, L. Gagliardi, C.J Cramer, *Phys. Chem. Chem. Phys.* **2014**, *16*, 10620. c) P. Verma, Z. Varga, J. E. M. N. Klein, C. J. Cramer, L. Que. Jr, D.G. Truhlar, *Phys. Chem. Chem. Phys.*, **2017**, *19*, 13049.
62. Z. Ertem, L. Gagliardi, C. J. Cramer, *Chem. Sci.* **2012**, *3*, 1293.
63. V. Barone, M. Cossi, *J. Phys. Chem. A.* **1998**, *102*, 1995.
64. M. Cossi, N. Rega, G. Scalmani, V. Barone, *J. Comput. Chem.* **2003**, *24*, 669.
65. J.P. Perdew, K. Burke, M. Ernzerhof, *Phys. Rev. Lett.* **1997**, *78*, 1396.
66. A.D Becke, *Phy. Rev. A.* **1988**, *38*, 3098.
67. a) J. P. Perdew, S. H. Chevary, K. A. Vosko, K. A. Jackson, M. R. Pederson, D. J Singh, C. Fiolhais, *Phys. Rev. B.* **1992**, *46*, 6671; b) J. P. Perdew, S. H. Chevary, K. A. Vosko, K. A. Jackson, M. R. Pederson, D. J. Singh, C. Fiolhais, *Phys. Rev. B.* **1993**, *48*, 4978; c) J. P. Perdew, K. Burke, Y. Wang, *Phys. Rev. B.*, **1996**, *54*, 16533; d) C. Adamo, V. Barone, *J. Chem. Phys.* 1998, *108*, 664; e) A. D Becke, *J. Chem. Phys.* **1993**, *98*, 5648; f) C. Lee, W. Yang, R. G. Parr, *Phys. Rev. B.* **1988**, *37*,

- 785; g) C. C. Roothan, *J. Rev. Mod. Phys.* **1960**, 3, 179; h) R. McWeeny, G. Dierksen, *J. Chem. Phys.* **1968**, 49, 4852; i) J. A. Pople, R. K. Nesbet, *J. Chem. Phys.* **1954**, 22, 571.
68. S. Hong, S. Jang, K.B. Cho, W. Nam, *Chem. Commun.* **2016**, 52, 12968.
69. W. Humphrey, A. Dalke, K. Schulten, *J. Mol. Graphics.* **1996**, 14, 33.

Chapter 4: Unraveling the role of counter anions in “Ge(II) inside a Molecular Cage” Systems

Chapter 4

Unraveling the role of counter anions in “Ge(II) inside a Molecular Cage” Systems

Abstract

The current work showcases general principles at play in systems consisting of Ge(II) dication present inside molecular cages. The very fact that such compounds exist appears highly unlikely, given the highly reactive nature of the Ge(II) dication. Our studies reveal what really occurs in solution when such complexes are formed: the Ge(II) dications are actually present as $[\text{Ge-X}]^+$ (where X is the “non-coordinating” counterion employed in such systems) during entry and subsequent existence at the center of the cage. Hence, what is actually present is a “pseudo monocation” that the experimentalists have completely missed detecting it.

4.1 Introduction

In chemistry, low oxidation state cations and di-cations of heavier group 13 and 14 elements have received a significant amount of attention in recent years.¹Of these, the most interesting family consists of single, isolated charged species surrounded by a cage, with no covalent interactions between the central cation and the surrounding cage. The genesis of this field lies in the discovery of the Ge(II)-cryptand system by Baines and co-workers in 2008.²The Ge(II) center is encapsulated within the cryptand and assumed to be stabilized by numerous weak donor–acceptor interactions due to the presence of six oxygen and two nitrogen atoms in the cavity. Following their discovery, many more such complexes have been reported, with various ligands acting as support to the central Ge(II) cation and possessing the same property as described before (Complexes 1-4, **Figure 4.1**). These include [12]-crown-4 and [18]-crown-6.^{3,4}Related compounds with tacn (1,4,7-triazacyclononane) and cyclam (1,4,8,11-tetramethyl-1,4,8,11-tetraazacyclotetradecane) ligands have also been reported (Figure 1).⁴Moreover, the field has further expanded to include other group 13 and 14 elements.¹In these systems (1-4), the primary interaction between the Ge(II) center and donor atoms (N and O) is primarily non-covalent electrostatic, as had been pointed out in the original report by Baines and co-workers² and also experimentally confirmed by the same group.⁵ This is quite interesting, since the central germanium has a single filled orbital and three empty orbitals, thereby making it a highly reactive species. So why does it stay isolated at the center of the cage, interacting only through electrostatic means with the atoms of the cage and forgoing almost any covalent interactions altogether? An even more interesting question pertains to the general expectation that had been observed about these systems when they were first reported nearly twelve years back: that they could be employed as the starting point for various synthetic routes, because of the ready availability of a highly reactive naked germanium dication that could be subjected to remote bond activation reactions on a variety of substrates.⁶Such an expectation has not been realized. This is not because of steric constraints, because the encapsulating cage provides ample space for the approach and departure of substrates. So, why the absence of any such chemistry for these set of compounds? A further question that indeed needs asking is the apparent ease by which such compounds have been reported to have formed. Most reports state a very high yield for these complexes.^{2,3,4}How does this come about?

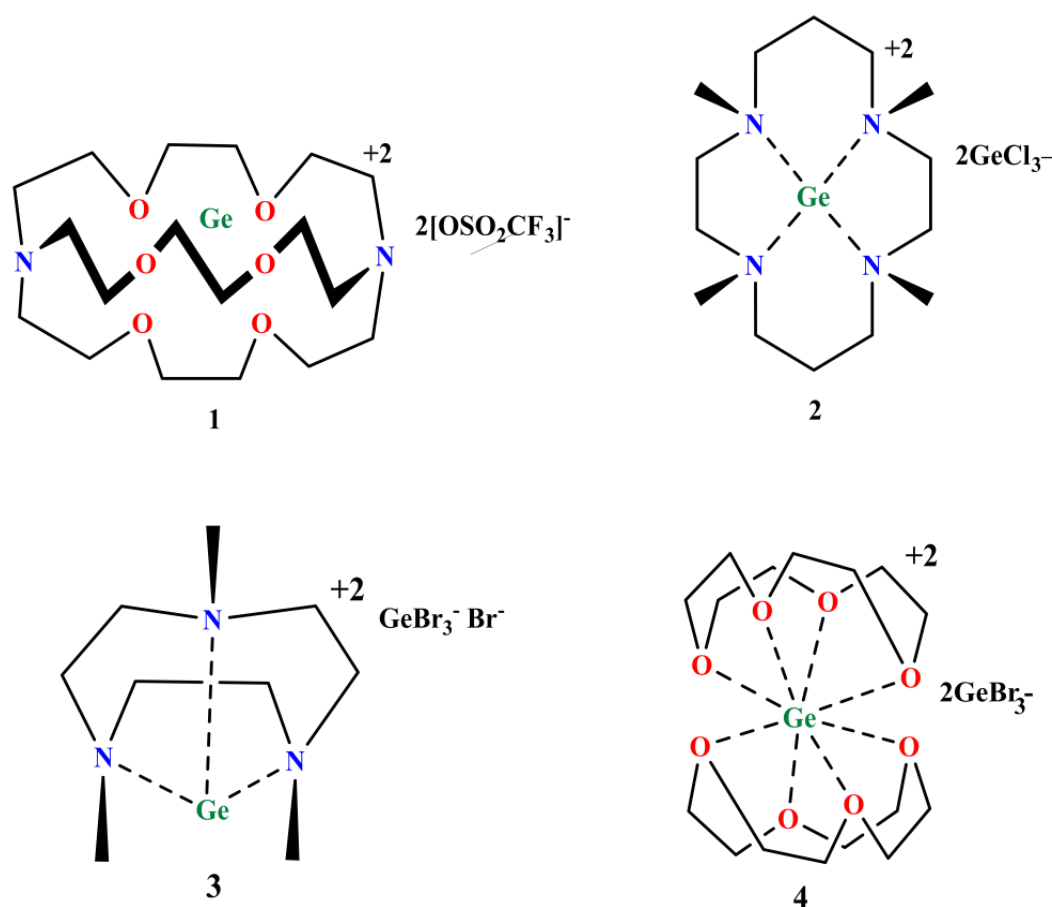


Figure 4.1 Cryptand and crown ether stabilized Ge(II) with their counter anions, as isolated in the crystal structure.

If the germanium dication were to enter unassisted into the cage, it would come into close proximity with the cage atoms while doing so, and this would lead to chemical interactions between the highly unsaturated germanium center and the cage atoms, which should result in the destruction of the cage. Indeed, as we will demonstrate in the Results and Discussion section, room temperature ab initio molecular dynamics (AIMD) simulations indicate that such decomposition reactions would occur in a matter of picoseconds. In other words, systems that show a naked germanium cation sitting unassisted in the center of a cage (Complexes 1-4, **Figure 4.1**) should have been difficult to synthesize and should have only been formed in low yields, if at all. And yet they are formed in very high yields. What accounts for this?

The current computational study, with high level static density functional theory (DFT), as well as AIMD simulations, seeks to address these issues, focusing on the compounds **1-4**. What is revealed is the hidden role played by the counterions: it is seen that the counterions facilitate the entry of such caged dications inside their encapsulating cages and ensure their subsequent stability. This insight is useful, because it then

allows us to understand how one could employ strategies to make the group 14 dications exist in isolation at the center of the cage, thereby opening up the possibility of further synthetic transformation of potential substrates at the cationic centers.

4.2 Methods

All the DFT calculations were carried out using the *Gaussian 09* suite of quantum-chemical programs.⁷ All Ge(II) complex geometries were optimized at the M06-2X/6-311G (d, p) level of theory.⁸ Frequency calculations on all the stationary points were carried out to characterize the nature of each stationary point and also to evaluate the respective molecular entropic terms. The solvent effect was added through the Conductor-like Polarization Continuum Model (C-PCM) using the actual solvent as used for all the Ge(II) complexes geometries considered.^{9,10} NBO charges have been used to calculate the net electrostatic force on the dicationic germanium center.¹¹ All the Wiberg bond indices (WBI) reported are the maximum values reported between Ge(II) and the heteroatoms (N, O and S), i.e., if there are four Ge(II)-O interactions, for instance, in a particular cage the WBI indicating the greatest interaction has been reported.

The binding energies of the all the Ge(II) complexes described in this work were calculated as follows:

$$\Delta G (\text{Binding}) = G_{\text{Ge(II)cage}} - G_{\text{cage}} - G_{\text{Ge(II)}}$$

The net force on the Ge(II) was calculated using Coulomb's law where the electrostatic force is given by:

$$F_{\text{electrostatic}} = (1/4\pi\epsilon) * (q_{\text{Ge(II)}}q_{\text{atom}}) / (r_{\text{Ge(II)-atom distance}})^2$$

where, $q_{\text{Ge(II)}}$ = charge on the Ge(II) atom, q_{atom} = charge on other atoms, $r_{\text{Ge(II)-atom distance}}$ = distance and ϵ = dielectric constant for the respective solvents between Ge(II) and other atoms. The charge was assigned from the NBO charge analysis. A vector summation was done at the Ge(II) center in order to determine the net electrostatic force at the Ge(II) due to the presence of the cage atoms. Likewise the electrostatic energy was calculated from:

$$E_{\text{electrostatic}} = (1/4\pi\epsilon) * (q_{\text{Ge(II)}}q_{\text{atom}}) / (r_{\text{Ge(II)-atom distance}})$$

The code to calculate the force and the energy was written in the Python Language.

Isotropic NMR shielding tensors were calculated at the M06-2X/6-311G (d, p) level of theory in *Gaussian 09* using the gauge-independent atomic orbital (GIAO) method.¹² The ab initio molecular dynamics (AIMD) simulations were performed with the *TeraChem 1.9* quantum chemistry and AIMD software packages,¹³⁻¹⁹

using the B3LYP density functional²⁰ and the def2-SVP basis set to calculate the Born–Oppenheimer potential energy surface. A different functional is employed when using the *TeraChem* software because the M06-2X functional has not been implemented in this suite of softwares. A slightly lower quality basis set has been employed in this case keeping the computational expense of the full quantum chemical molecular dynamics simulations in mind. The equations of motion were integrated numerically using Langevin dynamics with an equilibrium temperature of 300 K (also the starting temperature). The electronic state of the germanium dication was considered to be a singlet, or a closed shell configuration, in the AIMD simulations. Also, all our static DFT calculations have been done considering the singlet germanium dication as the ground state. The triplet state requires the excitation of one electron from the 4s orbital to the 4p orbital. Since the energy gap between 4s and 4p is considerably large, the former phenomenon should be highly unfeasible. Hence, this should make any involvement of triplet electronic state highly unfavourable. Non-covalent interaction (NCI) regions have been plotted using the *nciplot-3.0* suite of programs.²¹

4.3 Results and Discussion

As discussed in the Introduction, it is expected that there exist only non-covalent electrostatic interactions between the Ge(II) dication and the encapsulating cage in the considered cases 1-4 (see Figure 1).

Table 4.1 Different parameters associated with the reported Ge(II) complexes (1-4). The reported values are for the cationic fragment of the complex.

Compound	Solvent	NPA Charge on Ge(II) center	Wiberg Bond Index (WBI)	% of s character in Ge(II) center
1	tetrahydrofuran	1.5	0.0901 (O)	97.9
2	dichloromethane	1.4	0.2105 (N)	89.9
3	acetonitrile	1.4	0.3100 (N)	87.3
4	acetonitrile	1.6	0.0769 (O)	99.5

This has been verified: for the cases 1-4, an almost 100.0% 4s orbital with minimal orbital mixing was obtained by natural bond orbital (NBO) analysis (**Table 4.1**), and the plotting of non-covalent interactions

(NCI) for these systems (1-4) exemplifies (**Figure 4.2**) the fact that the electrostatic interaction is the primary factor between the molecular cages and their cationic hosts.

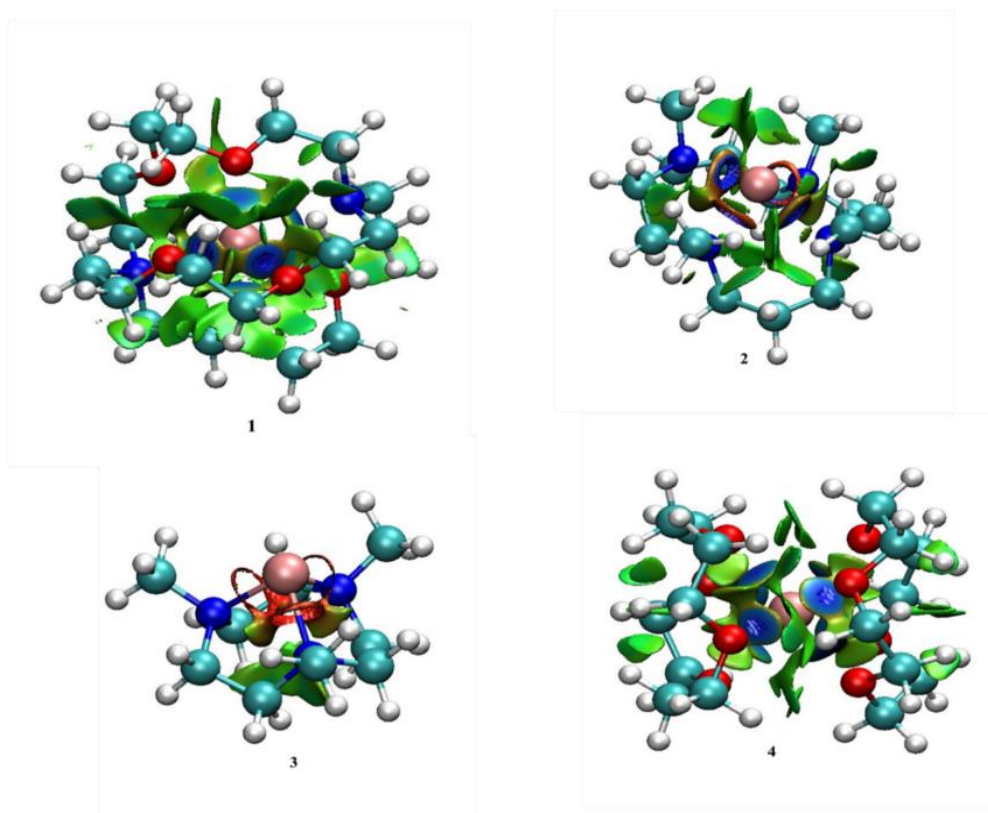


Figure 4.2 Noncovalent interaction (NCI) plot for Ge(II) complexes (1-4) illustrating the non-covalent electrostatic interaction between the germanium dication and the heteroatoms of the molecular cage. The green, blue and red regions respectively represent attractive, strongly attractive and repulsive interactions. Colour scheme: germanium = pink, oxygen = red, carbon = sky blue, nitrogen = blue and hydrogen= white.

Hence, as discussed in the Introduction, we have first attempted to understand whether the germanium dication could enter unassisted into the cages (1-4) and stay stabilized. To this end, we have employed ab initio molecular dynamics (AIMD) simulations. What was first investigated were AIMD simulations where the bare Ge(II) dication was kept on the outside of the cage and a counterion was located on the opposite side. The simulations were done for the Cases 1-4 discussed in the Introduction. For every case, a boundary radius of 9.0 Å was employed, in order to ensure that the Ge(II) dication did not fly away from the cage altogether during the AIMD simulations, a phenomenon known as the “evaporation” event. **Figure 4.3** and **4.4** below, showing snapshots of the results for Case 1, are very revealing. It is seen that in the absence of coordination to the counterion, the

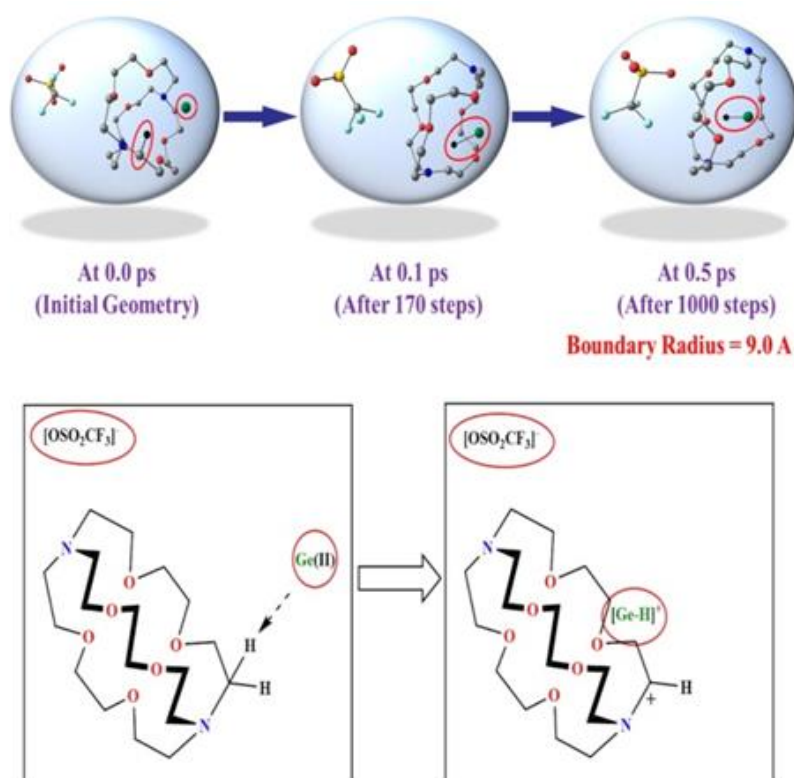


Figure 4.3 Snapshots depicting the trajectory of ab initio molecular dynamics (AIMD) simulations done for Case 1, where the Ge(II) and the counter anion, $[\text{OSO}_2\text{CF}_3]^-$, remain unattached. A red circle encloses the Ge(II) as well as the H atom abstracted by it during the course of the simulation. Colour scheme: germanium = deep green, oxygen = red, carbon = gray, hydrogen = black, nitrogen = blue, sulphur = yellow and fluorine = sky blue. Hydrogen atoms not pertinent to the reaction have been removed for clarity.

Ge(II) dication begins interacting with the cage, extracting a hydrogen (as hydride) from it and thus initiating the process of destroying it (see **Figure 4.3**). The fact that the H-abstraction happens as a hydride anion and not as a H-radical is proved by the net NPA charge of the $[\text{Ge-H}]^+$ moiety. A net NPA charge of 0.69 in the complex proves that the $[\text{Ge-H}]^+$ moiety is a monocationic species. This occurs after only a short time has elapsed in the course of the AIMD simulations. Though **Figure 4.3** shows this decomposition process for the original Baines system, Ge(II) with triflate ($\text{C}_{20}\text{H}_{36}\text{F}_6\text{GeN}_2\text{O}_{12}\text{S}_2$) and the cryptand cage, the same was seen to occur for all the other cases 2-4 as well. The corresponding figures for Cases 2-4 have been shown in **Figure 4.4**. The AIMD simulations therefore makes clear that that if the Ge(II) dication were to enter the cage in a naked, unassisted fashion, its reactive nature, as evidenced by its three empty orbitals and unsaturation, would lead to unwanted side reactions and cage decomposition. However, as mentioned earlier, very high yields have been reported for the formation of the encapsulated Ge(II)

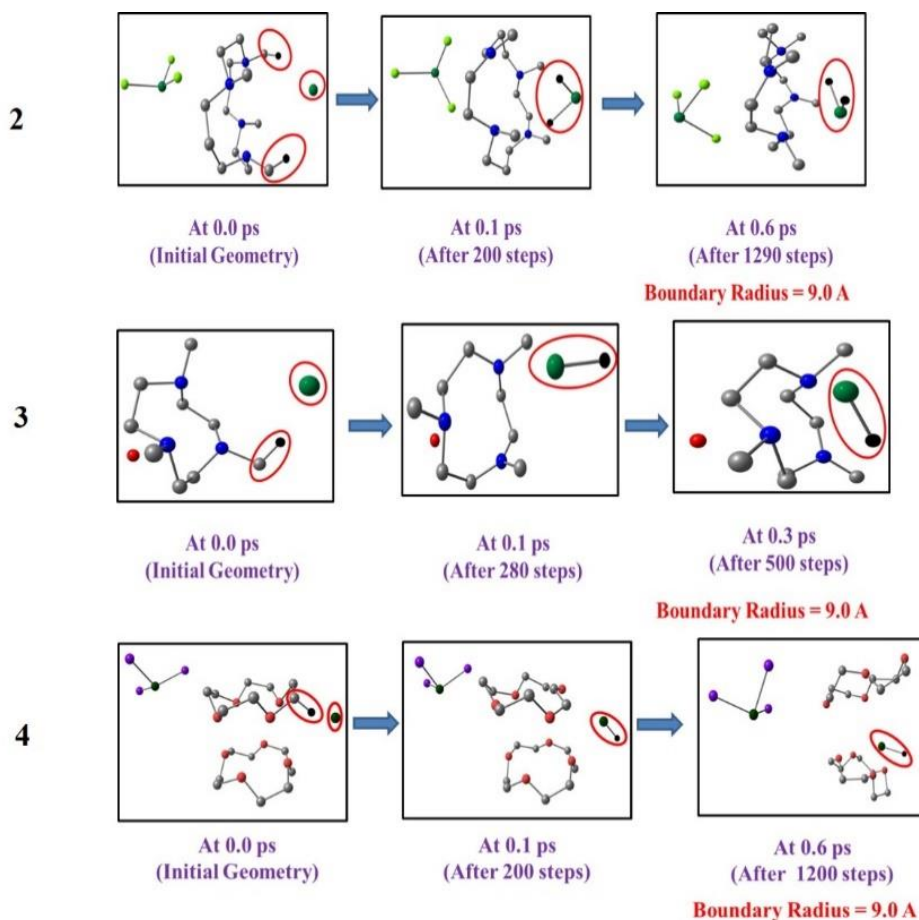


Figure 4.4 Snapshots depicting the trajectory of ab initio molecular dynamics (AIMD) simulations done for Cases 2, 3 and 4 where the Ge(II) and their respective counter anion remain unattached. A red circle encloses the Ge(II) as well as the H atom abstracted by it during the course of the simulation. Colour scheme: germanium = deep green, oxygen = red, carbon = gray, hydrogen = black, nitrogen = blue and violet = bromine. Hydrogen atoms not pertinent to the reaction have been removed for clarity.

systems, which suggests that such side reactions are completely absent during the formation of the caged Ge(II) compounds. In order to explain this apparent contradiction, we hypothesized that the reactive behavior of the Ge(II) dication could be reduced if it were to be coordinated with one of the counterions present in solution when it approached the cage. In order to test this hypothesis, AIMD simulations were done for all the cases Case (1-4), with the Ge(II) dication associated with the corresponding counterion in each case, and kept as before at the vicinity of the cage. The results are shown for Case 1 in **Figure 4.5**, and for Cases 2, 3 and 4 in **Figure 4.6**. Interestingly, what was seen now is that, for every case, the Ge(II)-counterion entered without interacting with the cage, and settled at the center. Hence, what the results indicate is that the reactivity of the Ge(II) dication is tamed by

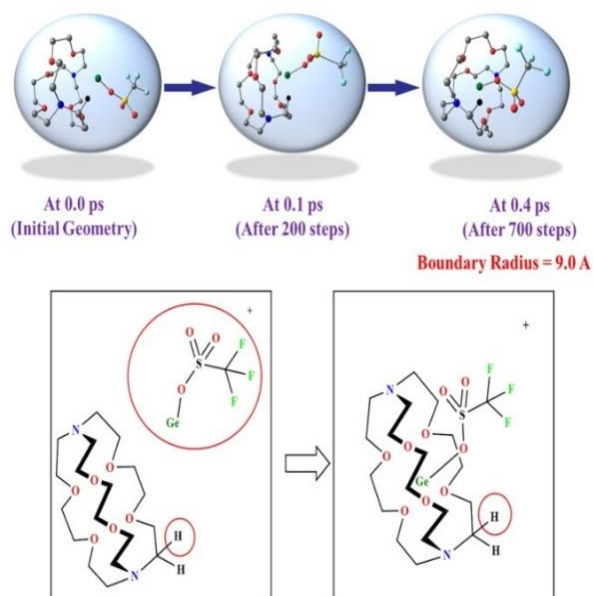


Figure 4.5 Snapshots depicting the trajectory of AIMD simulations for Case 1, where Ge(II) and the counter anion ($-\text{OSO}_2\text{CF}_3$) remain attached. Colour scheme: germanium = deep green, oxygen = red, carbon = gray, hydrogen = black, nitrogen = blue, sulphur = yellow and fluorine = sky blue. Hydrogen atoms not pertinent to the reaction have been removed for clarity.

the presence of a counterion, and this not only stops unwanted side reactions from taking place, but also ensures that the Ge(II) dication enters into the cage and settles at its center. For Case 4, an interesting deviation was observed. The counter anion (GeBr_3^- in this case) ferries the dicationic germanium into the sandwich crown ether cage during the course of the simulations, as was done by the other counterions for the other cases.

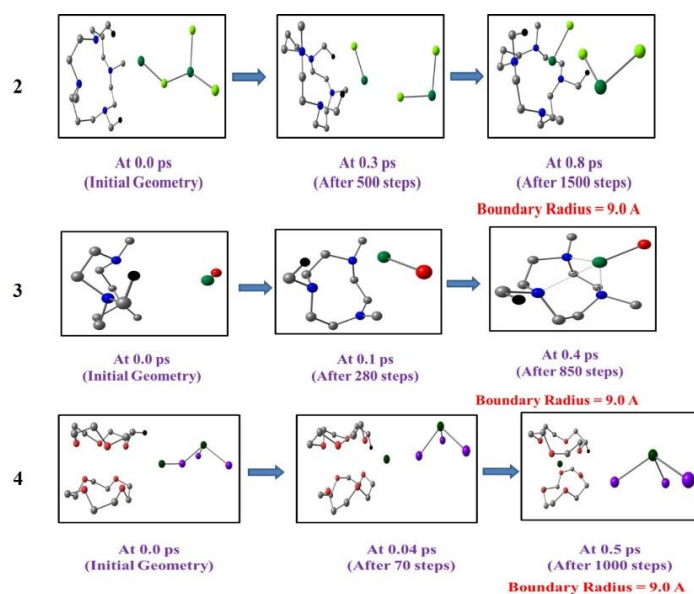


Figure 4.6 Snapshots depicting the trajectory of ab initio molecular dynamics (AIMD) simulations done for Cases 2, 3 and 4 where the Ge(II) and their respective counter anion remain attached. Colour scheme: germanium = deep green, oxygen = red, carbon = gray, hydrogen = black, nitrogen = blue and violet = bromine. Hydrogen atoms not pertinent to the reaction have been removed for clarity.

However, the counter anion does not itself enter the cage in this case. What happens instead is that one of the two crown ether moieties that make up the cage reorients itself to accommodate the Ge(II) (see **Figure 4.6**). This is an exception to the other cases where the counter anion enters into the cage along with the Ge(II).

For all the other three cases (1-3), AIMD simulations show that the counter anion remains coordinated to the Ge(II) even after its entry into the cage. The reason for this becomes clear from static DFT calculations, which show that the $[\text{Ge(II)-counter anion}]^+$ species inside the cage represents a stable structure. Indeed, it is seen that this complex is more stable than the corresponding system where the counter anion is stationed as a non-coordinating species at a much greater distance (see **Table 4.2** and **Figure 4.7** in the ESI).

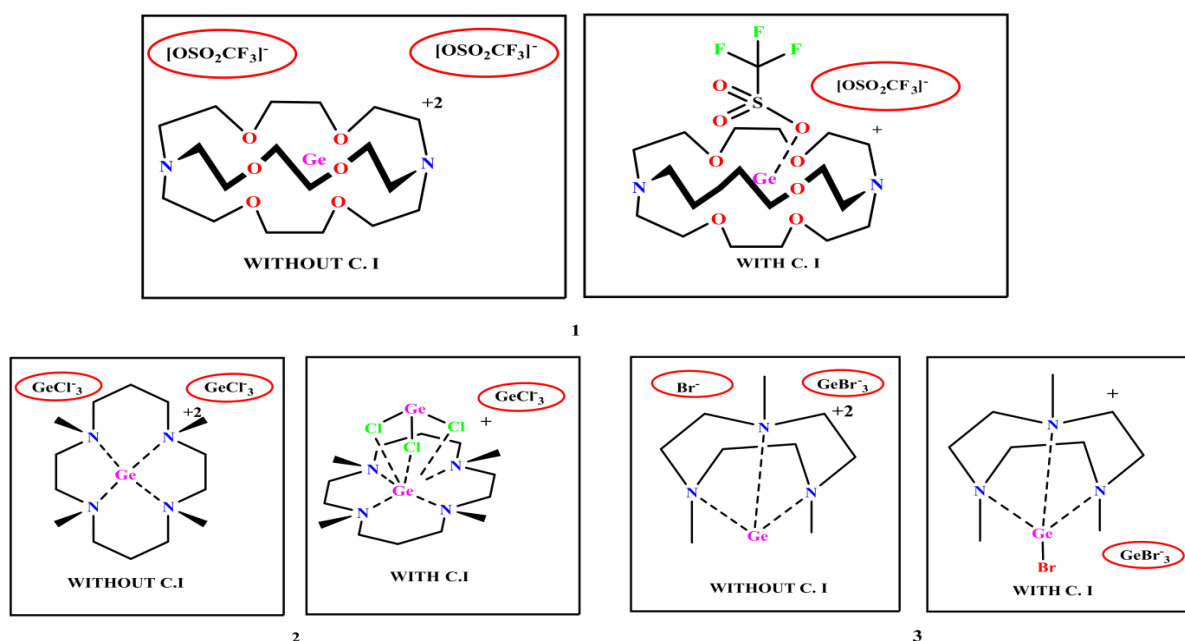


Figure 4.7 Geometries of free and counter anion bound crown ether and cryptand complexes (**1, 2, 3**) of Ge(II), optimized at the M06-2X/ 6-311G (d, p) level of theory.

This was observed for all the cases considered, with the exception of Case 4, where the counter anion (GeBr_3^-) left the Ge(II) dication center during the optimization process (**Figure 4.8**). (For Case 2, the Ge(II) - counter anion distance is $\sim 3.70 \text{ \AA}$, but this still represents a much

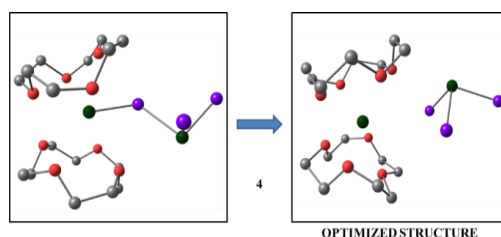


Figure 4.8 Geometry optimization trajectory of counter anion binding in Case 4. Colour scheme: germanium = deep green, oxygen = red, carbon = gray and bromine = violet. Hydrogen atoms not pertinent to the reaction have been removed for clarity.

closer distance than in the crystal structure). This result thus explains why the counter anion remains with the dication for cases 1-3 in the AIMD simulations, and also why the counter anion completely detaches from the Ge(II) cation after thrusting it into the molecular cage in Case 4. Therefore, in almost all the cases considered, the calculations indicate that the counterion stays in the proximity of the Ge(II) dication in solution. This is significant, because it reveals that the reality in solution is far removed from what is observed from the reported crystal structures. This also helps to explain perhaps why the systems are so stable and have been reported in high yields.

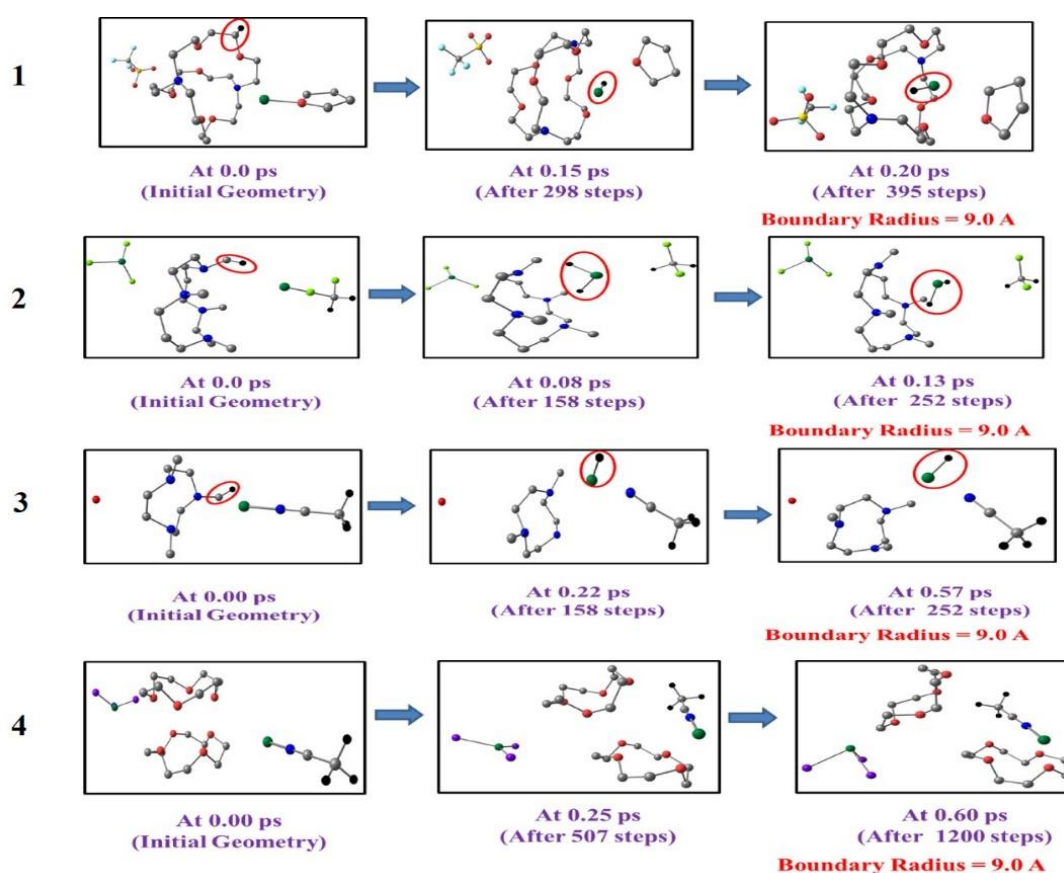


Figure 4.9 Snapshots depicting the trajectory of ab initio molecular dynamics (AIMD) simulations done for Cases 1, 2, 3 and 4 where the Ge(II) and their respective counter anion remain attached. Colour scheme: germanium = deep green, oxygen = red, carbon = gray, hydrogen = black, nitrogen = blue, yellow = sulphur, sky blue = fluorine and violet = bromine. Hydrogen atoms not pertinent to the reaction have been removed for clarity.

Furthermore, we have examined whether a similar phenomenon occurs when the Ge(II) dication is attached to the heteroatom of their respective solvents in which they were synthesized (similar to the case described earlier when the counter anion was attached to the dicationic germanium center). AIMD calculations have been carried out on each of the complexes (1-4). For every case, a similar boundary radius of 9.0 Å as imposed earlier was employed and the respective counter anions were placed unattached at a large distance apart from the Ge(II)-explicit solvent adduct centers (see **Figure 4.9**). Simulations illustrate that the Ge(II) destroys the cage by abstracting a hydride from the cage in all the complexes (see **Figure 4.9**), except in 4, where, earlier we had shown that the dication was unattached to the counter anion. For 4, though the dication does not destroy the cage as in previous cases (1-3), it forms a distorted structure which is geometrically different from the experimentally isolated structure (**Figure 4.9**). Hence, the presence of an explicit solvent molecule does not play a beneficial role that the counter anions display in stabilizing the dications inside the cages.

Table 4.2 Thermodynamic parameters of counterion binding of the respective counter anions in solution, at the M06-2X/6-311G (d, p) // M06-2X/6-311G (d, p) level of theory.

Molecule	Solvent	ΔG (kcal/mol)	Counter ion (C.I)
1	tetrahydrofuran	-8.8	OTf ⁻
2	dichloromethane	-4.2	GeCl ₃ ⁻
3	acetonitrile	-7.9	Br ⁻

A further important point that needs to be made here pertains to ^{19}F -NMR data that has been reported by Baines and co-workers for Case 1.5. When ^{19}F -NMR was done for this system, a single resonance signal akin to a triflate anion was obtained.² This would suggest that the triflate anion remains in a dissociated form outside the cage away from the Ge(II) dication, thus reinforcing the crystal structure orientation of the counterion and contradicting our current results. In order to investigate this seeming discrepancy, we have done ^{19}F -NMR DFT calculations to determine the shifts with the counterion (i) bound as well as (ii) not bound to the Ge(II) dication center.

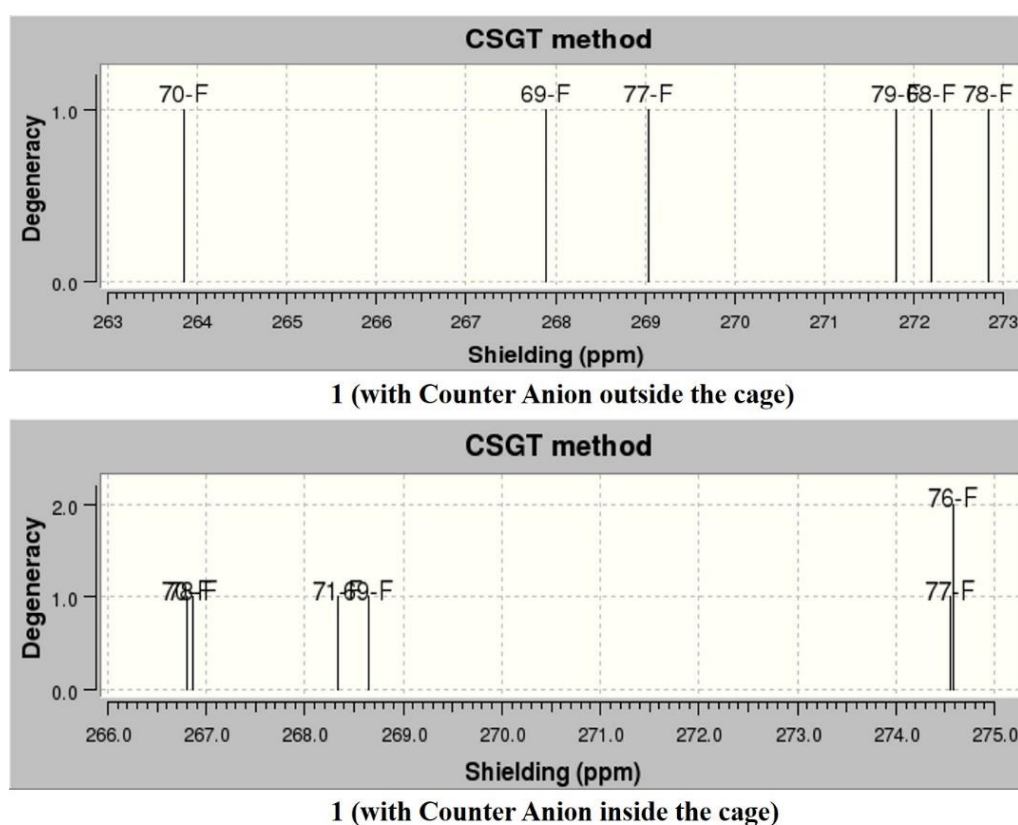


Figure 4.10 Computationally generated ^{19}F -NMR spectra for counterion (i) bound and (ii) not bound to the Ge(II) dication center in complex **1**.

What we found, was that the simulated ^{19}F -NMR shifts patterns were almost the same whether the triflate anion was bound to the Ge(II) center or stayed outside the cage (**Figure 4.10**). Hence the experimental ^{19}F -NMR data done for the Baines system (Case 1) in solution does not contradict the computational results, and allows for the likelihood of the counterion binding to the Ge(II) center inside the cage, when the caged system is present in solution. Moreover, the crystal structure for a crown ether complex of Ge(II) shows that one of the counter anions is attached to the central dication.³ Also, certain other Sn(II), In(I) and Ga(I)

crown ether and cryptand complexes show at least some interaction between the counterion and the cationic center.²²⁻²⁶

Hence, for the Cases 1-4, the counterion is seen to play an important role in keeping the Ge(II) inside the cage and reduce its propensity for unwanted side reactions. Another factor that makes it favorable for a charged species to be at the center of the cage is the energetic favorability of this configuration. In other words, once a monocation (or a dication) settles at the center of the cage, it is likely to remain there, because that is seen to be the most favoured configuration energetically by the simple concept of differential calculus.

Another important conclusion is that only one counterion out of the two binds to the dication at the center: when optimizations were done for Case 1 keeping both triflate counterions at the germanium center, the second triflate anion returned to the uncoordinated geometry during the optimization cycle (**Figure 4.11**). This is because the reduced charge on the Ge(II) center after one counter anion binding makes it less favourable to bind another negatively charged counterion at the same center. Other inhibiting factors such as steric effects could further reduce this favorability. The lower charge on the Ge(II) also serves to reduce its reactivity inside the cage. These observations can be extended to other cases where counter anion coordination was seen to be important (Cases 2 and 3).

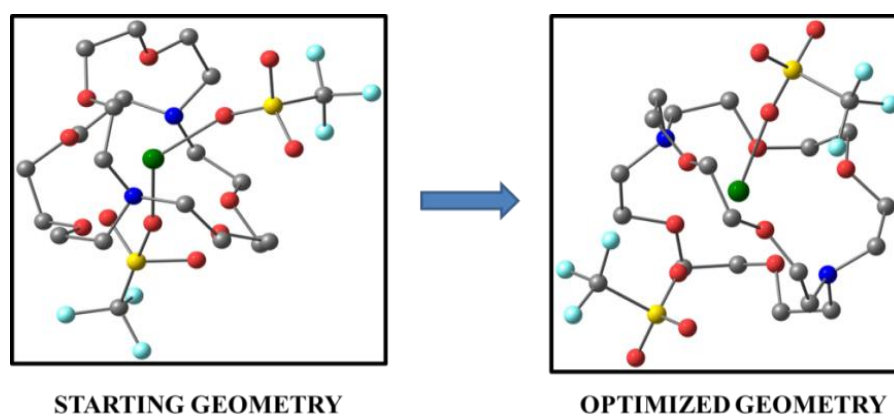


Figure 4.11 DFT Optimization trajectory for Case 1 keeping both triflate counterions at the germanium centre. Colour scheme: germanium = deep green, oxygen = red, carbon = gray, nitrogen = blue, sulphur = yellow and fluorine = sky blue. The cage hydrogen atoms are not shown for the purpose of clarity.

A further point worth considering is the strength of the dication – counter anion interaction when the two are encapsulated inside the cage. For this, we have looked into the interaction of Ge(II) with Br⁻ in Case 3. We have observed that in the optimized structure, there is an elongation of the bond length in [Ge-Br]⁺

(bond length = 2.79 Å), as compared to an unconfined and isolated $[\text{Ge-Br}]^+$ ion (bond length = 2.25 Å). The bond order in the encapsulated $[\text{Ge-Br}]^+$ is also seen to be significantly lower (see **Table 4.3**). In other words, there is a confinement, “cage effect”, on the interaction between the Ge(II) and the Br^- in Case 3, and this leads to the weakening of the interaction of the cation and the anion inside the cage. Why this occurs is due to the favorable electrostatic interactions between the two ions and the partial charges of the cage atoms. This cage effect helps explain perhaps why the counter anion dissociates during the crystallization process and is observed to be found outside the cage in the experimentally observed crystal structures in the Cases 1-4.

Table 4.3 Different parameters comparing the case of $[\text{Ge-Br}]^+$ in a bare state with the $[\text{Ge-Br}]^+$ encapsulated inside the cage in Case 3 in solution.

Complexes	Ge-Br bond length (Å)	WBI BOND INDEXES OF Ge-Br bond	NPA CHARGE ON Ge (II)
$[\text{Ge-Br}]^+$	2.25	1.00	1.42
3	2.79	0.45	1.30

Hence, the current computational investigations show that in almost all the cases investigated, it is likely that the counterion would bind to the Ge(II) at the center of the cage in solution, a situation very different from that envisaged from the obtained crystal structures, which show the two counterions to be present outside the cage. This is also significant in a different sense. In a commentary on the obtained results by Baines and co-workers, Lambert and Müller had suggested that these unusual compounds could be employed as the starting point for new synthetic strategies:^{6,27} since the Ge(II) dication lay uncoordinated and accessible at the center of the cage with plenty of space for substrates to enter, they could be approached by a range of substrates and new products could therefore be made from the subsequent interaction between the Ge(II) dication and the different substrates. However, no reports of such synthetic strategies have been reported to date. Only loosely coordinated adducts with water and ammonia molecules have been reported so far.²⁸ The current results help to explain why this is so: the Ge(II) dicationic center is not present in an accessible form in solution, but is coordinated to a counterion. Hence, an incoming substrate would first have to remove the counterion from the Ge(II) dication in order for new chemistry to take place, and this

would be difficult in the sterically constrained area in the caged structures. This hypothesis is further exemplified by the fact that a NHC stabilized $\text{Ge}(\text{OtBu})_2$ synthesized from the cryptand complex required a strong nucleophile like potassium tert-butoxide. Hence, the current work serves to explain the difficulties in exploiting such systems for new chemistry. But now that the explanation has been provided, can we also suggest means by which this problem could be overcome? The answer is a “yes”: Case 4 provides the clue. Though the $\text{Ge}(\text{II})$ dication was seen to enter the cage with the assistance from the counterion in Case 4, the counter anion did not remain with the $\text{Ge}(\text{II})$, as was discussed earlier. If the reasons why this happens could be understood, then this would serve as a means of designing new cages in future where the counterion would not be necessary for stabilizing the $\text{Ge}(\text{II})$ dication inside the cage in solution.

In order to understand why $\text{Ge}(\text{II})$ in Case 4 is stabilized without any attachment to the counterion, we have employed a new computational approach that we have recently developed, which determines the force and energy experienced by the $\text{Ge}(\text{II})$ dication when at the center of the cage. This is because the main interactions between $\text{Ge}(\text{II})$ and the cage atoms are electrostatic in nature. If the force pulling the $\text{Ge}(\text{II})$ away from its preferred position at the center of the cage is higher in some cases than in others, it would explain why the germanium dication needs a counterion to stay at the center of the cage in some cases and not in others. The computational strategy that we employed has been explained in detail in the Computational Details Section. We had previously shown that force can be employed to determine the strength of hydrogen bonding interactions.²⁹

Here, we have developed a strategy where we (i) have considered dicationic cases, where the cages were optimized with the $\text{Ge}(\text{II})$ dication at the center without any counterion, (ii) obtained the charges on the different atoms of the cage, as well as on the $\text{Ge}(\text{II})$ center (NPA charges were employed for this purpose) and (iii) determined the electrostatic force between the $\text{Ge}(\text{II})$ center and each atom, by using Coulomb's law, and (iv) then obtained the net force acting at the $\text{Ge}(\text{II})$ center by vectorially adding up all the individual force values. This is a simple strategy, and its effectiveness lies in the fact that the absolute values of the forces is not as significant as the relative values obtained for the different cases considered. Column 4 in **Table 4.4** below shows the results obtained for the Cases 1-4. For all the cases, the net electrostatic force was seen to be repulsive. Case 4 was seen to have the lowest repulsive force at the $\text{Ge}(\text{II})$ center, while the $\text{Ge}(\text{II})$ in Case 2 was seen to be experiencing the highest repulsive force. Indeed, the force was 13.7 times higher in

Table 4.4 The force at the $\text{Ge}(\text{II})$ center for reported $\text{Ge}(\text{II})$ complexes (1-4). The reported values are for the cationic fragment of the complex.

Compound	Solvent	Net Force on Ge (II) (pN)/NBO	Relative Values of the Force on Ge(II) for Each Case, Compared to Case 4	Relative Values of the Energy at the Ge(II) center for Each Case, Compared to Case 1
1	tetrahydrofuran	611.7	<i>10.9</i>	<i>1.0</i>
2	dichloromethane	769.0	<i>13.7</i>	<i>1.9</i>
3	acetonitrile	235.8	<i>4.2</i>	<i>10.8</i>
4	acetonitrile	56.1	<i>1.0</i>	<i>4.7</i>

Case 2 than in Case 4 (**Table 4.4**). This is largely due to the fact that, for Case 4, the Coulombic interactions between the heteratom oxygens and the almost oppositely placed Ge(II), which are the primary interactions, largely cancel each other out due to the orientation of the cage (**Figure 4.12**) and this leads to a reduced repulsive force at the Ge(II) center. This analysis indicates that the nature of the cage is very relevant in determining how favorably the Ge(II) would sit inside the cage without support from the counterion, and indeed, as we had seen, the counterion is not necessary for Case 4, and is present outside the cage in this case.

A similar computational strategy also allows us to calculate the electrostatic energy of the interaction of Ge(II) with the cage atoms (see column 5 in **Table 4.4**). A perusal of the values shows that it does not explain why the counter anion does not stay coordinated to Ge(II) in Case 4, but does so in the other three cases. Indeed, here Case 1 is seen to show the most favourable

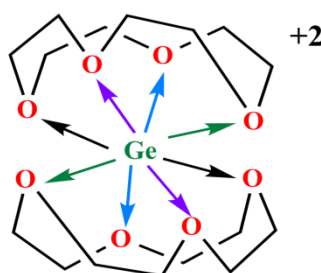


Figure 4.12 Illustration of cancellation of coulombic interactions between the Ge(II) center and the oxygen heteroatoms in Case 4.

electrostatic interactions between Ge(II) and the atoms of the enclosing cage. These results serve to show that the electrostatic force is a better parameter to understand cation-cage interactions than the electrostatic energy of interactions, because when charged species are present in close proximity, the distance between them becomes a crucial factor. This is because the energy of interaction varies as the inverse of the distance, while the force varies as the square of the inverse, and therefore the force becomes a more dominant entity. This result underlines the value of developing strategies to evaluate the force of electrostatic interaction between charged species that are present close together.

4.4 Conclusion

The value of the insights gained from this analysis is that it shows that the principal quality a cage should have to keep a naked cation at its center is to reduce repulsive electrostatic interactions with the cationic center as much as possible via efficient design of the cage. Hence, our work (i) reveals the hidden role played by the counterion in stabilizing the Ge(II) dication inside caged structures, and (ii) shows the principal factor necessary to have naked Ge(II) cations in cages. This has relevance for the development of synthetic strategies beginning from accessing naked cations in caged structures. Our hypothesis could also be extended to similar “cation in a cage” systems. This idea will be subsequently explored in the following chapter of this thesis.

4.5 References

1. V.S.V.S.N. Swamy, S. Pal, S. Khan, S. S. Sen, *Dalton Trans.* **2015**, *44*, 12903.
2. P. A. Rugar, V. N. Staroverov, K. M. Baines, *Science*. **2008**, *322*, 1360.
3. P.A. Rugar, R. Bandhopadhyay, B. F. T. Cooper, M. R. Stinchcombe, J. P. Ragogna, C. L. B. Macdonald, K. M. Baines, *Angew Chem. Int. Ed.* **2009**, *48*, 5257.

4. F. Cheng, A. L. Hector, W. Levason, G. Reid, M. Webster, W. Zhang, *Angew. Chem. Int. Ed.* **2009**, *48*, 5152.
5. M. J. Ward, P. A. Rugar, M. W. Murphy, Y. M. Yiu, K.M. Baines, T. K. Sham, *Chem Commun.* **2010**, *46*, 7016.
6. J. B. Lambert, *Science.* **2008**, *322*, 1333.
7. M. J. Frisch, G. W.Trucks, H. B. Schlegel, G. E. Scuseria, M. A. Robb, J. R. Cheeseman, G. Scalmani, V. Barone, B. Mennucci, G. A. Petersson, H. Nakatsuji, M. Caricato, X. Li, H. P. Hratchian, A. F. Izmaylov, J. Bloino, G. Zheng, J. L. Sonnenberg, M. Hada, M. Ehara, K. Toyota, R. Fukuda, J. Hasegawa, M. Ishida, T. Nakajima, Y. Honda, O. Kitao, H. Nakai, T. Vreven, J. A., Jr. Montgomery, J. E. Peralta, F. Ogliaro, M. Bearpark, J. J. Heyd, E. Brothers, K. N. Kudin, V. N. Staroverov, R. Kobayashi, J. Normand, K. Raghavachari, A. Rendell, J. C. Burant, S. S. Iyengar, J. Tomasi, M. Cossi, N. Rega, J. M. Millam, M. Klene, J. E. Knox, J. B. Cross, V. Bakken, C. Adamo, J. Jaramillo, R. Gomperts, R. E. Stratmann, O. Yazyev, A. J. Austin, R. Cammi, C. Pomelli, J. W. Ochterski, R. L. Martin, K. Morokuma, V. G. Zakrzewski, G. A. Voth, P. Salvador, J. J. Dannenberg, S. Dapprich, A. D. Daniels, Ö. Farkas, J. B. Foresman, J. V. Ortiz, J. Cioslowski, D. J. Fox, *Gaussian 09*, revision B.01; Gaussian, Inc.: Wallingford, CT, **2009**.
8. Y. Zhao, D. G. Truhlar, *Theor. Chem. Acc.* **2008**, *120*, 215
9. V. Barone, M. Cossi, *J. Phys. Chem. A.* **1996**, *102*, 1995.
10. M. Cossi, N. Rega, G. Scalmani, V. Barone, *J. Comput. Chem.* **2003**, *24*, 669.
11. A. E. Reed, R. B. Weinstock, F. Weinhold, *J. Chem. Phys.* **1985**, *83*, 735.
12. a) F. J. London, *Phys Radium, Paris* **1937**, *8*, 397; b) R. McWeeny, *Phys Rev.* **1962**, *126*, 102; c) R. Ditchfield, *Mol Phys.* **1974**, *27*, 789; d) J. L. Dodds, R. McWeeny, A. Sadlej, *J. Mol Phys* **1980**, *41*, 1419; e) K. Wolinski, J. F. Hilton, P. Pulay, *J. Am. Chem. Soc.* **1990**, *112*, 8251.
13. I. S. Ufimtsev, T. J. Martinez, *J. Chem. Theory Comput.* **2009**, *5*, 2619.
14. I. S. Ufimtsev, N. Luehr, T. J. Martinez, *J. Phys. Chem. Lett.* **2011**, *2*, 1789.
15. C. M. Isborn, N. Luehr, I. S. Ufimtsev, T. J. Martinez, *J. Chem. Theory Comput.* **2011**, *7*, 1814.
16. A. V. Titov, I. S. Ufimtsev, N. Luehr, T. J. Martinez, *J. Chem. Theory Comput.* **2013**, *9*, 213.
17. I. S. Ufimtsev, T. J. Martinez, *Comput. Sci. Eng.* **2008**, *10*, 26.
18. I. S. Ufimtsev, T. J. Martinez, *J. Chem. Theory Comput.* **2008**, *4*, 222.
19. I. S. Ufimtsev, T. J. Martinez, *J. Chem. Theory Comput.* **2009**, *5*, 1004.
20. a) J. P. Perdew, S. H. Chevary, K. A. Vosko, K. A. Jackson, M. R. Pederson, D. J. Singh, C. Fiolhais, *Phys. Rev. B.* 1992, *46*, 6671; b) J. P. Perdew, S. H. Chevary, K. A. Vosko, K. A. Jackson, M. R.

- Pederson, D. J. Singh, C. Fiolhais, *Phys. Rev. B.* **1993**, *48*, 4978; c) J. P. Perdew, K. Burke, Y. Wang, *Phys. Rev. B.* **1996**, *54*, 16533; d) C. Adamo, V. Barone, *J. Chem. Phys.* **1998**, *108*, 664; e) A. D. Becke, *J. Chem. Phys.* **1993**, *98*, 5648; f) C. Lee, W. Yang, R. G. Parr, *Phys. Rev. B.* **1988**, *37*, 785; g) C. C. J. Roothan, *Rev. Mod. Phys.* 1960, *36*, 179. h) R. McWeeny, G. Dierksen, *J. Chem. Phys.* **1968**, *49*, 4852. (i) J. A. Pople, R. K. Nesbet, *J. Chem. Phys.* **1954**, *22*, 571.
21. E. R. Johnson, S. Keinan, P. Mori-Sanchez, J. Contreas-Garcia, A. J. Cohen, Y. Weitao, *J. Am. Chem. Soc.* **2010**, *132*, 6498.
22. R. Bandyapadhyay, B. F. T. Cooper, A. J. Rossini, R. W. Schurko, C. L. B. Macdonald, *J. Organometal. Chem.* **2010**, *695*, 1012.
23. J. C. Avery, M. A. Hanson, R. H. Herber, K. J. Blodek, P. A. Rugar, I. Novik, Y. Huang, K. M. Baines, *Inorg. Chem.* **2012**, *51*, 7306.
24. B. F. T. Cooper, C. L. B. Macdonald, *J. Organomet. Chem.* **2008**, *693*, 1707.
25. C. G. Andrews, C. L. B. Macdonald, *Angew. Chem. Int. Ed.* **2005**, *117*, 7619.
26. J. L. Bourque, P. D. Boyle, K. M. Baines, *Chem. Eur. J.* **2015**, *21*, 9790.
27. T. Muller, *Angew. Chem. Int. Ed.* **2009**, *48*, 3740.
28. R. Bandyopadhyay, J. H. Nguyen, A. Swidan, C. L. B. Macdonald, *Angew. Chem., Int. Ed.* **2013**, *125*, 3553.
29. M. K. Tiwari, K. Vanka, *Chem. Sci.* **2017**, *8*, 1378.

**Chapter 5: Hidden Role of Counter Anions: Implications in
Biology and Surface Science**

Chapter 5

Hidden Role of Counter Anions: Implications in Biology and Surface Science

Abstract

We have earlier deduced that a dicationic Ge(II) actually resides as a pseudo monocation inside a molecular cage in solution by the involvement of their corresponding counter anions. Interestingly, such pseudo monocation encapsulated cages are seen to be equally relevant in systems of biological importance, such as for dicationic s block based ionophores. In explaining such cases, the concept of “isoionicity” is introduced, demonstrating that the counterion coordinated dications are isoionic with a monocation, such as Li(I), isolated in the same ionophore. This leads to the realization that two monocations inside a cage represents a stable assembly, which, in turn, provides important insights into surface chemistry, while considering the case of a recently isolated C₁₈ molecule on a NaCl surface.

5.1 Introduction

A model that deserves a closer look is that of a cation inside an enclosing molecular caged structure. This chemical system is of relevance to several important areas of chemistry, biology and surface science. For instance, pendant molecular cage structures in polymer electrolyte membranes (PEMs) serve to transport protons from the anode to the cathode in state-of-the-art fuel cells;¹ a crown ether is seen to flit from one cationic polypeptide site to the next, serving as a relevant model for understanding dynamics in biology² and the progress of a cation through an ion-channel can be visualized as its passage through a successive series of molecular cages linked together. In the previous chapter, we had elucidated the subtle role of the counter anions in Ge(II). The current theoretical and computational investigation is to carefully look at this “cation in a cage” model across different disciplines, and finds surprising insights with it in a) biology: for the behavior of dications of groups 1 and 2 encased in ionophores and in b) surface science: for explaining the role of C₁₈ ring to encompass two monocations inside its periphery.

Furthermore, we have taken the insights gained from the studies of these group 14 complexes in the previous chapter, and looked across the Periodic Table into other systems, such as the biologically relevant dicationic group 2 ionophores: Mg-Ionophore VII and, and shown that factors similar to group 14 dications are in play in these systems as well. What is especially important in these studies is the realization that the counterion coordinated dication systems {such as [Mg-Cl]⁺} have a net charge at the center that matches almost exactly the charge of a lithium monocation: Li(I) at the center of the same cage. The counterion coordinated dication is, therefore, like a “pseudo monocation”, or, in other words, it is isoionic with a monocation. This isoionic analogy has relevance, because it provides a possible explanation for the unusual similarity that has been observed in the behavior of Mg(II) and Li(I) cations in biology.³ A further important consequence is that the isoionic analogy allows us to postulate that two monocations inside the same cage represents a stable configuration, by looking at an experimentally identified structure where two counterion coordinated dications (i.e. two “pseudo monocations”) were present together in a valinomycin cage.⁴ This insight has enabled us to explain the success of employing an NaCl surface in the recently reported stabilization of the C₁₈ molecule, which is a remarkable new development in materials chemistry.⁵

Hence, the current computational exploration of cation encapsulated cage systems reveals the hidden role of counterions in biologically important ionophores, introduces the isoionic analogy, and exploits them to shed light on the behavior of important caged systems in chemistry, as well as in biology and surface sciences.

5.2 Methods

All the DFT calculations were carried out using the *Gaussian 09* suite of quantum-chemical programs.⁶ All the ionophore complex geometries were optimized at the M06-2X/6-31G (d)//M06-2X / 6-311G (d, p) level of theory. The C₁₈ molecule on the fixed NaCl surface was optimized at the M06-2X/ 3-21G (d) level of theory. This was done keeping the computational expense in mind, due to the larger size of the ionophore complexes. Frequency calculations on all the stationary points were carried out to characterize the nature of each stationary point and also to evaluate the respective molecular entropic terms. The solvent effect was added through the Conductor-like Polarization Continuum Model (C-PCM) using the actual solvent as used for all the Ge(II) complexes geometries considered and using water as a solvent for the described ionophore complexes.^{7,8} NBO charges have been used to estimate the partial charge on the cationic center.⁹ All the Wiberg bond indices (WBI) reported are the maximum values reported between the cation and the heteroatoms (N, O and S), i.e., if there are four cation-O interactions, for instance, in a particular cage the WBI indicating the greatest interaction has been reported. Non-covalent interaction (NCI) regions have been plotted using the *nciplot-3.0* suite of programs.¹⁰

5.3 Results and Discussions

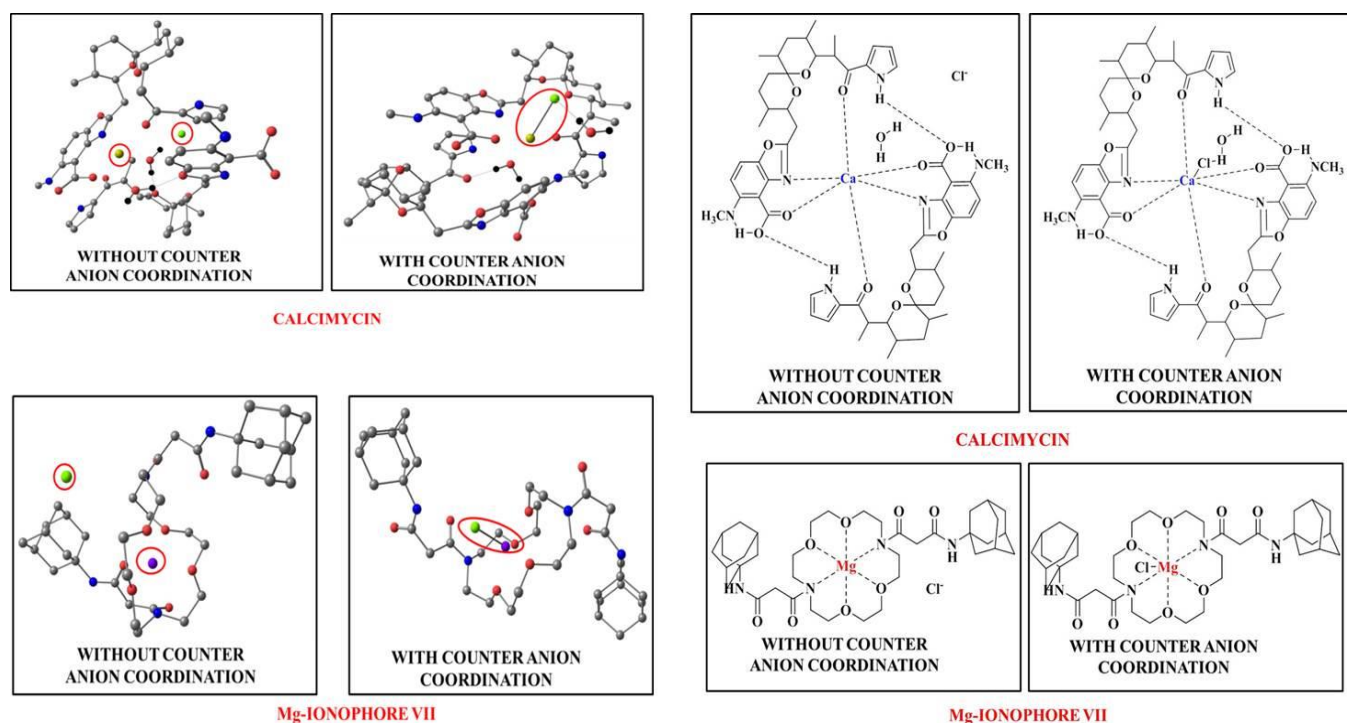


Figure 5.1 Optimized geometries of free and counter anion bound ionophore complexes of Mg(II) and Ca(II), with Cl⁻ considered as the counter anion. Colour scheme: magnesium = violet, calcium = yellow,

oxygen = red, carbon = gray, nitrogen = blue and chlorine = green. Hydrogen atoms on the ionophore cages are not shown for the purpose of clarity.

The previous chapter detailed insights into group 14 chemistry, specifically showing how Ge(II) dications are stabilized by the presence of a counter anion inside the enclosing cage in solution. What is important to note in this is that the interactions that had to be considered were primarily electrostatic in nature. This point to a significant fact: that the insights gained from the study of group 14 systems might be equally relevant across the Periodic Table. This is because, for instance, alkali and alkaline earth metal cations interact primarily through electrostatic interactions, and if one were to investigate cages encapsulating such cations, the principal interaction between the cage and the cations would also be electrostatic in nature. Specifically, one could consider the important area of ionophores enclosing dicationic group 2 ions, which are of significant interest in biology.

Ionophores are molecules that catalyze the transport of ions across hydrophobic cell membranes.¹¹The role of the ionophore is to reversibly and selectively coordinate to a cation and shield it from the cell membrane and hence facilitate the diffusion of the cation into the ion channel. In other words, the ionophore serves to insulate the charge of the cation from the hydrophobic cell membrane, and therefore, their function is even more significant when the charge on the cation is +2, i.e. for dicationic systems. These dications are usually Mg(II) or Ca(II).

Table 5.1 Highest Wiberg Bond Indices (WBI) of the ionophore cation and a heteroatom in the ionophore cage in all the ionophores reported.

Ionophores		Highest WBI Value of M-E bond (M=Mg²⁺, Ca²⁺, Li⁺; E = Heteroatom of the Cage)
Mg-Ionophore VII (Mg²⁺)	Without Counter anion	0.13(O)
	With Counter anion	0.10(O)
Calcimycin (Ca²⁺)	Without Counter anion	0.08(O)
	With Counter anion	0.17(O)
Mg-Ionophore VII with Mg²⁺ substituted by Li⁺ (Li⁺)	–	0.09(O)

Hence we have chosen two molecular cages that specifically bind to dication magnesium (Mg-Ionophore VII) and calcium (Calcimycin) respectively. Such encapsulated dicationic ionophore systems such as Mg-Ionophore VII and Calcimycin (see **Figure 5.1**) have a lot in common with the encapsulated group 14 dications that have been discussed in the previous section. Since they have an octet configuration, it is likely that they would have negligible covalent interactions with the heteroatoms of the ionophore cage after coordination (**Table 5.1**). NCI plots also illustrate the large non-covalent electrostatic interaction present within these systems (**Figure 5.2**).

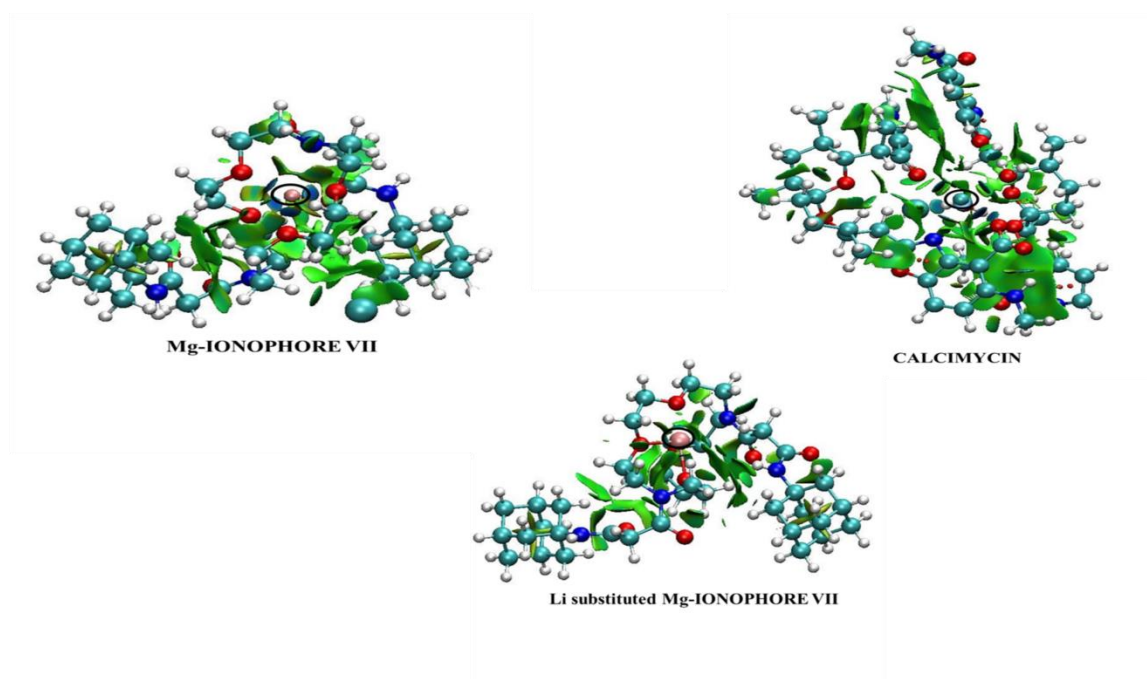


Figure 5.2 Noncovalent interaction (NCI) plot for Mg/Ca/Li based ionophore illustrating the non-covalent electrostatic interaction between the Mg/Ca centers and the heteroatoms of the ionophore cage. The green, blue and red regions respectively represent attractive, strongly attractive and repulsive interactions. The central metal cations are encircled for clarity.

The results with the group 14 systems had indicated the significance of the coordination of one counter anion to the dicationic center. The purpose of looking at the ionophores encapsulating Mg(II) and Ca(II) dications was to check whether the same holds true for group 2 systems as well.

In biological systems, phosphate (PO_4^{3-}) and chloride (Cl^-) are the principal counter anions and there is at least one previous report that has indicated the presence of a counterion (chlorate, ClO_4^- , in that case) that was present inside the valinomycin ionophore cage, coordinated to a Ba(II) dication, with two such Ba(II)- ClO_4^- ions being present together inside the cage.⁴In the current investigation, we have focused on the

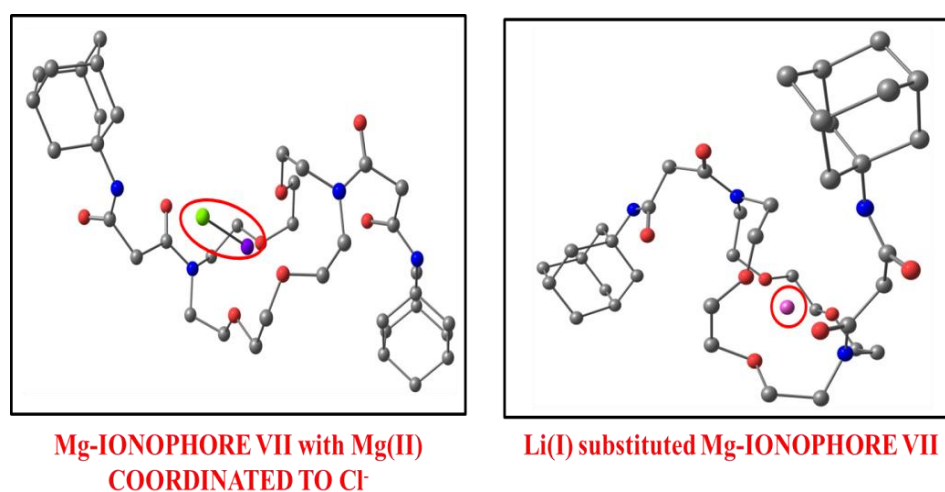
possibility of coordinating a Cl^- counter anion to the dicationic center in the Mg-Ionophore VII and Calceimycin ionophore systems.

The free energy of chloride binding was seen to be favourable for the Mg(II) case by 3.7 kcal/mol and feasible in the Ca(II) case (marginally unfavourable by 0.1 kcal/ml). In other words, for the Mg(II) case, the equilibrium would strongly favour counter anion binding to the Mg(II) center, while in the case of Ca(II), there would be equal probability of the counter anion existing inside or outside the ionophore cage. Ionophores function as a shield to the charged dication from the hydrophobic membranes of the channel and thus help in the smooth transfer of the cations. Hence, this counter anion binding to the dication (that reduces the formal charge on the cation) serves as a secondary layer of insulation of the charge from the membrane layer.

At this point, it is worth noting that the counter anion coordination in the group 14, as well as the group 2, dications inside molecular cages effectively reduces the formal charge on the dication from +2 to +1. In other words, coordination of a counterion to the dication results in the formation of a net “pseudo monocation” at the center of the cage. Since monocationic alkali metal systems encapsulated by cryptands and crown ethers have been widely reported and discussed in the literature,^{12,13} these stable pseudo monocationic systems situated at the center of the cryptand and crown ether cages appear strikingly similar. Hence, one could consider the pseudo mono-cationic systems to be “isoionic” to an alkali metal encapsulated inside the same molecular cage.

One begins to understand the significance of the isoionic analogy when considering and comparing dicationic magnesium and monocationic lithium ions. Recent experimental results suggest that Mg(II) can interact with the ATP triphosphate side chain and Li(I) can co-bind with the native Mg(II) to form ATP-Mg-Li and hence modulate the receptor response.¹⁴ The net charge has been demonstrated to play a pivotal role in the competition between Li(I) and Mg(II) for metal-binding sites and subsequent inhibition of key enzymes involved in specific neurotransmission pathways.¹⁵ Dudev and Lim had demonstrated, via computational studies, that Mg(II) binds in a tridentate fashion to the phosphate groups of ATP and Li(I) binds to the same anionic phosphate groups in a bidentate fashion.¹⁶ Hence, there is evidence to suggest that dicationic magnesium and monocationic lithium act on a specific site by modulation of counter anion coordination, so that they become isoionic with each other during the interaction. That, coupled with the similarity of their radii due to their diagonal relationship in the Periodic Table, might explain the similarity of their observed biological behavior. In order to investigate whether the isoionic analogy holds for Mg(II) and Li(I) in caged structures, we decided to replace $[\text{Mg(II)-Cl}]^+$ in the Mg-Ionophore VII with an Li(I). A

comparison of the NPA charges revealed that Li(I) and $[\text{Mg-Cl}]^+$ have almost the same partial charges (0.61 and 0.66 respectively) and are therefore isoionic to each other (**Figure 5.3**).



Cation	NPA Charge
$[\text{Mg(II)-Cl}]^+$	0.66
Li(I)	0.61

Figure 5.3 Illustration of the isoionic phenomenon. Colour scheme: magnesium = violet, lithium = pink, oxygen = red, carbon = gray, nitrogen = blue and chlorine = green. Hydrogen atoms on the ionophore cages are not shown for the purpose of clarity.

One conclusion from this is that Li(I) can compete and replace an $[\text{Mg(II)-counter anion}]^+$ ion inside ionophores such as Mg-Ionophore VII, which provides fresh new insight into competition between alkali and alkaline earth metal systems in biology. However, there is a larger point that can be made here. The isoionic analogy allows us to also consider the interesting case of the valinomycin encapsulated Ba(II)-chlorate system that had been mentioned previously.⁴ Spectroscopic studies revealed that there were two Ba(II)-chlorate ions present inside the valinomycin ionophore. In the context of the current work, this indicates the presence of two pseudo monocations inside the caged structure. This was made possible because of the flexible valinomycin cage undergoing a conformational change, thereby adopting a novel conformation different from the uncomplexed valinomycin ionophore,⁴ which allowed it to successfully stabilize the two pseudo monocations inside the cage. Now, with the insights that we have developed in the current work on pseudo monocations, as well as of the isoionic analogy, this experimental result makes it clear that it should be possible to stabilize two monocations isoionic with the counter anion coordinated dication inside similar flexible molecular cages.

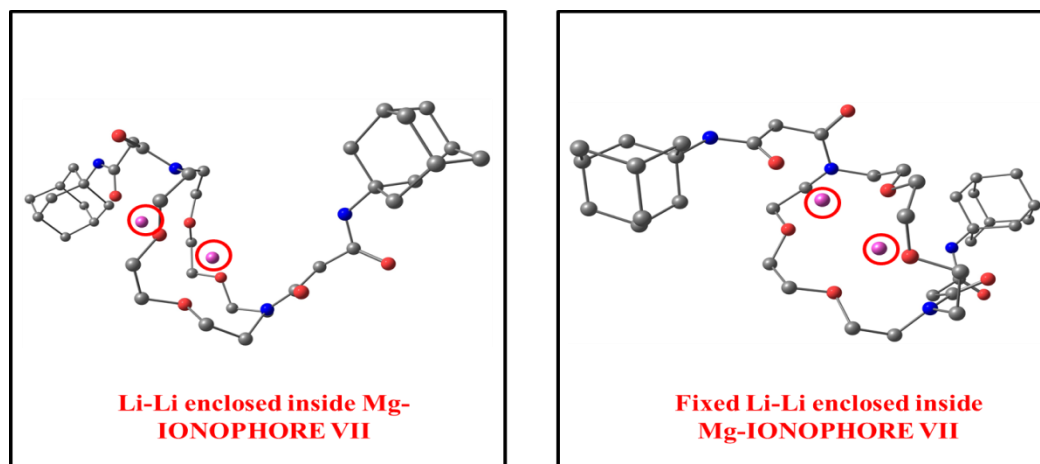


Figure 5.4 Optimized geometries of two Li(I) cations encompassed by Mg-Ionophore VII (the two lithium unfixed and fixed) at the M06-2X/6-31G* level of theory.

In order to drive home this point, we have looked at Mg-Ionophore VII, and encapsulated two Li(I) monocations inside the cage, instead of one, as done earlier. We considered two cases here, one where the two Li(I) ions were allowed to relax into a stable configuration inside the cage, and one where the distance between the two Li(I) ions was kept fixed inside the cage (**Figure 5.4**). What was interesting is that the energy difference between the two optimized structures was only 6.1 kcal/mol. This is due to fact that the flexible ionophore ligand was able to reorient itself to stabilize the two mutually repelling Li(I) cations inside the ionophore cavity via interactions with the negatively charged heteroatoms of the molecular cage, even when the distance between the two positive ions was kept fixed. Hence, molecular cages possessing a flexible, electron rich and large cavity size possess the ability not only to stabilize dications in the form of pseudo monocations, but also two monocations located inside its periphery.

Why is this important? Because of the relevance it may have in the area of surface chemistry. A very recent experimental report details the stabilization of a cyclo[18] carbon (C_{18}) structure on a bilayer (1,0,0) NaCl surface, which was itself positioned on a Cu (1,1,1) surface.⁵The C_{18} thus stabilized was characterized using high-resolution atomic force microscopy (AFM), which revealed a polynic structure with defined positions of alternating triple and single bonds. Now, as discussed above, if a ring is large and flexible, then it has the potential to make a stable complex with two monocations, even if the cations were constrained to be at fixed positions. C_{18} , like valinomycin, is sufficiently large and flexible, thereby enabling it to possess the ability to stabilize two monocations in its encompassing space, even if the monocations were only to be available at fixed positions. Moreover, the fact that it possesses alternating single and triple bonds facilitates bond polarization, the other criterion required for successful electrostatic interaction with two monocations.

Hence, one would expect that C_{18} would be able to make a stable complex if two monocations were to be housed inside of it. In this case, the rare C_{18} was isolated on a (1,0,0) NaCl lateral cut over a (1,1,1) Cu surface, which would lead to both sodium and chloride ions being present inside the C_{18} “cage“, i.e., this is not the system under discussion here. However, if, instead, the (1,1,1) NaCl lateral cut were present on the (1,1,1) lateral cut of Cu, the uppermost layer of atoms would be made up of only sodium monocations at fixed distances from each other and thus the C_{18} ring would enclose two monocations inside its periphery. Such a scenario is shown in **Figure 5.5** below. The insights gained from two pseudo-monocations present in a polarizing, enclosing ring, discussed above, suggest that such a situation would lead to a stable configuration, as exemplified by DFT calculations. They indicate that the binding energy of this specific kind of conformation is significantly higher ($\Delta E = -219.7$ kcal/mol) than the stabilization of the C_{18} over the NaCl (1,0,0) surface ($\Delta E = -65.6$ kcal/mol). The fact that the ΔE values appear high is because of the cluster model employed for the NaCl surface layers considered in each case, and donot, therefore represent the exact binding energy values of the C_{18} on the two NaCl surfaces considered. What is important, however, is that a qualitative comparison can be made between the two binding energy values, which would indicate that the stabilization of the C_{18} on the NaCl (1,1,1) lateral cut would be significantly higher than on the NaCl (1,0,0) lateral cut, which was experimentally employed. This insight can act as a guide for the stabilization of C_{18} , and analogous ring structures in the future, especially because the NaCl can be epitaxially grown as a (1,1,1) lateral cut on the (1,1,1) copper surface, and therefore experiments can be done where the C_{18} would be stabilized on a (1,1,1) NaCl surface rather than a (1,0,0) NaCl surface. Also, it should be noted that (1, 1, 1) surface is less stable than a (1, 0, 0) surface.⁵Indeed, the current calculations suggest that such a situation would lead to reduced movement of the C_{18} ring on the NaCl (1,1,1) surface, unlike in the experiments reported, where the C_{18} was observed to be move more frequently on the NaCl (1,0,0) surface.⁵In short, employing the NaCl (1,1,1) surface would lead to greater likelihood of observing phenomena, such as the stabilization of rare carbon rings, in surface science.

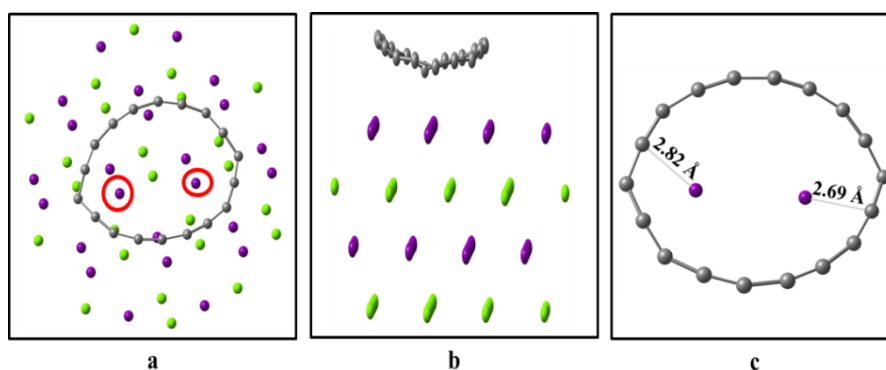


Figure 5.5 Optimized geometry of C₁₈ on an NaCl surface as seen (a) from the top (b) from the side and (c) from the top showing the distances of the two enclosed Na(I) cations from the nearest carbon of the C₁₈ molecule, at the M06-2X/3-21G* level of theory. The two Na (I) cations that the C₁₈ encompasses are shown enclosed in red circles. Colour Scheme: Gray = Carbon, Violet = Sodium and Green = Chloride

5.4 Conclusion

The insights inherited from the earlier chapter are applied to group 2 systems important to biology: to dicationic Ca(II) and Mg(II) binding ionophores, and the same pseudo monocation model is found to fit perfectly in these cases as well. Furthermore, for the Mg(II) binding ionophore, we show that [Mg(II)-Cl]⁺ can be replaced by a Li(I) inside the same ionophore and the two systems - one a pseudo monocation and the other a monocation – would possess the same charge inside the cage. This leads to the formulation of the “isoionic analogy”, and indicates that Li(I) can compete with Mg(II) for the same ionophore center, which has implications for the biochemistry of ionophores. The isoionic analogy also leads to the realization that two monocations can be stabilized inside a sufficiently flexible and polarizable cage, which provides a means of analyzing similar systems in future.

Our current work therefore provides insights into the behavior of cations enclosed in molecular cages, and explains a wide range of experimentally observed phenomena in such systems. It is easy to see that the insights gained from the current studies would have implications for other phenomena observed for caged systems. For example, in polymer electrolyte membranes (PEMs), low proton transfer barriers are coveted for efficient transfer of protons through the membrane. The tendency of cation to stabilize itself at the center of molecular cages can aid in understanding the mechanism of the hopping of the proton through pendant cages in certain PEMs.¹

5.5 References

1. M. V. Mane, K. Vanka, *J. Phys. Chem. C* **2014**, *118*, 784.
2. D. P. Weimann, H. D. F. Winkler, J. A. Falonski, B. Kokschi, C. A. Schalley, *Nat. Chem.* **2009**, *1*, 573.
3. E. Jakobsson, O. Arguello-Miranda, S.-W. Chiu, Z. Fazal, J. Kruczek, S. Nunez-Corrales, S. Pandit, L. Pritchett, *J. Membr. Biol.* **2017**, *250*, 587.
4. S. Devarajan, C. M. K. Nair, K. R. K. Easwaran, M. Vijayan, *Nature*. 1980. 286, 640.
5. K. Kaiser, L. M. Scriven, F. Schulz, P. Gawel, L. Gross, H. L. Anderson, *Science*, **2019**, *365*, 1299.

6. M. J. Frisch, G. W. Trucks, H. B. Schlegel, G. E. Scuseria, M. A. Robb, J. R. Cheeseman, G. Scalmani, V. Barone, B. Mennucci, G. A. Petersson, H. Nakatsuji, M. Caricato, X. Li, H. P. Hratchian, A. F. Izmaylov, J. Bloino, G. Zheng, J. L. Sonnenberg, M. Hada, M. Ehara, K. Toyota, R. Fukuda, J. Hasegawa, M. Ishida, T. Nakajima, Y. Honda, O. Kitao, H. Nakai, T. Vreven, J. A., Jr. Montgomery, J. E. Peralta, F. Ogliaro, M. Bearpark, J. J. Heyd, E. Brothers, K. N. Kudin, V. N. Staroverov, R. Kobayashi, J. Normand, K. Raghavachari, A. Rendell, J. C. Burant, S. S. Iyengar, J. Tomasi, M. Cossi, N. Rega, J. M. Millam, M. Klene, J. E. Knox, J. B. Cross, V. Bakken, C. Adamo, J. Jaramillo, R. Gomperts, R. E. Stratmann, O. Yazyev, A. J. Austin, R. Cammi, C. Pomelli, J. W. Ochterski, R. L. Martin, K. Morokuma, V. G. Zakrzewski, G. A. Voth, P. Salvador, J. J. Dannenberg, S. Dapprich, A. D. Daniels, Ö. Farkas, J. B. Foresman, J. V. Ortiz, J. Cioslowski, D. J. Fox, *Gaussian 09*, revision B.01; Gaussian, Inc.: Wallingford, CT, **2009**.
7. V. Barone, M. Cossi, *J. Phys. Chem. A* **1996**, *102*, 1995.
8. M. Cossi, N. Rega, G. Scalmani, V. Barone, *J. Comput. Chem.* **2003**, *24*, 669.
9. A. E. Reed, R. B. Weinstock, F. Weinhold, *J. Chem. Phys.* **1985**, *83*, 735.
10. E. R. Johnson, S. Keinan, P. Mori-Sanchez, J. Contreas-Garcia, A. J. Cohen, Y. Weitao, *J. Am. Chem. Soc.* **2010**, *132*, 6498.
11. E. Bakker, P. Buhlmann, E. Pretsch, *Chem. Rev.* **1997**, *97*, 3083.
12. H. J. Buschmann, *Journal of Inclusion Phenomena and Molecular Recognition in Chemistry*. **1989**, *7*, 581.
13. B. L. Haymore, J. D. Lamb, R. M. Izatt, J. J. Christensen, *Inorg. Chem.* **1982**, *21*, 1598.
14. K. T. Briggs, G. G. Giulian, G. Li, J. P. Y. Kao, J. P. Marino, *Biophys. J.* **2016**, *111*, 294.
15. T. Dudev, C. Lim, *J. Am. Chem. Soc.* **2011**, *133*, 9506.
16. T. Dudev, C. Grauffel, C. Lim, *Sci. Rep.* **2017**, *7*, 42377.

Chapter 6: Computational Investigation on the Role of External and Local Electric Fields in Macrocyclic Chemical and Biological Systems

Chapter 6

Computational Investigation on the Role of External and Local Electric Fields in Macrocylic Chemical and Biological Systems

Abstract

Investigating the role of electric field in systems of widespread interest via computational techniques is a blossoming field of research. In this respect, we have chosen two macrocyclic systems of chemical and biological importance for a comprehensive theoretical analysis. The outcome of applying an oriented external electric field (OEEF) on the geometric and electronic properties of the chemically unique π -conjugated carbon ring compounds has been studied. The distinct changes in its critical features inspired us to investigate the specific function of built-in local electric field (LEF) present in naturally occurring macrocyclic systems like valinomycin. We have deduced the role of counter anions like chloride (Cl^-) in biological systems and its different conformational status in potassium (K^+) and sodium (Na^+) coordinated valinomycin macrocycle. Furthermore, this divergence has been proposed to be one of the possible reason for the selectivity of the valinomycin macrocycle for a K^+ cation over Na^+ .

6.1 Introduction

The interaction between matter and electric field specifically in the context of chemistry has been captured over some period now.¹ One of the most commonly encountered phenomenon is Stark effect. However, electric fields have captured the imagination of researchers recently and has fueled interest to investigate this field into various aspects of chemistry.²⁻⁴ The role of oriented external electric field (OEEF) i.e external electric field applied along a particular direction in space has also been explored in this context with respect to its implementation in modulating reaction rates, regio-selectivity and spin-selectivity.⁵ Though conceptualized theoretically in the initial periods, it's practical application provided a very limited scope as an outcome of the experimental limitations associated with application of oriented electric. However in recent years, various methods have been designed and proposed for the actual realization of these concepts into real term use.⁴

Angle strained π -conjugated carbon rings are attractive molecules due to their distinctive electronic and structural properties.⁵ Due to the low overlap between p orbitals as a result of the structural constraints, these molecules are highly reactive but also finds applicability in practical use via numerous means.⁶⁻¹⁰ These group of cyclocarbons can be broadly be categorized into three classes i.e a) cyclocarbon b) cycloparaphenylene (CPP) and c) cycloparaphenylacetylene (CPPA) (**Figure 6.1**).¹¹ Considering their relatively elastic structural and stand-out electronic properties, an application of an OEEF can tune the existing properties to a considerable extent and thus rendering these molecules an interesting subject to investigate in the context of OEEF research. Previously, external electric field application on carbon systems like fullerene, graphite and nanotubes were performed.¹²

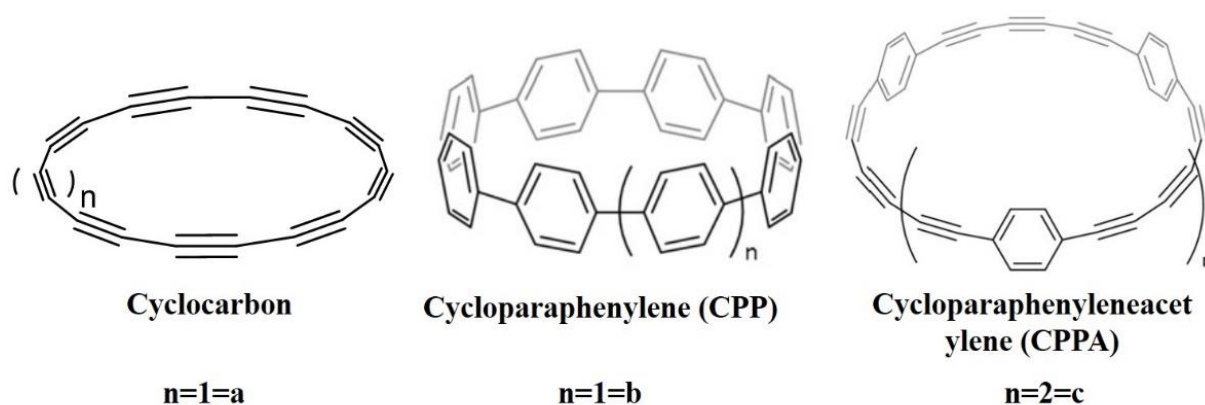


Figure 6.1 a) cyclocarbon b) cycloparaphenylene (CPP) c) cycloparaphenylacetylene (CPPA)

An alternate manifestation of electric field observed in matter are local electric fields (LEFs). This field as the term suggests is introduced via charged functional groups present in the periphery of the molecules.³In biomolecules, this field is generated by polar side chain of the framework.¹³ Moreover, the origin of the catalytic activity in enzymes has been explained via the concept of LEF by Warshel and co-workers.¹⁴This explanation has been experimentally corroborated by Boxer and co-workers on the basis of vibration Stark effect measurement whereby an extremely high electric field was successfully quantified in ketosteroid isomerase enzyme.¹⁵Further experimental proof elucidating the importance of LEF has been provided by Spackmann and co-workers.¹⁶All these key findings have stressed the importance of estimating the electric field strength in the active sites of enzymes. This would be helpful not only to understand fundamental properties in biologically relevant systems but also provide important clue for novel molecular design for useful applications.

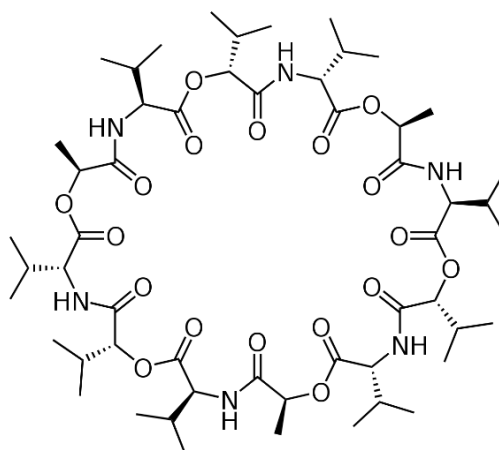


Figure 6.2 Valinomycin ionophore macrocycle.

In this work, we have computationally explored the effect of both OEEF and LEF in important systems using state of the art quantum chemical methods. The structural and electronic effects of OEEF in π -conjugated carbon rings has been studied via exploring all the three classes of molecules integral to it (**Figure 6.1**). Furthermore, we have comprehensively abstracted the implications of LEF in the important biological macrocyclic ionophore molecule of valinomycin (**Figure 6.2**). Valinomycin is an ionophore that selectively coordinates and transports K^+ across cellular membranes.¹⁷In summary, we have illustrated how electric field, both manually applied and inherent, plays a pivotal role in tuning the properties and activity of relevant systems.

6.2 Methods

6.2.1 π -conjugated macrocycles

All the calculations were done using *Gaussian09* suite of quantum chemical programs.¹⁸ All results presented in this work were calculated by using ω B97XD exchange-correlation functional¹⁹ in conjunction with def2-TZVP²⁰ (for **a**) and 6-311g** (for **b** and **c**) basis set respectively in the gas phase. The ω B97XD functional reproduced the geometry generated by the more robust coupled-cluster singles and doubles (CCSD) theory and can also reasonably depict electronic structure of the cyclo[18]carbon.²¹ The EEF was applied via "field" keyword in Gaussian program.

6.2.2 Valinomycin macrocycle

All the DFT calculations were carried out using the *Turbomole 7.1* suite of programs.²² Geometry optimizations were performed using the Perdew, Burke, and Erzenhof density functional (PBE)²³ functional, the electronic configuration of the atoms was described by a triple- ζ basis set augmented by a polarization function (Turbomole basis set TZVP).²⁴ The resolution of identity (ri)²⁵ along with the multipole accelerated resolution of identity (marij)²⁶ approximations were employed for an accurate and efficient treatment of the electronic Coulomb term in the density functional calculations. The real (not model) system has been employed for all the calculations. The option "disp" provided in the Turbomole package (DFT-D3) was used for dispersion-corrected DFT calculations for all the calculations with Turbomole.²⁷ The values reported in manuscript are ΔG values, with zero point energy, internal energy, and entropic contributions, with the temperature taken to be 298.15 K. Solvent effects were introduced by using the COSMO model²⁸ with the dielectric constant $\epsilon = 20$. NBO and Mullikan charges have been used to calculate the net electrostatic force on the anionic chloride center.²⁹ The net force was calculated according to the protocol described in our previous report.³⁰ All the Wiberg bond indices (WBI) reported are the maximum values reported between the central cation (K^+ and Na^+) and the heteroatoms (N, Cl and O), i.e., if there are four interactions, for instance, in a particular cage the WBI indicating the greatest interaction has been reported utilizing the NBO analysis module prescribed in the *Gaussian09* program¹⁸ at M06-2X/6-311G(d) level of theory.³¹

6.3 Results and Discussion

6.3.1 Oriented External Electric field (OEEF) in π -conjugated macrocycles

OEEFs have been known to be boosting catalysis, inhibition, bond dissociation, region/stereo-selectivity, spin-selectivity, and so on as was discussed before.^{5,32} This versatility of this area makes it an alluring

interest of comprehensive research. Also, external electric fields can also bring about observable change in molecular geometry. Previously, an ammonia molecule changes its geometry on modulating the direction of the OEEF has been recorded.³ Also, spin flipping under an influence of external electric field can induce geometric changes.³³ The molecules that would be most affected structurally are flexible and large supra-molecules held by weak electrostatic attraction by electric field of very low strength. Very low strength electric field has been found to force change in structural frameworks of molecular networks,³⁴ protein folding³⁵ and water cluster.³⁶

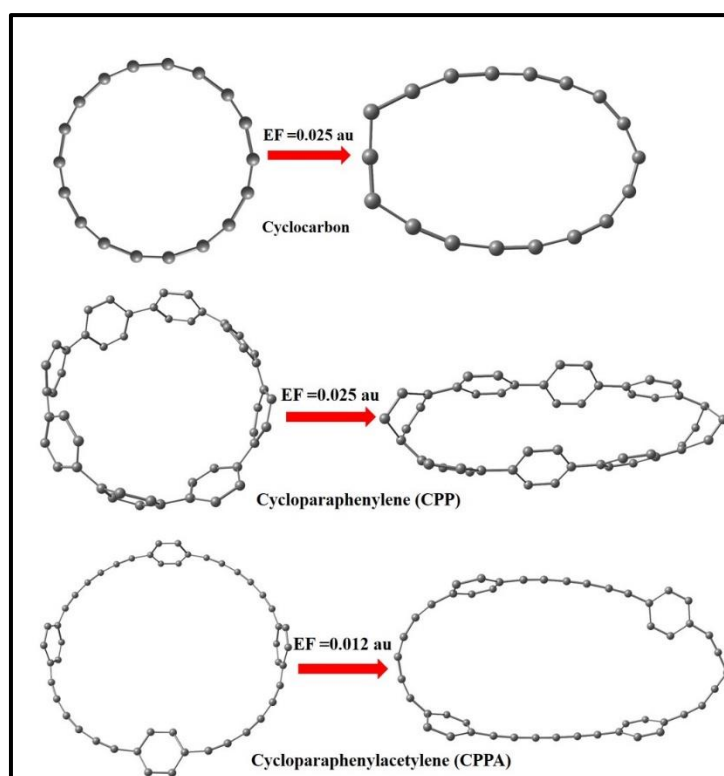


Figure 6.3 Illustration of the optimized geometries, involving the three molecules from three families (cyclocarbon, CPP and CPPA) transforming to a distorted structure under OEEF. The magnitude of field strength of OEEF is mentioned on the top of the arrow. The arrow also denotes the direction of the OEEF. Color code: carbon: grey.

As discussed in the introduction, the flexible nature of the family of π -conjugated carbon rings make it a prospectus candidate to study the effect of applying electric field on it. Its geometric features makes it susceptible to distortion under the influence of a low electric field strength. Recently, a molecule $C_{18}(a)$ of cyclocarbon family was recently isolated in a landmark work.³⁷ Subsequently, the geometric and electronic effects of an OEEF on this molecule was thoroughly studied via computational techniques.³⁸ Hence to

extend the scope of this area, we attempted to check a similar likelihood existing for molecules of other families of π -conjugated carbon rings. Henceforth, we performed OEEF calculations using density functional theory (DFT) quantum chemical technique on a molecule (a, b and c) from each of the three families (cyclocarbon, CPP, CPPA) including the C₁₈ (**a**) molecule from the cyclocarbon family.

On applying an electric field along the plane of the molecule, all the three molecules show considerable distortion (**Figure 6.3**). It is to be noted that the field was taken to be of minimal strength under which the molecule exhibits a clear cut and recognizable structural deformation. The molecule aligns itself with the direction of the external electric field. The geometric changes enforced by the external brings about change in its electronic properties as well. This is reflected in the HOMO-LUMO energy gap values of the distorted structure (**Table 6.1**). HOMO-LUMO gap is a key determinant for many properties of a molecule. It is noted that the molecule **c** relatively distorts under a lower electric field strength (**Figure 6.3**) as compared to the other two molecules (**a** and **b**). The higher susceptibility towards external electric field is also reflected in its large variation of electronic properties from the original geometry i.e HOMO-LUMO gap (**Table 6.1**). This is an important point that could be useful for experimentalist as a low electric field strength is beneficial for seamless actual technical use for harnessing OEEF effect on molecules in real life.

Our theoretical study via choosing a molecule each from the three families of the intriguing group of compounds like π -conjugated carbon rings stresses the importance of finding novel systems to study the consequences of implementing OEEF. Computational techniques can predict beforehand several important characteristics which may be of critical help to recreate it in actual use.

Table 6.1 HOMO-LUMO Energy of Original and Distorted Structure for molecule **a-c**.

Molecule	HOMO-LUMO Energy Gap (kcal/mol)	
	Original Structure	Distorted Structure
a	155.8	124.9
b	38.2	129.8
c	138.3	69.0

6.3.2 Local Electric field (LEF) in Valinomycin

It is an established fact that electrostatics plays a pivotal role in biology.³⁹ Over the years, it has been agreed that electric field is the best parameter to quantify and understand the electrostatic interactions in biomolecules that modulates its specific functions.¹³ Strong electric fields are also found to manifest themselves in membrane proteins.⁴⁰ For example, it is observed that a small change in membrane potential via electric field modulation can have a profound effect on the properties of an ion-channel.⁴¹ As discussed earlier, the role of electric field in the active sites of enzymes has been affirmed. Hence, explaining biological phenomena on the basis of electric field is an attractive area to explore on account of the predominant electrostatic interaction present in the biological systems.

Table 6.2 Binding Energies and WBI Values for Cl⁻ incorporated K⁺ and Na⁺ valinomycin complexes. The WBI values are the maximum values for the interaction between the central mono cation and the cage atoms (the atoms are mentioned in parenthesis)

Valinomycin Cage	$\Delta E_{\text{binding}}$ (kcal/mol)	Wiberg Bond Index (WBI)
		Value
KCl-Valinomycin	-22.4	0.06 (Cl)
NaCl-Valinomycin	-16.7	0.08 (Cl)

We have discussed the structural and electronic effects of OEEF on macrocyclic carbon based systems earlier. We also underlined the outcome of applying a directional electric field on a distinct macromolecular π -conjugated carbon ring system in terms of conformation and electronics. A directional field modifies the symmetrical ring into an unsymmetrical structure. It has been recorded that an equivalent electric field strength as strong that of an external electric field could be induced into a system by chemical methods like introducing a divalent alkaline earth metal cation.³⁸ It could also be introduced into a symmetrical macrocyclic system by introducing polar groups in the molecular framework that would generate polarity and a net electric field into the system. These facts have made us inquisitive to enquire about the role of these effects in biomolecules where likewise systems can be encountered. Since electrostatic interaction plays a key role in determining several of its properties, the local electric field that is generated by polar side groups of the molecule itself, is an important parameter to visualize and comprehend. Hence, we have chosen an important class of macrocyclic compounds present in biological systems known as ionophores. Ionophores are molecules that catalyze the transport of ions across hydrophobic cell

membranes.⁴² Valinomycin (**Figure 6.2**) is an ionophore that selectively binds K^+ cation over Na^+ ($\Delta\Delta E_{\text{binding}} = 5.7$ kcal/mol) cation in for transport across membranes (**Table 6.2**). The coordination of the cage to the cation happens via predominantly electrostatic stabilization of the positively charged monocation utilizing the heteroatoms of the cage framework (**Table 6.2**). Hence it is expected that this inherent electric field, generated by the polar side group of the valinomycin, plays a critical role in determining its specific property and function.

Table 6.3 Thermodynamic parameters of Cl^- binding at the PBE/TZVP // PBE/TZVP level of theory

Type of valinomycin cage	ΔG (kcal/mol)
K-valinomycin complex	2.0
Na-valinomycin complex	-1.7

In our earlier work, we had shown that counter anions present in biological systems (like Cl^-) can remain coordinated to the a dication inside ionophore cages.³⁰ For valinomycin ionophore, counter anions (ClO_4^-) along with Ba^{2+} dication have been characterized experimentally to be present inside a synthetic cage complex.⁴³ Hence it would be interesting to examine the possibility of a similar scenario for an actual case whereby counter anions present in biological systems (like Cl^-) can remain inside a valinomycin macrocycle along with biologically pertinent cations (like K^+ and Na^+) that can bind to the cage. Henceforth, we confirmed such a possibility by performing high level state of the art density functional theory (DFT) calculations on the valinomycin macrocycle coordinated to both K^+ and Na^+ cation. It is to be noted that a dielectric constant (ϵ) of 20 was incorporated while performing the calculations. It has reported that the dielectric constant value of water inside biological ion-channel could be reduced by a significant extent due to change in its local environment.⁴⁴ Result indicate that this possibility does exist for the Na^+ binded valinomycin (**Table 6.1**). In other words, Cl^- anion can stay inside the Na^+ -valinomycin as a stable geometry. This scenario is not possible for analogous K^+ case as such a geometry is not thermodynamically feasible. What explains this dichotomy in conformation?

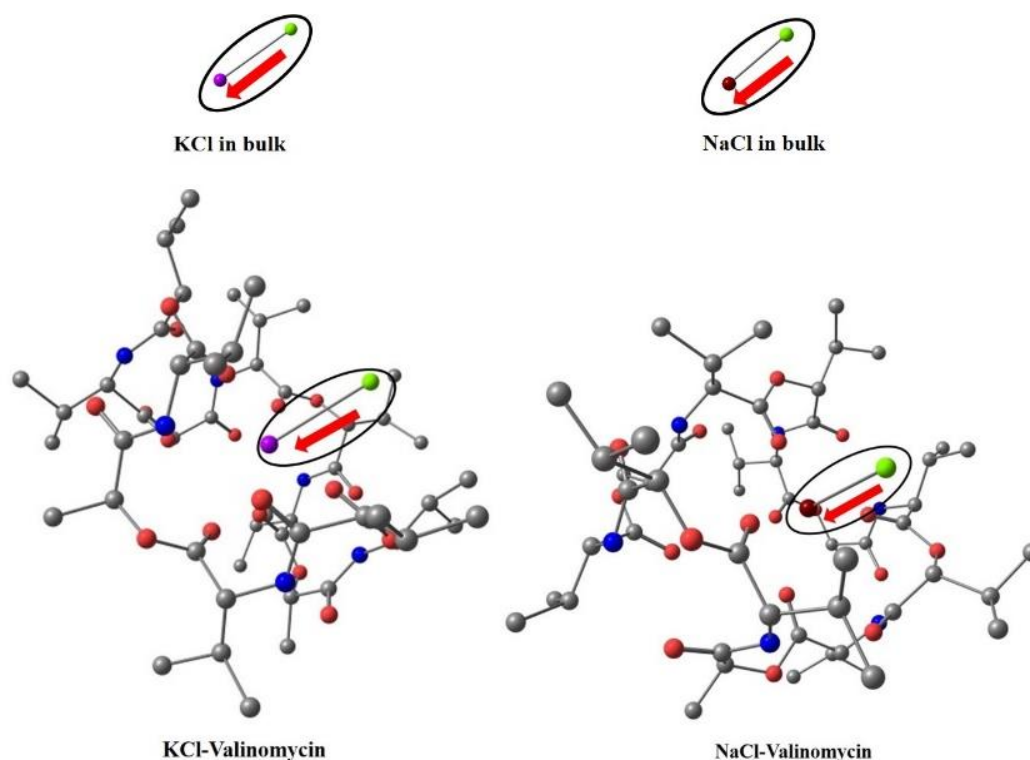


Figure 6.4 Illustration denoting the direction of the net force on Cl⁻ in the counter anion incorporated K⁺/Na⁺ valinomycin complex and the NaCl/KCl moiety in bulk solution. Colour scheme: potassium = violet, sodium = brown, oxygen = red, carbon = gray, nitrogen = blue and chlorine = green. Hydrogen atoms on the valinomycin cage are not shown for the purpose of clarity.

To explain this anomalous observation, we have to again recall the fact that electric field is the best parameter to explain any observed event in biological systems like valinomycin. Hence we attempted to explain this occurrence via invoking the concept of local electric field. This electric field generates an electrostatic force inside the macrocycle that is felt by every single moiety present in the framework. Hence we calculated the net force on the Cl⁻ anion in both the counter anion included K⁺/Na⁺-valinomycin complex optimized structure and Cl⁻ in KCl/NaCl moiety in bulk solution without the cage to illustrate a comprehensive relative idea regarding the extent of interaction. It is to be noted that the bulk solution refers to the medium containing the K-Cl/Na-Cl moiety sans the valinomycin macrocycle in an identical dielectric medium. Hence, the Cl⁻ in bulk solution is devoid of any interaction from the macrocyclic cage. The net force was calculated following Coulomb's law exploiting Mullikan and Natural Population Analysis (NPA) charge method of denoting atom charges. The direction of the net force that the Cl⁻ feels (**Figure 6.4**) is oriented towards the central mono-cation in each case. We introduced a new parameter, designated by σ , which signifies the ratio between net force on the Cl⁻ anion in bulk solution and inside the valinomycin

cage in in a similar dielectric medium to get an authentic comparative quantification of the force on Cl^- . Results indicate a higher σ value for the K^+ -valinomycin system as compared to the Na^+ -valinomycin system (**Table 6.4**). This signifies that, in the former case, the instantaneous force felt by the Cl^- anion is markedly reduced going from the bulk solution to that present inside the macrocyclic valinomycin cage as compared to the latter case where the σ value is comparatively higher. This explains the bias of the Na-valinomycin towards the incorporation of Cl^- counter-anion inside the cage framework as a result of the apparent change in relative attractive force felt by the Cl^- towards the central cation as compared to that in the bulk.

Table 6.4 Values of the two parameter (Ω and σ) using different charge analysis methods.

Population Analysis Method	Ratio (Ω) for K-valinomycin cage	Ratio (Ω) for Na-valinomycin cage	Ratio (σ) for K-valinomycin cage	Ratio (σ) for Na-valinomycin cage
NPA	3.8	2.8	3.4	2.6
Mullikan	3.2	2.3	4.4	3.3

Since electric field is the force felt is by a unit positive charge, any change in force is related to electric field disparity. Hence the change in net force on Cl^- is related to parallel local electric field strength variation. Hence to affirm this hypothesis, we assigned another parameter, designated by Ω , which denotes the ratio between net electric field strength on the Cl^- anion in the bulk solution and inside the valinomycin cage in in a similar dielectric medium. The electric field strength on Cl^- can be easily calculated from the magnitude of the force if the exact value of the charge on the Cl^- is estimated. We find that there is an equivalent change in the Ω value mirroring the trend shown for σ values (**Table 6.4**). The absolute values of Ω suggest that there is differential change in the local electric field strength experienced by the Cl^- on going from the bulk to confinement inside the cage between the two cationic valinomycin complexes. Since electric field strength is directly proportional to the magnitude of the force, the trends satisfy our expectation according to our hypothesis. Hence the local electric field generated by the Na^+ -valinomycin and K^+ -valinomycin complexes utilizing its polar groups are quantitatively different from that in the bulk and this

in turn could dictate the counter anion association feasibility. What is the implication of this atypical behavior of the valinomycin cages regarding its coordination to K^+ and Na^+ ?

One of the remarkable features of natural systems like valinomycin is its selectivity towards one cation between two mono cation like Na^+/K^+ which differs by less than 0.4 Å in size.⁴⁵ While, the driving force behind the ion-selectivity in K^+/Na^+ ion channels has been studied extensively over the years,⁴⁶ similar efforts have been undertaken to unravel the selectivity query in smaller molecular systems like valinomycin. A quantum chemical study conducted earlier attributed the selectivity in valinomycin towards K^+ over Na^+ to structural constraints that prevents the reorganization of the molecule to coordinate the Na^+ cation.⁴⁷ Earlier, in this report, we have showcased the preferential behavior of the K^+ -valinomycin complex towards including the counter anions inside its framework over the Na^+ -valinomycin complex (**Table 6.1**). Since explaining the driving force for the selectivity is a major goal for studying a cation selective molecule like valinomycin, it was enticing enough to examine the specific fall-out of our earlier deduced observation pertaining to counter anions influences the ion selectivity.

To this effect we have conducted a linear transit scan calculation for calculating the potential energy surface (PES) for the comparing the counter anion effect in Na^+ -valinomycin/ Cl^- complex. Linear transit scan refers to deducing the PES via optimization by freezing one degree of freedom (which is systematically varied after each cycle during the scan) while keeping the remaining degree of freedoms relaxed.

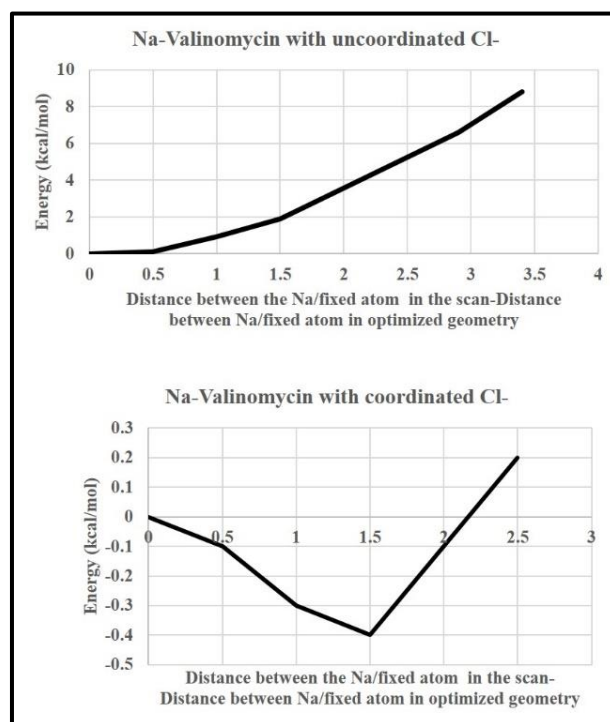


Figure 6.5 Potential Energy Surface (PES) for the path of Na^+ exiting the valinomycin cage computed via linear transit scan. Top: when the Cl^- remains uncoordinated to Na^+ inside the cage and below: when the Cl^- remains coordinated to Na^+ outside the cage. It is to be noted that the value of the energy and the distance between the Na^+ cation and the fixed atom (which is varied during the after each cycle in the scan) is assumed to be nil for convenience of illustration.

Hence we undertook this scan for the two cases of Na^+ -valinomycin/ Cl^- complex, a case where the counter anion Cl^- is located outside and where counter anion Cl^- is located inside the cage in another case, starting the scan from the optimized structures in both occasions and gradually increasing the distance from a particular atom in the cage to the central Na^+ cation (this distance is freeze in each cycle of the scan). This is to attain an idea regarding the role of Cl^- in aiding the exit of Na^+ from the macrocyclic cage. Results from the linear transit scan confirms that the counter anion present in the cage makes the Na^+ more energetically labile to leave the macrocycle when compared to the case when the counter anion is located outside the cage (**Figure 6.5**). This calculation is irrelevant for the K^+ -valinomycin/ Cl^- complex whereby the counter anion prefers thermodynamically to stay outside the macrocyclic cage. Hence varying local electric field induced on the cage atoms in Na^+/K^+ -valinomycin complexes dictates the different conformational preference of two complexes. This in turn influences the selectivity of valinomycin molecule towards K^+ over Na^+ thus thrusting the important part played by counter anions whose specific role is predefined on the basis of local electric field strength.

6.4 Conclusion

Researchers have remained oblivious of the role play by electric field in important systems of relevance over the years. It is with recent advancement of research directed towards unraveling the intricacies involved in directed electric fields within molecules that its significance is being understood. For example, inducing an extra positive charge in biomimetic iron complexes boosts its catalytic capacity by several folds.⁴⁸ This results can be credited to electric field effect which modulates the catalytic activity of the complexes.

In this work, we have stressed the significance of applying an external field and also deducing ingrained electric fields in diverse and important molecules. Computational technique can easily premeditate the critical features arising out of applying an OEEF. It can easily predict the susceptibility of a molecular system to external electric field and also the field strength with precision to enforce observable changes in the molecule according to our targeted goal. It will also aid scientists to suitably tune the systems to

influence the necessary outcomes according to our specific need. Parallel to this, sophisticated experimental techniques are being developed for real life usage in a synergistic manner along with computational predictions.⁴Also, new venues like subjecting other flexible macrocyclic rings⁴⁹under OEEF could be attempted in future in continuation of work under this section. All these clues promises an exciting new field of research.

In the case of local electric fields, computational techniques could also be of great help to comprehend the standard behavior of systems of general interest. In this work, the well-known principle of selectivity in biologically relevant valinomycin has been explained on the basis of variation in local electric field imposed by the macrocycle on the Cl⁻ ion. This is a significant addition to a hot area of research as all previous reports have primarily focused on biological enzymes. Also, a new ionophore with better selectivity between K⁺ and Na⁺ cations has been synthesized.⁵⁰The selectivity query could also be settled here through the spectrum of LEF. Also, it would be interesting to visualize the effect of OEEF on systems with profound LEF thus merging the two strands discussed here. In summary, our present work creates a promising platform for potentially relevant future computational and experimental exploration.

6.5 References

1. S. Shaik, D. Mandal, R. Ramanan, *Nat. Chem.* **2016**, *8*, 1091.
2. A. C Aragonés, N. L Haworth, N. Darwish, *Nature.* **2016**, *531*, 88.
3. S. Shaik, R. Ramanan, D. Danovich, D. Mandal, *Chem. Soc. Rev.* **2018**, *47*, 5125.
4. S. Ciampi, N. Darwish, H. M. Aitken, I. Diez-Pérez, M. L Coote, *Chem. Soc. Rev.* **2018**, *47*, 5146.
5. S. Shaik, T. Stuyver, J. Joy, Z. Wang, *J. Am. Chem. Soc.* **2020**, *142*, 12551.
6. H. Hopf, J. Grunenberg in *Strained Hydrocarbons (Ed.: H. Dodziuk)*, Wiley-VCH, Weinheim, **2009**, 375.
7. E. M. Sletten, C. R. Bertozzi, *Acc. Chem. Res.* **2011**, *44*, 666.
8. M. F. Debets, S. van Berkel, J. Dommerholt, A. J. Dirks, F. P. J. T. Rutjes, F. L. van Delft, *Acc. Chem. Res.* **2011**, *44*, 805.
9. J. C. Jewett, C. R. Bertozzi, *Chem. Soc. Rev.* **2010**, *39*, 1272. C. M. Gampe, E. M. Carreira, *Angew. Chem. Int. Ed.* **2012**, *51*, 3766–3778; *Angew. Chem.* **2012**, *124*, 3829.
10. P. M. Tadross, B. M. Stoltz, *Chem. Rev.* **2012**, *112*, 3550.
11. K. Miki, K. Ohe, *Chem. Eur. J.* **2020**, *26*, 2529.
12. a) M. Wahadoszamen, T. Nakabayashi, S. Kang, H. Imahori, N. Ohta, *J. Phys. Chem. B.* **2006**, *110*, 20354; b) Y.-W. Son, M. L. Cohen, S. G. Louie, *Nature.* **2006**, *444*, 347; c) O. Hod, V. Barone, G.

- E. Scuseria, *Phys. Rev. B.* **2008**, *77*, 035411; d) X.-Q. Tian, X.-R. Wang, Y.-D. Wei, L. Liu, Z.-R. Gong, J. Gu, Y. Du, B. I. Yakobson, *Nano Lett.* 2017, *17*, 7995-8004; e) J. Klinovaja, M. J. Schmidt, B. Braunecker, D. Loss, *Phys. Rev. B.* **2011**, *84*, 085452; f) M. Khazaei, A. A. Farajian, S. U. Lee, R. V. Belosludov, Y. Kawazoe, *Jpn. J. Appl. Phys.* **2010**, *49*, 115103.
13. S. D. Fried, S. G. Boxer, *Annu Rev Biochem.* **2017**, *86*, 387.
14. A. Warshel, *Acc. Chem. Res.* **1981**, *14*, 284.
15. S. D. Fried, S. Bagchi, S. G. Boxer, *Science.* **2014**, *346*, 1510.
16. M. W. Shi, S. P. Thomas, V. R. Hathwar, *J. Am. Chem. Soc.* **2019**, *141*, 3965.
17. L. Rose, A. T. A. Jenkins, *Bioelectrochemistry*, **2007**, *70*, 387.
18. M. J. Frisch, G. W. Trucks, H. B. Schlegel, G. E. Scuseria, M. A. Robb, J. R. Cheeseman, G. Scalmani, V. Barone, B. Mennucci, G. A. Petersson, H. Nakatsuji, M. Caricato, X. Li, H. P. Hratchian, A. F. Izmaylov, J. Bloino, G. Zheng, J. L. Sonnenberg, M. Hada, M. Ehara, K. Toyota, R. Fukuda, J. Hasegawa, M. Ishida, T. Nakajima, Y. Honda, O. Kitao, H. Nakai, T. Vreven, J. A., Jr. Montgomery, J. E. Peralta, F. Ogliaro, M. Bearpark, J. J. Heyd, E. Brothers, K. N. Kudin, V. N. Staroverov, R. Kobayashi, J. Normand, K. Raghavachari, A. Rendell, J. C. Burant, S. S. Iyengar, J. Tomasi, M. Cossi, N. Rega, J. M. Millam, M. Klene, J. E. Knox, J. B. Cross, V. Bakken, C. Adamo, J. Jaramillo, R. Gomperts, R. E. Stratmann, O. Yazyev, A. J. Austin, R. Cammi, C. Pomelli, J. W. Ochterski, R. L. Martin, K. Morokuma, V. G. Zakrzewski, G. A. Voth, P. Salvador, J. J. Dannenberg, S. Dapprich, A. D. Daniels, Ö. Farkas, J. B. Foresman, J. V. Ortiz, J. Cioslowski, D. J. Fox, *Gaussian 09*, revision B.01; Gaussian, Inc.: Wallingford, CT, **2009**.
19. J. D. Chai, M. Head-Gordon, *Phys. Chem. Chem. Phys.* **2008**, *10*, 6615.
20. F. Weigend, R. Ahlrichs, *Phys. Chem. Chem. Phys.* **2005**, *7*, 3297.
21. Z. Liu, T. Lu, Q. Chen. *Carbon.* **2020**, *165*, 468.
22. R. Ahlrichs, M. Bar, M. Haser, H. Horn, C. Kolmel, *Chem. Phys. Lett.* **1989**, *162*, 165.
23. J. P. Perdew, K. Burke, M. Ernzerhof, *Phys. Rev. Lett.* **1997**, *78*, 1396.
24. S. Ansgar, H. Christian, A. Reinhard, *J. Chem. Phys.* **1994**, *100*, 5829.
25. K. Eichkorn, O. Treutler, O. H. M. Haser, R. Ahlrichs, *Chem. Phys. Lett.* **1995**, *240*, 283.
26. M. Sierka, A. Hogekamp, R. Ahlrichs, *J. Chem. Phys.* **2003**, *118*, 9136.
27. a) J. Hepburn, G. Scoles, R. Penco, *Chem. Phys. Lett.* **1975**, *36*, 451; b) R. Ahlrichs, R. Penco, G. Scoles, *Chem. Phys.* **1977**, *19*, 119; c) S. J. Grimme, *Comput. Chem.* **2004**, *25*, 1463; d) S. J. Grimme, *Comput. Chem.* **2006**, *27*, 1787; e) S. Grimme, J. Antony, S. Ehrlich, H. J. Krieg, *Chem. Phys.* **2010**, *132*, 154104.

28. A. Klamt, G. Schuurmann, *Chem. Soc, Perkin Trans.* **1993**, 2, 799.
29. A. E. Reed, R. B. Weinstock, F. Weinhold, *J. Chem. Phys.* **1985**, 83, 735.
30. A. Mukherjee, S. Ghule, M. K. Tiwari, K. Vanka, *J. Phys. Chem. A* **2020**, 124, 8040.
31. Y. Zhao, D. G. Truhlar, *Theor. Chem. Acc.* **2008**, 120, 215.
32. T. Stuyver, D. Danovich, J. Joy, S. Shaik, *WIREs Comput Mol Sci.* **2019**, e1438.
33. P. M. De Biase, D. A. Paggi, F. Doctorovich, *J. Am. Chem. Soc.* **2009**; 131, 16248.
34. a) G. Velpula, J. Teyssandier, S. De Feyter, K. S. Mali, *ACS Nano.* **2017**; 11, 10903; b) A. K. Jissy, A. Datta. *ChemPhysChem.* **2012**, 13, 4163; c) M. Novak, C. Foroutan-Nejad, R. Marek. *J Chem Theor Comput.* **2016**, 12, 3788.
35. N. J. English, D. A. Mooney, *J Chem Phys.* **2007**, 126, 1105.
36. a) S. Vaitheeswaran, J. C. Rasaiah, G. Hummer. *J Chem Phys.* **2004**, 121, 7955; b) S. Vaitheeswaran, H. Yin, J. C. Rasaiah. *J Phys Chem B.* **2005**, 109, 6629.
37. K. Kaiser, L. M. Scriven, F. Schulz, P. Gawel, L. Gross, H. L. Anderson, *Science.* **2019**, 365, 1299.
38. T. Liu, Q. Chen, *ChemPhysChem.* **2021**, Just Accepted.
39. a) F. B. Sheinerman, B. Honig, *J. Mol. Biol.* **2002**, 318, 161; b) R. Rohs, S. M. West, A. Sosinsky, P. Liu, R. S. Mann, B. Honig, *Nature.* **2009**, 461, 1248; c) M. K. Gilson, B. H. Honig, *Nature*, **1987**, 330, 84; d) A. Mulgrew-Nesbitt, K. Diraviyam, J. Wang, S. Singh, P. Murray, *Biochim. Biophys. Acta.* **2006**, 1761, 812; e) T. Simonson, *Curr. Opin. Struct. Biol.* **2001**, 11, 243.
40. H. G. L. Coster, T. C. Chillcott, *Bioelectrochemistry.* **2002**, 56, 141.
41. A. Mathie, L. E. Kennard, E. L. Veale, *Radiation Protection Dosimetry.* **2003**, 106, 311.
42. E. Bakker, P. Buhlmann, E. Pretsch, *Chem .Rev.* **1997**, 97, 3083.
43. S. Devarajan, C. M. K. Nair, K. R. K. Easwaran, M. Vijayan, *Nature.* **1980**, 286, 640.
44. M. Aguilera-Arzo, A. Andrido, V. M. Aguilera, A. Alcaraz, *Phys. Chem. Chem. Phys.* **2009**, 11, 358.
45. Dobler, M. Ionophores and their structures. John Wiley & Sons, Inc; **1981**.
46. B. Roux, *Essays Biochem.* **2017**, 61, 201.
47. S. Varma, D. Sabo, S. B. Rempe, *J Mol Biol.* **2008**, 376, 13.
48. a) S. R. Bell, J. T. Groves, *J. Am. Chem. Soc.* **2009**, 131, 9640; b) A. Mukherjee, S. Pattanayak, S. Sen Gupta, K. Vanka, *Phys. Chem. Chem. Phys.* **2018**, 20, 13845.
49. K. T. Mortensen, T. J. Osberger, T. A. King, H. F. Sore, D. R. Spring, *Chem. Rev.* **2019**, 119, 10288.

50. A. Casnati, A. Pochini, R. Ungaro, C. Bocchi, F. Ugozzoli, Richard J. M. Egberink, Helma Struijk, R. Lugtenberg, F. de Jong, D. N. Reinhoudt, *Chem. Eur. J.* **1996**, *4*, 436.

Chapter 7: Summary and Future Outlook

Chapter 7

Summary and Future Outlook

7.1 Theme of the Thesis

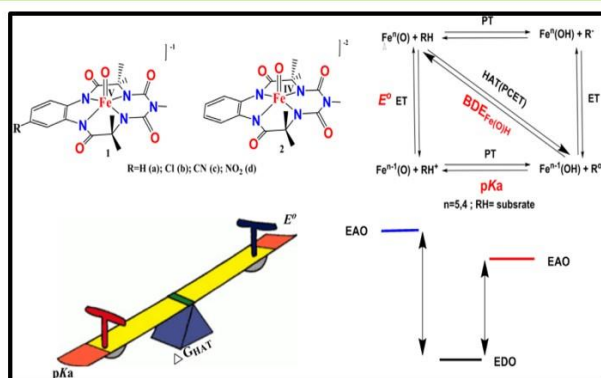
The interaction between an electric field and matter has always been an attractive subject to study. Electric fields are generated by electric charges and they mutually varies with each other.¹ However, it has special relevance in chemical and biological systems as electrostatic interactions plays a major role in these systems. This field is introduced in these systems by charged polar groups. Considering this fact, these electrostatic interactions would be best quantified by an electric field.² This is helpful in understanding existing chemical phenomenon and also estimating the driving force behind various biological processes.³ Also, the role of an external electric field (EEF) in inducing fundamental changes in molecules has generated a lot of interest in recent years specially with regards to its utility in smart chemistry.^{3,4} Our thesis addresses these points by investigating several instances of systems relevant to both chemistry and biology. Due to impediments from technical difficulties, experimental techniques could be cumbersome to estimate the electric field of actual systems.⁵ Hence computational tools could be alternatively used to not only comprehend important observations in biology but also predict the outcome of applying an EEF on relevant systems for an actual judicious application in future.^{3,4} In this thesis, we have used state of the art quantum chemical computational analysis to present a comprehensive understanding of important chemical and biological systems via the prism of the interlinked concepts of electric field and charge. In short, our work adds significant new insight in this already developing and exciting field. The entire thesis can be summarized as follows

- (i) Firstly, we focused on the family of biomimetic iron complexed biuret based tetra-amido macrocyclic ligands (bTAML) to exemplify. Density Functional Theory (DFT) calculations showcased the role of an extra positive charge on the complex in enhancing the hydrogen atom transfer (HAT) reaction over its precursor. This fact has been explained on the basis of the reduction in energy gap between the electron donating molecular orbital (EDO) of the substrate and electron accepting molecular orbital (EAO) of the iron complex on account of the local electric field (LEF) generated by an extra positive charge. Also, the variation in reaction rate in substituted complexes has been explained on the basis of the change in local electric field on the iron center induced by the substituent effects. This work highlighting a biomimetic system

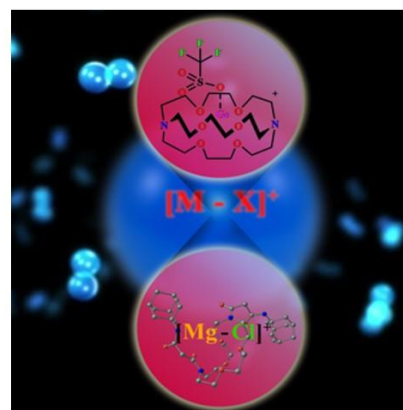
could be useful in explaining similar processes in actual biomolecules which could subsequently be exploited for designing new biomimetic structures.

- (ii) Electric field are modulated by change in orientation and quantity of electric charges. In a molecular system, charged could be tuned by ionic species or more specifically, counter ions. Hence we deduced the exact role played by counter ions in an array of Ge(II)-cryptand/crown ether cage complexes by extensive DFT and *ab initio* molecular dynamics (AIMD) calculations. Results indicate that the counter anions could be present alongside the Ge(II) dication inside the macrocycles in these complexes in solution. This outcome stabilizes the highly reactive dication inside the cage by preventing its interaction with the cage framework.
- (iii) The insight from our preceding work were applied to similar and biologically relevant ionophore cage molecules that encompasses dications like Mg^{2+} and Ca^{2+} respectively utilizing theoretical methods. DFT calculations illustrate that similar possibility exists for these complexes whereby biological anions like Cl^- could be present inside the Mg^{2+}/Ca^{2+} -valinomycin cage in a stable geometry in solution p. Hence it is actually a pseudo monocation that is present inside the cages. Herein, we introduced the “iso-ionic” analogy to explain certain existent biological phenomenon. These results serves as a conduit to explain the role of NaCl surface in stabilizing the extremely rare C_{18} molecule. Hence our computational study thrusts the role of charge and the subsequent outcome on its systematic tuning in important systems of interest.
- (iv) Lastly, in addition to the self-generated field, we have studied the effects of applying a theoretical oriented external electric field (OEEF) on macrocyclic all carbon systems known for their distinct properties. This form of study is now a major area of interest as an electric field can considerably induce primary changes in fundamental molecular properties. Furthermore, we have also explored the important function of LEF in naturally occurring valinomycin macrocycle. Similar to our previous report, we have deduced by performing DFT calculations that counter anions could be associated inside a valinomycin ionophore along with a monocation in a stable geometry. This factor has been shown to direct the important ion selectivity property of the macrocycle.

Charge and Electric field effects in biomimetic systems



Role of counter anions in macrocycles



Electric Field in Macrocyclic systems

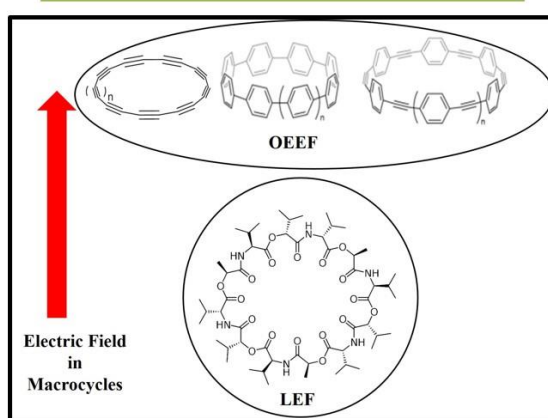


Figure 7.1 Pictorial summary of the work presented in this thesis.

7.2 Computational Methods

The static DFT calculation has been carried out utilizing the *Gaussian09*⁶ and *Turbomole 7.1*⁷ suite of programs. The ab initio molecular dynamics simulations were conducted using the *TeraChem 1.9* quantum chemistry and AIMD software packages,⁸⁻¹⁴ using the B3LYP density functional¹⁵ and the def2-SVP basis set to calculate the Born–Oppenheimer potential energy surface. For static DFT calculations, M06-L,¹⁶⁻¹⁸ M06-2X,¹⁸ PBE,¹⁹ BP86²⁰ and B3LYP functionals have been used. Solvent effects were added employing C-PCM^{21,22} and COSMO²³ solvation model. Mullikan and NPA²⁴ charge analysis have been used to calculate the partial charges of each atoms in the systems studied. Additionally, Wiberg Bond Indices (WBI) and Non Covalent interaction (NCI)²⁵ analysis were performed to ascertain the degree of non-covalent interactions in molecules. Frequency calculations were carried out to characterize the nature of each stationary point and also to evaluate the respective molecular entropic terms which were included into the energy value to report the absolute ΔG value.

7.3 Future Directions from this Thesis.

Considering the multi-disciplinary nature of our thesis, a wide range of directions protrudes out of it for consideration in future. Since, electrostatic interactions are key determinants of different properties of chemical and biological systems, the insights gained from our thesis could be extended to similar important systems. In this scenario, computational estimation of charge and electric field becomes highly resourceful. We have explained several important functions in biomolecules from the viewpoint of charge and electric field in this thesis by computational methods. This ideas could be applied to other important biological bodies by performing similar theoretical calculations as conducted in this thesis. Out of the numerous potentials, one particular case could that of ion channels. We have explained the role of charge and electric field in ionophore molecules in details in our work. Ionophore cages are considered the seeds of biological ion channels that are present in intercellular membrane. The insight deduced from these macrocycles could be used to provide clarity on various important functions of ion channels like ion conduction and selectivity of different channels. Also, existing properties of other bio-enzymes could be explained on the basis of electric field caused by charge distribution in these molecular systems. Our insights on the biomimetic iron catalyst could be replayed in actual biological enzymes by focusing on the effect of alteration in charges. A high precision theoretical prediction of the outcome of applying an external electric field (EEF) on important systems could be a useful methodology before an actual practical implementation of the process. This is helpful to get a comprehensive picture of the potential fallouts of the experimental application beforehand which may make the technologies cost-effective and more beneficial.

7.4 References

1. R. Chabay, B. Sherwood, *Matter and interactions (4th ed.)*. Wiley. **2015**, 867.
2. J. D. Slocum, L. J. Webb, *Annu. Rev. Phys. Chem.* **2018**, 69, 253.
3. S. Shaik, T. Stuyver, J. Joy, Z. Wang, *J. Am. Chem. Soc.* **2020**, 142, 12551.
4. T. Stuyver, D. Danovich, J. Joy, S. Shaik, *WIREs Comput Mol Sci.* **2019**, e1438.
5. S. Ciampi, N. Darwish, H. M. Aitken, I. Diez-Pérez, M. L Coote, *Chem. Soc. Rev.* **2018**, 47, 5146.
6. M. J. Frisch, G. W.Trucks, H. B. Schlegel, G. E. Scuseria, M. A. Robb, J. R. Cheeseman, G. Scalmani, V. Barone, B. Mennucci, G. A. Petersson, H. Nakatsuji, M. Caricato, X. Li, H. P. Hratchian, A. F. Izmaylov, J. Bloino, G. Zheng, J. L. Sonnenberg, M. Hada, M. Ehara, K. Toyota, R. Fukuda, J. Hasegawa, M. Ishida, T. Nakajima, Y. Honda, O. Kitao, H. Nakai, T. Vreven, J. A., Jr. Montgomery, J. E. Peralta, F. Ogliaro, M. Bearpark, J. J. Heyd, E. Brothers, K. N. Kudin, V. N.

- Staroverov, R. Kobayashi, J. Normand, K. Raghavachari, A. Rendell, J. C. Burant, S. S. Iyengar, J. Tomasi, M. Cossi, N. Rega, J. M. Millam, M. Klene, J. E. Knox, J. B. Cross, V. Bakken, C. Adamo, J. Jaramillo, R. Gomperts, R. E. Stratmann, O. Yazyev, A. J. Austin, R. Cammi, C. Pomelli, J. W. Ochterski, R. L. Martin, K. Morokuma, V. G. Zakrzewski, G. A. Voth, P. Salvador, J. J. Dannenberg, S. Dapprich, A. D. Daniels, Ö. Farkas, J. B. Foresman, J. V. Ortiz, J. Cioslowski, D. J. Fox, *Gaussian 09*, revision B.01; Gaussian, Inc.: Wallingford, CT, **2009**.
7. R. Ahlrichs, M. Bar, M. Haser, H. Horn, C. Kolmel, *Chem. Phys. Lett.* **1989**, *162*, 165.
 8. I. S. Ufimtsev, T. J. Martinez, *J. Chem. Theory Comput.* **2009**, *5*, 2619.
 9. I. S. Ufimtsev, N. Luehr, T. J. Martinez, *J. Phys. Chem. Lett.* **2011**, *2*, 1789.
 10. C. M. Isborn, N. Luehr, I. S. Ufimtsev, T. J. Martinez, *J. Chem. Theory Comput.* **2011**, *7*, 1814.
 11. A. V. Titov, I. S. Ufimtsev, N. Luehr, T. J. Martinez, *J. Chem. Theory Comput.* **2013**, *9*, 213.
 12. I. S. Ufimtsev, T. J. Martinez, *Comput. Sci. Eng.* **2008**, *10*, 26.
 13. I. S. Ufimtsev, T. J. Martinez, *J. Chem. Theory Comput.* **2008**, *4*, 222.
 14. I. S. Ufimtsev, T. J. Martinez, *J. Chem. Theory Comput.* **2009**, *5*, 1004.
 15. a) J. P. Perdew, S. H. Chevary, K. A. Vosko, K. A. Jackson, M. R. Pederson, D. J. Singh, C. Fiolhais, *Phys. Rev. B.* 1992, *46*, 6671; b) J. P. Perdew, S. H. Chevary, K. A. Vosko, K. A. Jackson, M. R. Pederson, D. J. Singh, C. Fiolhais, *Phys. Rev. B.* **1993**, *48*, 4978; c) J. P. Perdew, K. Burke, Y. Wang, *Phys. Rev. B.* **1996**, *54*, 16533; d) C. Adamo, V. Barone, *J. Chem. Phys.* **1998**, *108*, 664; e) A. D. Becke, *J. Chem. Phys.* **1993**, *98*, 5648; f) C. Lee, W. Yang, R. G. Parr, *Phys. Rev. B.* **1988**, *37*, 785; g) C. C. J. Roothan, *Rev. Mod. Phys.* 1960, *36*, 179. h) R. McWeeny, G. Dierksen, *J. Chem. Phys.* **1968**, *49*, 4852. (i) J. A. Pople, R. K. Nesbet, *J. Chem. Phys.* **1954**, *22*, 571.
 16. Y. Zhao, D. G. Truhlar, *J. Chem. Phys.* **2006**, *125*, 194101.
 17. Y. Zhao, D. G. Truhlar, *Acc. Chem. Res.* **2008**, *41*, 157.
 18. Y. Zhao, D. G. Truhlar, *Theor. Chem. Acc.* **2007**, *120*, 215.
 19. J.P. Perdew, K. Burke, M. Ernzerhof, *Phys. Rev. Lett.* **1997**, *78*, 1396.
 20. A.D Becke, *Phy. Rev. A.* **1988**, *38*, 3098.
 21. V. Barone, M. Cossi, *J. Phys. Chem. A.* **1998**, *102*, 1995.
 22. M. Cossi, N. Rega, G. Scalmani, V. Barone, *J. Comput. Chem.* **2003**, *24*, 669.
 23. A. Klamt, G. Schuurmann, *Chem. Soc. Perkin Trans.* **1993**, *2*, 799.
 24. A. E. Reed, R. B. Weinstock, F. Weinhold, *J. Chem. Phys.* **1985**, *83*, 735.
 25. E. R. Johnson, S. Keinan, P. Mori-Sanchez, J. Contreas-Garcia, A. J. Cohen, Y. Weitao, *J. Am. Chem. Soc.* **2010**, *132*, 6498.

ABSTRACT

Name of the Student: Anagh Mukherjee**Registration No. :** 10CC15J26010**Faculty of Study:** Chemical Sciences**Year of Submission:** 2021**AcSIR academic centre/CSIR Lab:** CSIR-National**Name of the Supervisors:** Dr. Kumar Vanka

Chemical Laboratory Pune

(Supervisor)/Dr. Sayam Sengupta (Co-supervisor)

Title of the thesis: Computational Studies on the Effect of Charge and Electric Fields on Systems of Chemical and Biological Interest.

The interaction between an electric field and matter has always been an attractive subject to study. Electric fields are generated by electric charges and they mutually varies with each other. The judicious use of electric field in smart chemistry is a promising new area of investigation. Computational techniques involving high level quantum chemical calculations can predict the outcome of the applied electric field. This theoretical technique can be best utilized to estimate the intricacies of electric field in natural systems to explain their basic properties. In this thesis, we computationally deduce the role of electric field in chemical and biological systems.

Firstly, we explored this field effect in high-valent intermediates in non-heme biomimetic systems. We selected the iron complexed biuret based tetra-amido macrocyclic ligand (bTAML) and illustrated the role of an extra positive charge on the iron center in enhancing the HAT rate by several folds over the former. DFT calculations have been exploited to deduce the effect of this LEF on the frontier molecular orbitals which leads to the stabilization of the TS. Hence our investigation explains the reactivity of an important bio-mimic on the basis of the variation of electric field.

This study provides a seed for understanding actual physical observations in entities where the electric field is induced by the systems itself. As we know, charge modulation can lead to change in the electric field. One of way to alter charged species is to bind more charged species to it. Hence we explored of role of counter anions in the intriguing group of Ge(II)-crown ether/cryptand complexes. By performing an ab initio molecular dynamics (AIMD) simulations and DFT calculations, we deduced the exact function of the corresponding counter anion in solution. The implications of this result is felt in biological ionophore systems involving dications whereby similar observations involving counter-anions are recorded. We proposed a new concept of “isoionicity” based upon our findings which further explains biological phenomenon. This idea was further applied in an important system of surface science. This exhibits the function of a charged species (counter-anions) in modifying the charge and subsequently the local electric field and its ramifications in chemistry and biology.

Similarly, the electronic and geometric effect of an electric field along a certain direction of space in unique macromolecular systems has also been computationally studied. Furthermore, we emphasized the importance of LEFs in biological macrocycle of valinomycin which can regulate its primary functions.

Our thesis thus adds significantly new insights to an already booming research area. We have successful showcased the applicability of the intertwining concept of electric field and charge on important chemical and biological systems via computational techniques.

List of publication(s) in SCI Journal(s) (published & accepted) emanating from the thesis work

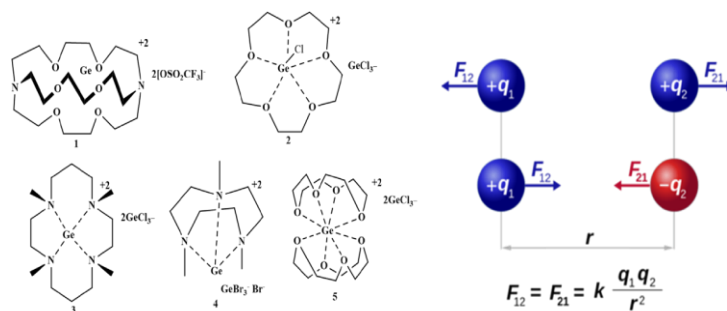
1. A. Mukherjee, S. Pattanayak, S. S. Gupta, K. Vanka, What Drives the H-abstraction Reaction in Bio-mimetic Oxoiron/TAML Complexes? A Computational Investigation. *Phys. Chem. Chem. Phys.* **2018**, *20*, 13845.
2. A. Mukherjee, S. Ghule, M. K. Tiwari, K. Vanka, Unraveling the Hidden Role of the Counteranion in “Cation in a Cage” Systems. *J. Phys. Chem. A* **2020**, *124*, 8040.

List of Papers with abstract presented (oral/poster) at national/international conferences/seminars with complete details.

- i) **Presented an oral entitled** “Deciphering the Factors behind the Stability of Low Valent pblock Cations in Molecular Cages: A Computational Study” at **International Conference Structural and Inorganic Chemistry (ICSIC-II)** IISER Pune, 18-19, March 2019.

Abstract

Low oxidation state cations and dications of groups 13 and 14 have received a lot of attention in recent years, partly owing to the fact that they are difficult to isolate synthetically. Baines and coworkers demonstrated, for the first time in 2008, the successful implementation of the polyether ligation approach to stabilize a “naked” germanium (II) di-cation using an electron rich [2.2.2]-cryptand.¹ Subsequent studies found that reacting differently sized crown ethers, such as [12]-crown-4, [15]-crown-5, and [18]-crown-6, with $\text{GeCl}_2 \cdot \text{dioxane}$ led to a range of caged Ge(II) mono- and dications. In all of these complexes, the interaction between the Ge(II) centre and donor atoms (N and O) of the enclosing cage was found to be predominantly non-covalent, electrostatic in nature. Why such unusual compounds remain stable after being formed is finally revealed through the current computational investigation. We have found that the role of the counter-ions in stabilizing the caged cations is significantly more important than had been previously realized. The presence of the counter-ion was seen to reduce the propensity of the cation to exit the cage. Moreover, *ab initio* molecular dynamics simulations have revealed that even if the cation leaves the cage, it is likely to re-enter it if the counter-ion is present in its vicinity. As such, the current work considerably expands on the understanding of the nature and stability of these important *p* block cationic caged compounds.

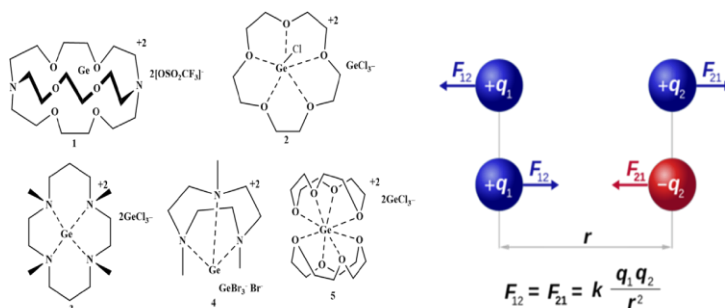
**References**

1. I. Rugar, P. A.; Staroverov, V. N.; Baines, K. M. A Cryptand-Encapsulated Germanium (II) Dication. *Science*, **2008**, *322*, 1360-1362.

- ii) **Presented a poster entitled** " Deciphering the Factors behind the Stability of Low Valent p-block Cations in Molecular Cages: A Computational Study" at **Science day, CSIR NCL Pune**, 26-27 Feb 2019.

Abstract

Low oxidation state cations and dications of groups 13 and 14 have received a lot of attention in recent years, partly owing to the fact that they are difficult to isolate synthetically. Baines and coworkers demonstrated, for the first time in 2008, the successful implementation of the polyether ligation approach to stabilize a “naked” germanium (II) di-cation using an electron rich [2.2.2]-cryptand.¹ Subsequent studies found that reacting differently sized crown ethers, such as [12]-crown-4, [15]-crown-5, and [18]-crown-6, with $\text{GeCl}_2 \cdot \text{dioxane}$ led to a range of caged Ge(II) mono- and dications. In all of these complexes, the interaction between the Ge(II) centre and donor atoms (N and O) of the enclosing cage was found to be predominantly non-covalent, electrostatic in nature. Why such unusual compounds remain stable after being formed is finally revealed through the current computational investigation. We have found that the role of the counter-ions in stabilizing the caged cations is significantly more important than had been previously realized. The presence of the counter-ion was seen to reduce the propensity of the cation to exit the cage. Moreover, *ab initio* molecular dynamics simulations have revealed that even if the cation leaves the cage, it is likely to re-enter it if the counter-ion is present in its vicinity. As such, the current work considerably expands on the understanding of the nature and stability of these important *p* block cationic caged compounds.



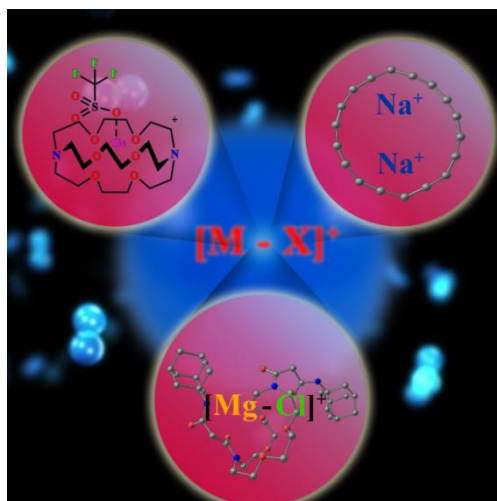
References

- Rupar, P. A.; Staroverov, V. N.; Baines, K. M. A Cryptand-Encapsulated Germanium (II) Dication. *Science*, **2008**, 322, 1360-1362.
- iii) **Presented a poster entitled** “Understanding Behaviour in Systems of Chemical and Biological Interest with the Remarkably Versatile "Cation in a Cage" Model” at **National Symposium on Convergence of Chemistry & Materials (CCM-2019)** BITS-Pilani, Hyderabad Campus, 17-18 December 2019.

Abstract

The current work showcases general principles at play in systems consisting of cations present inside molecular cages. Such systems, relevant to chemistry, biology and surface science, have been carefully investigated with computational methods. The important Ge(II) encapsulating cage systems have been studied first. The very fact that such compounds exist appears a near impossibility, given the highly reactive nature of the Ge(II) dication. Our studies reveal what really occurs in solution when such complexes are formed: the Ge(II) dications are actually present as $[\text{Ge-X}]^+$ (where X is the “non-coordinating” counterion employed in such systems) during entry and subsequent existence at the centre of the cage. Hence, what is actually present is a “pseudo monocation”. Interestingly, such pseudo monocation encapsulated cages are

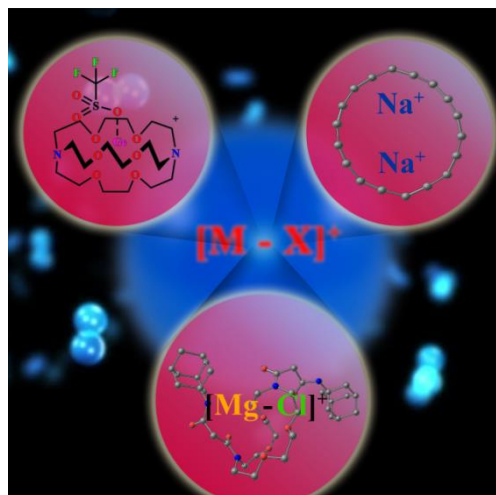
seen to be equally relevant in systems of biological interest, such as for dicationic *s* block based ionophores. In explaining such cases, the concept of “isoionicity” is introduced, demonstrating that the counterion coordinated dications are isoionic with a monocation, such as Li(I), isolated in the same ionophore. This leads to the realization that two monocations inside a cage represents a stable assembly, which, in turn, provides interesting insights into surface chemistry, helping to explain the recently reported, remarkable stabilization of a C₁₈ molecule on an NaCl surface.



- iv) **Presented a poster entitled**, “Understanding Behaviour in Systems of Chemical and Biological Interest with the Remarkably Versatile "Cation in a Cage" Model” at the **Conference on Recent Trends in Catalysis (RTC 2020)**, NIT Calicut, 26-29 Feb 2020.

Abstract

The current work showcases general principles at play in systems consisting of cations present inside molecular cages. Such systems, relevant to chemistry, biology and surface science, have been carefully investigated with computational methods. The important Ge(II) encapsulating cage systems have been studied first. The very fact that such compounds exist appears a near impossibility, given the highly reactive nature of the Ge(II) dication. Our studies reveal what really occurs in solution when such complexes are formed: the Ge(II) dications are actually present as [Ge-X]⁺ (where X is the “non-coordinating” counterion employed in such systems) during entry and subsequent existence at the centre of the cage. Hence, what is actually present is a “pseudo monocation”. Interestingly, such pseudo monocation encapsulated cages are seen to be equally relevant in systems of biological interest, such as for dicationic *s* block based ionophores. In explaining such cases, the concept of “isoionicity” is introduced, demonstrating that the counterion coordinated dications are isoionic with a monocation, such as Li(I), isolated in the same ionophore. This leads to the realization that two monocations inside a cage represents a stable assembly, which, in turn, provides interesting insights into surface chemistry, helping to explain the recently reported, remarkable stabilization of a C₁₈ molecule on an NaCl surface.



A copy of all SCI publication(s), emanating from the thesis, to be bound at the end of the thesis.



Cite this: *Phys. Chem. Chem. Phys.*,
2018, 20, 13845

What drives the H-abstraction reaction in bio-mimetic oxoiron-bTAML complexes? A computational investigation†

Anagh Mukherjee,^a Santanu Pattanayak,^a Sayam Sen Gupta^{id}*^b and Kumar Vanka^{id}*^a

Received 28th February 2018,
Accepted 10th April 2018

DOI: 10.1039/c8cp01333k

rsc.li/pccp

Monomeric iron-oxo units have been confirmed as intermediates involved in the C–H bond activation in various metallo-enzymes. Biomimetic oxoiron complexes of the biuret modified tetra-amido macrocyclic ligand (bTAML) have been demonstrated to oxidize a wide variety of unactivated C–H bonds. In the current work, density functional theory (DFT) has been employed to investigate the hydrogen abstraction (HAT) reactivity differences across a series of bTAML complexes. The cause for the differences in the HAT energy barriers has been found to be the relative changes in the energy of the frontier molecular orbitals (FMOs) induced by electronic perturbation.

Introduction

Numerous model complexes and functional mimics have been studied for the purpose of understanding the chemical reactions taking place in heme and nonheme based enzyme systems. One important question in this respect regards the H-atom transfer (HAT) reactivity difference during C–H abstraction in such systems. The existence of reactive intermediates, oxoiron(v) and oxoiron(iv) species, has been confirmed experimentally during the mechanistic elucidation of HAT, oxygen activation and oxygen-atom transfer (OAT) reactions.^{1–15} A plethora of theoretical models and functional mimics have been employed to study and explain the sluggish C–H abstraction reactivity of Cpd II (Compound II, oxoiron(iv) porphyrins) with respect to Cpd I (Compound I; oxoiron(iv) porphyrin π -cation radicals), with theoretical calculations yielding a 2.0–5.0 kcal mol^{–1} higher H-abstraction barrier for Cpd II mimics in comparison to the mimics of Cpd I.^{16–22} Theoretical insight into the HAT reactivity of a proposed nonheme oxoiron(v) and its one electron reduced intermediate indicates higher reactivity of the former but the inherent reason elucidating the reactivity difference was not provided.¹⁴ However, a related comparison between pure monomeric Fe^V(O) and Fe^{IV}(O), experimentally isolated with high purity, has not been reported in the literature

until recently. In a recent study, our group has compared the spectroscopy and H-atom abstraction activity of nonheme oxoiron(v) and oxoiron(iv) complexes of the biuret based tetra-amido macrocyclic ligand (bTAML) system (**1a** and **2**), which are isoelectronic to Cpd I and Cpd II, respectively (Fig. 2).^{23,24} **1a** showed a 2500-fold increase in reactivity in comparison to **2** when benzyl alcohol was employed as the substrate. However, the stability of both the oxoiron complexes is pH dependent: while **1a** is stable below pH 10, **2** can only be synthesized above pH 11. Hence, it was not possible to experimentally study the reactivity of both complexes at a common pH. Though HAT was found to be the principal rate influencing step for both the complexes (**1a** and **2**), a certain amount of quantum chemical tunnelling was also observed during the H-abstraction in **1a**.²³ Hence, the exact reason for the reactivity difference was not illustrated clearly in our earlier report. This provides the impetus for the current work. We have employed density functional theory (DFT) based calculations to evaluate the thermodynamics and kinetics that guide the HAT reactions involving the above mentioned complexes. This is significant, as a computational approach with a suitable solvent model yields an ideal common ground for a comparative study that was not possible in the experimental case, due to the pH related complexity mentioned earlier. For high valent metal-oxo moieties, the counteracting roles of the redox potential of the oxo species (E^0) and the basicity of the terminal oxo species, expressed in terms of the pK_a of the protonated oxo moiety (Fe–OH), affect the reactivity involving C–H abstraction reactions.^{25–31} These two factors, steering the formation of the H-abstraction transition state (TS), are expressed in terms of the thermodynamic parameter of bond dissociation energy (BDE). These two effects have been

^a Physical and Material Chemistry Division, CSIR-National Chemical Laboratory, Pune-411008, India. E-mail: k.vanka@ncl.res.in

^b Department of Chemical Sciences, Indian Institute of Science Education and Research (IISER) Kolkata, Mohanpur 741246, India

† Electronic supplementary information (ESI) available: Computational details, xyz coordinates of relevant structures and additional figures. See DOI: 10.1039/c8cp01333k

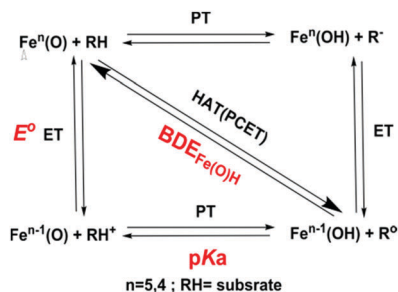


Fig. 1 Square scheme with associated thermodynamic parameters involved in HAT reactions.

further illustrated through the use of the thermodynamic square scheme shown in Fig. 1.

$$\text{BDE}_{\text{Fe(O)H}} = 1.37\text{p}K_{\text{a}} + 23.06E^0 + C$$

$E^0 = 1e^-$ is the reduction potential of the high valent iron-oxo species and $\text{p}K_{\text{a}}$ mentioned here refers to $\text{p}K_{\text{a}}$ of the $1e^-$ reduced Fe(O)H species. C is a constant dependent on the solvent.

Results and discussion

Neese and co-workers have associated the differential HAT reactivity for a series of hypothetical iron oxo and iron nitride complexes (exhibiting varying oxidation states on iron) with the unequal compensation of mutually opposing electron and proton affinities.³² Also, to explain the reactivity difference between the oxoiron(v) and oxoiron(IV) biuret-TAML species, it is important to know the $\text{p}K_{\text{a}}$ of both $\text{Fe}^{\text{IV}}(\text{OH})$ and $\text{Fe}^{\text{III}}(\text{OH})$. Although the $\text{p}K_{\text{a}}$ of $\text{Fe}^{\text{IV}}(\text{OH})$ can be experimentally measured (~ 10), it is not possible to experimentally measure the $\text{p}K_{\text{a}}$ of $\text{Fe}^{\text{III}}(\text{OH})$.²³ A significantly high $\text{p}K_{\text{a}}$ value of $\text{Fe}^{\text{III}}(\text{OH})$ could well offset the reported higher reactivity of **1a** over **2**. Keeping in mind that both the E^0 and $\text{p}K_{\text{a}}$ values are very important constituents in the overall thermodynamics governing a HAT process, we have performed calculations utilizing different density functionals, including the quantitative calculation of the $\text{p}K_{\text{a}}$ of $\text{Fe}^{\text{III}}\text{-OH}$. Thermodynamic calculations suggest a favourable hydrogen abstraction process for **1a** over **2** (Table 1).

Calculations confirm that the basicity of $\text{Fe}^{\text{III}}(\text{O})$ (calculated $\text{p}K_{\text{a}} = 54.35$, Table S1, ESI[†]) is indeed not sufficient to compensate for the large redox potential difference between **1a** and **2** ($\Delta E_{\text{exp}}^0 = 0.75$ V, $\Delta E_{\text{cal}}^0 = 1.68$ V) that contributes to a more

Table 1 Thermochemical free energy analysis for HAT reactions of **1a** and **2** in acetonitrile medium (C-PCM model) using benzyl alcohol as the substrate. All energies are reported in kcal mol^{-1}

Level of theory	1a	2
ΔG_{HAT} BP86/TZVP, LANL2DZ (Fe)	0.4	14.1
ΔG_{HAT} PBE/6-31G*, LANL2DZ (Fe)	1.1	16.4
ΔG_{HAT} M06-L/6-31G*, LANL2DZ (Fe)	-3.3	7.9

Table 2 The Gibb's free energy activation barrier (ΔG^{\ddagger}) and free energy change in initial electron transfer ($\Delta G_{\text{E.T}}$) or proton transfer ($\Delta G_{\text{P.T}}$) for the HAT step, using benzyl alcohol as the substrate for various bTAML complexes that have been investigated at the M06-L/6-311G*/LANL2DZ (Fe)//M06-L/6-311G*/LANL2DZ (Fe), C-PCM (acetonitrile) level of theory. All energies are reported in kcal mol^{-1}

Catalyst	ΔG^{\ddagger}	$\Delta G_{\text{E.T}}$	$\Delta G_{\text{P.T}}$
1a	13.9	51.5	58.9
1d	12.8	44.5	62.3
2	20.4	117.6	36.0

conductive HAT reaction for **1a**. Subsequently, an ~ 7.0 kcal mol^{-1} lowering of the HAT activation free energy barrier for **1a** in comparison to **2** (Table 2) was observed. The computed HAT activation barrier for **1a** (13.9 kcal mol^{-1}) without tunnelling correction indicates a minimal tunnelling influence on the HAT reactivity when it was compared to the experimental activation barrier ($\sim 15 \pm 1$ kcal mol^{-1}). Apart from this, the higher reactivity of the Cpd I mimics over their Cpd II counterparts has also been attributed to the spin state crossover phenomenon.²² The calculated free energy profile shows no spin state crossing en route to the TS for both **1a** and **2** (ESI[†]). This has also been illustrated previously while performing toluene oxidation with **1a**.³³ For **2**, the large triplet-quintet energy gap confines the HAT reaction pathway to a single spin state.²³ A closer look into the optimized transition state geometries reveals substantial differences in the bond lengths of the C-H bond in benzyl alcohol, the O-H bond in Fe-OH and the Fe-O bond (Fig. 3). Our calculations suggest significant scission of the C-H bond (1.45 Å) for $\text{Fe}^{\text{IV}}(\text{O})$, signifying a late transition state, since the BDE of $\text{Fe}^{\text{III}}\text{O-H}$ and benzyl alcohol is similar. The high basicity of O in $\text{Fe}^{\text{III}}(\text{O})$ in comparison to $\text{Fe}^{\text{IV}}(\text{O})$, as suggested by the weaker and longer $\text{Fe}^{\text{III}}(\text{O})$ bond relative to $\text{Fe}^{\text{IV}}(\text{O})$, leads to significant weakening of the C-H bond in the transition state.

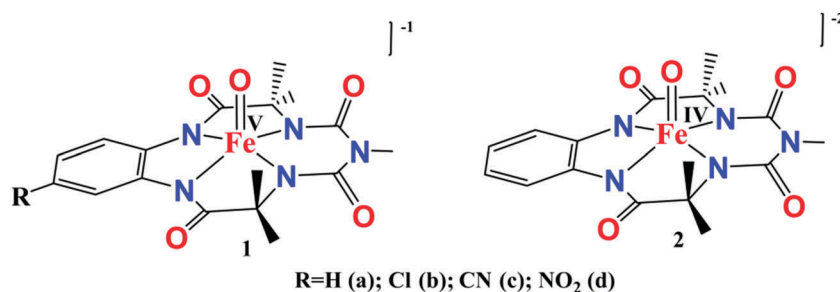


Fig. 2 Biuret TAML based iron complexes used for this study.

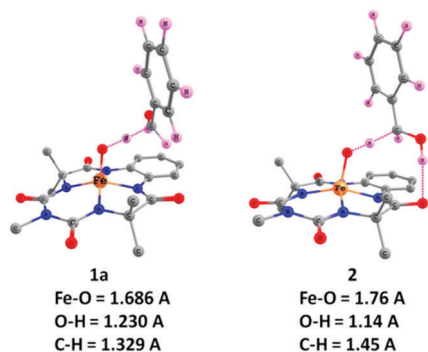


Fig. 3 Optimized TS geometries of C–H abstraction in benzyl alcohol employing **1a** and **2** at the M06-L/6-311G*/LANL2DZ (Fe)/C-PCM (acetonitrile) level of theory.

Apart from the thermodynamic stabilization of **1a** over **2**, we have also explained their HAT reactivity on the basis of frontier molecular orbital (FMO) theory. Subsequently, the effect of the overall charge of the complex was also investigated. A positive charge is supposed to generate an electrostatic field that would reduce the energies of both the electron acceptor orbital (EAO) and the electron donor orbital (EDO).^{34–37} Additionally, it has been outlined that even slight changes in the EAO–EDO energy gap value can modulate the activation barrier and subsequently alter the HAT reaction rates.³⁸ If in close structural proximity of the catalyst and the substrate, the overall charge modulates the energies of frontier molecular orbitals (FMOs), *i.e.*, reduces the energy gap between the EDO based on the substrate

(benzyl alcohol) and the $\pi^*(d_{xz}, d_{yz})$ metal centred EAO, the HAT barrier is lowered. Recently, in order to explain the reactivity difference between Cpd I and Cpd II, the overall effect of the relative charge differences in its mimicking system, the $[(4\text{-TMPyP})^+\text{Fe}^{\text{IV}}\text{O}]^{5+}\{4\text{-TMPyP} = 5,10,15,20\text{-tetrakis}(N\text{-methyl-4-pyridinium})\text{porphyrinate}\}$ complex and its one electron reduced analogue were investigated.¹⁸ The extra positive charge in the porphyrin ligand periphery stabilized both the metal based and the substrate orbitals and thus modulated the EDO–EAO energy gap. This observation explained the higher HAT reactivity of the poly-cationic Cpd I mimic over its Cpd II counterpart. Therefore, in order to observe analogous charge effects in the purely metal centred high valent oxoiron–bTAML systems (**1a** and **2**), differing only by a net single overall charge (–1 and –2, respectively), we have analyzed the electronic structure of the encounter complex of both **1a** and **2**. The encounter structures analyzed were taken to be such that there would be negligible chance of mixing between EAO and EDO, giving us a reliable model to study charge induced orbital stabilization (Fig. 4). The results show that an extra positive charge on **1a** has a more pronounced effect on the EAOs than EDOs due to the relative differences in proximity from the charge and shielding from the solvent.³ A higher downhill shift of EAO in **1a** lowers the energy gap between EAO and EDO ($\Delta E = 1.0$ eV) to a larger extent than in **2** ($\Delta E = 1.9$ eV) and hence explains the lowering of the HAT barrier height in **1a**.

The role of axially substituted donating groups in regulating the pK_a value of the high valent iron species in different heme proteins has been studied for various heme containing proteins.^{39,40} Therefore, as in the case with variable oxidation states, looking into

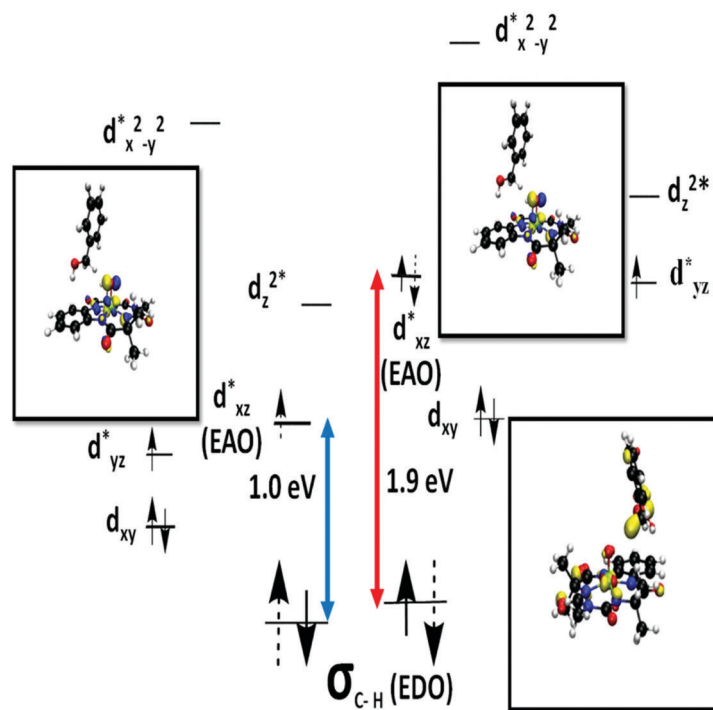


Fig. 4 Schematic diagram of the key MOs (EDO and EAO) at an O–H distance of 2.0 Å in the solution phase of the encounter complexes (the left and right side indicate the MOs of **1a** and **2**, respectively) at the BP86/def2-TZVPP, C-PCM (acetonitrile) level of theory. The dotted arrow indicates the trajectory of the electron transfers (π pathway). The MOs of the EAOs and the EDO are provided in the inset.

ligand structural variation effects on the counter balancing electron and proton transfer processes that regulate the HAT, and the subsequent effect on the overall reaction, is of utmost importance. Previously, experimental analysis in this direction has been performed on a metal hydride species.⁴¹ A ligand promoted electronic perturbation on a copper hydroxide unit has also been reported.⁴² Recently, a similar thermodynamic analysis on the hydrogen abstraction thermodynamics for a superoxo-dicopper complex has also been performed.⁴³ Ligand fields can be tuned to provide an ideal environment for C–H activation.⁴⁴ Recently, our group has developed a mechanism guided nitro substituted analogue (**1d**) of the previously reported **1a** complex for highly selective C–H bond activation.⁴⁵ Experiment (KIE) has suggested the HAT as the rate determining step. We have, therefore, analyzed the four equatorially located phenyl ring substituted bTAML sets that were supposed to perturb the overall electronics on the high valent iron centres in **1(a–d)**, thereby affecting the overall HAT reaction. To this end, we have calculated the thermodynamics facilitating the HAT reactions of the four substituted complexes of sets of oxoiron(v) complex using benzyl alcohol as the substrate, by employing different density functionals. This included the theoretical estimation of the pK_a and E values (Tables S1 and S2, ESI[†]), in order to understand the relative displacement of these two aspects that would result from structural alteration. Theoretical calculations can be a reliable alternative for quantitative estimation of the electrochemical reduction potential (E^0) and pK_a values; as a means to mitigate various possible inaccuracies in the experimental evaluations.^{46,47} Our calculations show a minimal change in the overall energetics of the HAT reactions across the ligand series, implying a “see-saw” equal and opposite compensation of an unfavourable factor with a favourable one and *vice versa*. A ligand with lower electron donating characteristics (like $-\text{NO}_2$) does not stabilize the high valent oxo species well enough, leading to a lower pK_a value, but this penalty is equally compensated for by a feasible electrochemical reduction potential (E^0). Quantitative calculation of pK_a and E^0 does not exactly coincide with the corresponding experimental values.²³ However, our approach sheds considerable light upon the underlying principles of the internal processes of HAT. Despite this internal compensation, a calculated difference in reaction rates across the electronically variable ligand series arises due to the subtle change in the relative barrier heights of the H-abstraction reaction. A thorough thermochemical analysis has already shown minimal energy changes on moving across variant substituents (**1a–1d**). However, **1d** exhibits a higher turn-over number (TON) than **1a** in their corresponding HAT reactions.⁴⁵ Calculations reveal a lower hydrogen atom abstraction barrier height for the nitro substituted catalysts (Table 2) in comparison to the unsubstituted catalysts. Very similar to the case pertaining to **1a** and **2**, axial and equatorial ligand mediated reactivity differences have also been adjudged to be due to the interaction between the EDO and EAO, which therefore also contributes significantly to the driving force of the reaction.^{48–54} An analysis of the electronic structures of the **1d** complex shows relative stabilization of the anti-bonding π^* EAO by almost 4.0 kcal mol⁻¹ in its

free structure, compared to that in **1a** (Table S4, ESI[†]). The strongly donating tetra-amido framework induces a strong equatorial ligand field, as shown by Mulliken and Natural Population Analysis (NPA) charge estimation (Table S3, ESI[†]). This reveals that substitution of the phenyl ring by an electron-withdrawing group somewhat reduces electron donation to the iron centre. This, in fact, directly leads to minimization of the anti-bonding interaction between the metal and ligand orbitals and indirectly reduces the electronic charge density on the metal centre, leading to a relative stabilization of the EAO, as a result of the charge effect. This effectively reduces the energy gap between EDO and EAO. Thus, this fine-tuning of the frontier orbital energy induced due to variable electronic environments plays a critical role in reducing the barrier height and thereby explains the decrease in the HAT activation barrier, going from **1a** to **1d**. Furthermore, in all the HAT cases that we have analysed, the question of a stepwise electron transfer/proton transfer (PT/ET) mechanism does not arise. Our calculations indicate a concerted HAT, as the free energy for initial electron or proton transfer ($\Delta G_{E,T}$ and $\Delta G_{P,T}$) is considerably higher than the free energy of activation for hydrogen abstraction in the reported HAT processes (Table 2). Thus, the concerted mechanism is a constant phenomenon in all our cases, irrespective of any electronic perturbation.

Computational details

All the calculations were carried out using the Gaussian09 suite of quantum chemical programs.⁵⁵ All the transition states were optimized at the (DFT)-M06-L/6-311G*-LANL2DZ (Fe) level of theory.^{56–58} The M06-L density functional accounts for the medium-range electron correlation effects⁵⁶ and has proven to be robust for the modeling of redox non-innocent ligands⁵⁹ and iron spin-state splitting energies.^{60,61} Also, it has been used for the quantum chemical analysis of the mechanism of water oxidation using a structurally similar iron-based TAML catalyst.⁶² The zero point vibrational energy corrections and thermal corrections were applied to the “bottom-of-the-well” values to obtain values for the Gibbs free energy at 298.15 K. Solvent effects were added using a conductor-like polarizable continuum model (C-PCM) using a dielectric continuum of acetonitrile ($\epsilon = 37.6$).^{63,64} M06-L, PBE⁶⁵ and BP86⁶⁶ levels of theory were employed for evaluating the thermo-chemistry involving the HAT reactions. Furthermore, all the pK_a and E^0 values were calculated at the B3LYP/6-31G*-LANL2DZ (Fe)//B3LYP/6-31G*-LANL2DZ (Fe) level of theory using a dielectric continuum of water ($\epsilon = 80.1$) employed *via* a C-PCM solvation model.⁶⁷ For analyzing the electronic structures of our reported complexes, the BP86/def2-TZVPP level of theory was used. This is because this particular functional and basis set combination produces a better spin state ordering and electron distribution, as has been demonstrated by Nam *et al.* before.⁶⁸ Mulliken and natural-population analysis (NPA) atomic partial charges were calculated for the mentioned bTAML catalysts to understand the intramolecular charge distribution. Mulliken charge analysis was carried out at three different levels of theory

in combination with three basis sets to get a better viewpoint. MO images were created from the Gaussian outputs using the VMD software.⁶⁹

Conclusions

In summary, we have extended the beneficial effect of an extra positive charge on the observed HAT reactivity involving heme based systems to a pair of non-isoelectronic nonheme systems. Also, looking at the effect of ligand modulation across a set of bTAML complexes (**1a–1d**), there is negligible change in hydrogen atom transfer (HAT) energetics, due to internal balancing between the pK_a and E^0 values. The difference in the HAT activation barriers arises due to modulation of frontier molecular orbitals (FMOs), because of the differential electronic environments of the ligand systems. Calculations suggest that FMO energies are more affected by the charge on the system than by ligand modulation. The current work therefore provides a comprehensive, theoretical analysis of the HAT process, and it is expected that the insights gained will aid in the rational design of efficient biomimetic nonheme complexes for C–H abstraction.

Conflicts of interest

The authors declare no competing financial interests.

Acknowledgements

A. M. and S. P. acknowledge UGC-New Delhi for fellowships. The authors thank Tamal Das (CSIR-NCL), Turbasu Sengupta (CSIR-NCL), Mrityunjay Tiwari (CSIR-NCL) and Mursaleem Ansari (IIT Bombay) for help and fruitful discussions. K. V. thanks the Department of Science and Technology (DST) for funding.

Notes and references

- I. G. Denisov, T. M. Makris, S. G. Sligar and I. Schlichting, *Chem. Rev.*, 2005, **105**, 2253.
- L. Que and W. B. Tolman, *Nature*, 2008, **455**, 333.
- J. Rittle and M. T. Green, *Science*, 2010, **330**, 933.
- J. T. Groves, In *Cytochrome P450: Structure, Mechanism, and Biochemistry*, ed. Ortiz de Montellano, P. R., Kluwer-Academic/Plenum, New York, 3rd edn, 2005, p. 183.
- P. R. O. de Montellano, *Chem. Rev.*, 2010, **110**, 932.
- M. Sono, M. P. Roach, E. D. Coulter and J. H. Dawson, *Chem. Rev.*, 1996, **96**, 2841.
- W. Nam, *Acc. Chem. Res.*, 2007, **40**, 522.
- J. Hohenberger, K. Ray and K. Meyer, *Nat. Commun.*, 2012, **3**, 720.
- M. Costas, M. P. Mehn, M. P. Jensen and L. Que, *Chem. Rev.*, 2004, **104**, 939.
- H. Fujii, *Coord. Chem. Rev.*, 2002, **226**, 51.
- H. P. Hersleth, U. Ryde, P. Rydberg, C. H. Gorbitz and K. K. J. Andersson, *Inorg. Biochem.*, 2006, **100**, 460.
- M. Puri and L. Que, *Bull. Jpn. Soc. Coord. Chem.*, 2016, **67**, 10.
- W. N. Oloo and L. Que, *Acc. Chem. Res.*, 2015, **48**, 2612.
- P. Comba, M. Maurer and P. Vadivelu, *J. Phys. Chem. A*, 2008, **112**, 13028.
- W. N. Oloo, R. Banerjee, J. D. Lipscomb and L. Que, *J. Am. Chem. Soc.*, 2017, **139**, 17313.
- A. Altun, S. Shaik and W. Thiel, *J. Am. Chem. Soc.*, 2007, **129**, 8978.
- L. Tahsini, M. Bagherzadeh, W. Nam and S. P. de Visser, *Inorg. Chem.*, 2009, **48**, 6661.
- G. Ricciardi, E. J. Baerends and A. Rosa, *ACS Catal.*, 2016, **6**, 568.
- J. F. Berry, S. D. George and F. Neese, *Phys. Chem. Chem. Phys.*, 2008, **10**, 4361.
- O. Y. Lyakin, K. P. Bryliakov and E. Talsi, *Inorg. Chem.*, 2011, **50**, 5526.
- W. N. Oloo, Y. Feng, S. Iyer, S. Parmelee, G. Xue and L. Que, *New J. Chem.*, 2013, **37**, 3411.
- S. R. Bell and J. T. Groves, *J. Am. Chem. Soc.*, 2009, **131**, 9640.
- S. Pattanayak, A. Jasniewski, A. Rana, A. Draksharapu, K. K. Singh, A. Weitz, M. Hendrich, L. Que, A. Dey and S. Sen Gupta, *Inorg. Chem.*, 2017, **56**, 6352.
- M. Ghosh, K. K. Singh, C. Panda, A. Weitz, M. P. Hendrich, T. J. Collins, B. B. Dhar and S. Sen Gupta, *J. Am. Chem. Soc.*, 2014, **136**, 9524.
- A. S. Borovik, *Chem. Soc. Rev.*, 2011, **40**, 1870.
- J. J. Warren, T. A. Tronic and J. M. Mayer, *Chem. Rev.*, 2010, **110**, 6961.
- D. Dhar and W. B. Tolman, *J. Am. Chem. Soc.*, 2015, **137**, 1322.
- J. M. Mayer and I. J. Rhile, *Biochim. Biophys. Acta, Bioenerg.*, 2004, **1655**, 51.
- J. M. Mayer, *Annu. Rev. Phys. Chem.*, 2004, **55**, 363.
- F. G. Bordwell, J. P. Cheng and J. A. Harrelson Jr, *J. Am. Chem. Soc.*, 1988, **110**, 1229.
- J. M. Mayer, *Acc. Chem. Res.*, 2011, **44**, 36.
- C. Geng, S. Ye and F. Nesse, *Dalton Trans.*, 2014, **43**, 6079.
- K. K. Singh, M. K. Tiwari, B. B. Dhar, M. Ghosh, C. Panda, A. Weitz, M. P. Hendrich, B. B. Dhar, K. Vanka and S. Sen Gupta, *Inorg. Chem.*, 2015, **54**, 1535.
- L. Bernasconi and E. J. Baerends, *Eur. J. Inorg. Chem.*, 2008, 1672.
- L. Bernasconi and E. J. Baerends, *J. Am. Chem. Soc.*, 2013, **135**, 8857.
- A. Kazaryan and E. J. Baerends, *ACS Catal.*, 2015, **5**, 1475.
- P. C. Andrikopoulos, C. Michel, S. Chouzier and P. Sautet, *ACS Catal.*, 2015, **5**, 2490.
- S. Ye, C. Y. Geng, S. Shaik and F. Neese, *Phys. Chem. Chem. Phys.*, 2013, **15**, 8017.
- T. H. Yosca, J. Rittle, C. M. Krest, E. L. Onderko, A. Silakov, J. C. Calixto, R. K. Behan and M. T. Green, *Science*, 2013, **342**, 825.
- T. H. Yosca, R. K. Behan, C. M. Krest, E. L. Onderko, M. C. Langston and M. T. Green, *J. Am. Chem. Soc.*, 2014, **136**, 9124.

- 41 M. Tilset in *Electron Transfer in Chemistry*, ed. Balzani, V., Wiley-VCH Verlag GmbH, Weinheim, Germany, 2001, p. 677.
- 42 D. Dhar, G. M. Yee, A. D. Spaeth, D. W. Boyce, H. Zhang, B. Dereli, C. J. Cramer and W. B. Tolman, *J. Am. Chem. Soc.*, 2016, **138**, 356.
- 43 N. Kindermann, C. J. Gunes, S. Dechert and F. Meyer, *J. Am. Chem. Soc.*, 2017, **139**, 9831.
- 44 L. Bernasconi, M. J. Louwerse and E. J. Baerends, *Eur. J. Inorg. Chem.*, 2007, 3023.
- 45 M. Ghosh, S. Pattanayak, B. B. Dhar, K. K. Singh, C. Panda and S. Sen Gupta, *Inorg. Chem.*, 2017, **56**, 10852.
- 46 A. V. Marenich, J. Ho, M. L. Coote, C. J. Cramer and D. G. Truhlar, *Phys. Chem. Chem. Phys.*, 2014, **16**, 15068.
- 47 B. Thapa and H. B. Schlegel, *J. Phys. Chem. A*, 2016, **120**, 5726.
- 48 S. Shaik, W. Lai, H. Chen and Y. Wang, *Acc. Chem. Res.*, 2010, **43**, 1154.
- 49 W. Lai, C. Li, H. Chen and S. Shaik, *Angew. Chem., Int. Ed.*, 2012, **51**, 5556.
- 50 J. C. Schoneboom, S. Cohen, H. Lin, S. Shaik and W. Thiel, *J. Am. Chem. Soc.*, 2004, **126**, 4017.
- 51 R. Latifi, M. Bagherzadeh and S. P. de Visser, *Chem. – Eur. J.*, 2009, **15**, 6651.
- 52 L. W. Chung, X. Li, H. Hirao and K. Morokuma, *J. Am. Chem. Soc.*, 2011, **133**, 20076.
- 53 P. K. Das, S. Chatterjee, S. Samanta and A. Dey, *Inorg. Chem.*, 2012, **51**, 10704.
- 54 C. Y. Geng, S. Ye and F. Neese, *Angew. Chem., Int. Ed.*, 2010, **49**, 5717.
- 55 M. J. Frisch, G. W. Trucks, H. B. Schlegel, G. E. Scuseria, M. A. Robb, J. R. Cheeseman, G. Scalmani, V. Barone, B. Mennucci, G. A. Petersson, H. Nakatsuji, M. Caricato, X. Li, H. P. Hratchian, A. F. Izmaylov, J. Bloino, G. Zheng, J. L. Sonnenberg, M. Hada, M. Ehara, K. Toyota, R. Fukuda, J. Hasegawa, M. Ishida, T. Nakajima, Y. Honda, O. Kitao, H. Nakai, T. Vreven, J. A. Montgomery Jr, J. E. Peralta, F. Ogliaro, M. Bearpark, J. J. Heyd, E. Brothers, K. N. Kudin, V. N. Staroverov, R. Kobayashi, J. Normand, K. Raghavachari, A. Rendell, J. C. Burant, S. S. Iyengar, J. Tomasi, M. Cossi, N. Rega, J. M. Millam, M. Klene, J. E. Knox, J. B. Cross, V. Bakken, C. Adamo, J. Jaramillo, R. Gomperts, R. E. Stratmann, O. Yazyev, A. J. Austin, R. Cammi, C. Pomelli, J. W. Ochterski, R. L. Martin, K. Morokuma, V. G. Zakrzewski, G. A. Voth, P. Salvador, J. J. Dannenberg, S. Dapprich, A. D. Daniels, Ö. Farkas, J. B. Foresman, J. V. Ortiz, J. Cioslowski and D. J. Fox, *Gaussian 09, revision B.01*, Gaussian, Inc., Wallingford, CT, 2009.
- 56 Y. Zhao and D. G. Truhlar, *J. Chem. Phys.*, 2006, **125**, 194101.
- 57 Y. Zhao and D. G. Truhlar, *Acc. Chem. Res.*, 2008, **41**, 157.
- 58 Y. Zhao and D. G. Truhlar, *Theor. Chem. Acc.*, 2007, **120**, 215.
- 59 P. Milko and M. A. Iron, *J. Chem. Theory Comput.*, 2014, **10**, 220.
- 60 (a) K. R. Delle Chiaie, A. B. Biernesser, M. A. Ortuno, B. Dereli, D. Iovon, M. J. T. Wilding, B. Li, C. J. Cramer and J. A. Byers, *Dalton Trans.*, 2017, **46**, 12971; (b) M. A. Ortuno, B. Dereli, K. R. Delle Chiaie, A. B. Biernesser, M. Qi, J. A. Byers and C. J. Cramer, *Inorg. Chem.*, 2018, **57**, 2064.
- 61 (a) M. Swat, *Chem. Phys. Lett.*, 2013, **580**, 166; (b) T. R. Rensen, J. R. Nitschke, L. Gagliardi and C. J. Cramer, *Phys. Chem. Chem. Phys.*, 2014, **16**, 10620; (c) P. Verma, Z. Varga, J. E. M. N. Klein, C. J. Cramer, L. Que Jr and D. G. Truhlar, *Phys. Chem. Chem. Phys.*, 2017, **19**, 13049.
- 62 Z. Ertem, L. Gagliardi and C. J. Cramer, *Chem. Sci.*, 2012, **3**, 1293.
- 63 V. Barone and M. Cossi, *J. Phys. Chem. A*, 1998, **102**, 1995.
- 64 M. Cossi, N. Rega, G. Scalmani and V. Barone, *J. Comput. Chem.*, 2003, **24**, 669.
- 65 J. P. Perdew, K. Burke and M. Ernzerhof, *Phys. Rev. Lett.*, 1997, **78**, 1396.
- 66 A. D. Becke, *Phys. Rev. A: At., Mol., Opt. Phys.*, 1988, **38**, 3098.
- 67 (a) J. P. Perdew, S. H. Chevary, K. A. Vosko, K. A. Jackson, M. R. Pederson, D. J. Singh and C. Fiolhais, *Phys. Rev. B: Condens. Matter Mater. Phys.*, 1992, **46**, 6671; (b) J. P. Perdew, S. H. Chevary, K. A. Vosko, K. A. Jackson, M. R. Pederson, D. J. Singh and C. Fiolhais, *Phys. Rev. B: Condens. Matter Mater. Phys.*, 1993, **48**, 4978; (c) J. P. Perdew, K. Burke and Y. Wang, *Phys. Rev. B: Condens. Matter Mater. Phys.*, 1996, **54**, 16533; (d) C. Adamo and V. Barone, *J. Chem. Phys.*, 1998, **108**, 664; (e) A. D. Becke, *J. Chem. Phys.*, 1993, **98**, 5648; (f) C. Lee, W. Yang and R. G. Parr, *Phys. Rev. B: Condens. Matter Mater. Phys.*, 1988, **37**, 785; (g) C. C. Roothan, *J. Rev. Mod. Phys.*, 1960, **3**, 179; (h) R. McWeeny and G. Dierksen, *J. Chem. Phys.*, 1968, **49**, 4852; (i) J. A. Pople and R. K. Nesbet, *J. Chem. Phys.*, 1954, **22**, 571.
- 68 S. Hong, S. Jang, K. B. Cho and W. Nam, *Chem. Commun.*, 2016, **52**, 12968.
- 69 W. Humphrey, A. Dalke and K. Schulten, *J. Mol. Graphics*, 1996, **14**, 33.

Unraveling the Hidden Role of the Counteranion in “Cation in a Cage” Systems

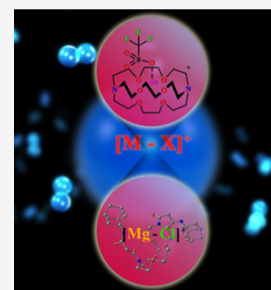
Anagh Mukherjee, Siddharth Ghule, Mrityunjay K. Tiwari, and Kumar Vanka*

 Cite This: *J. Phys. Chem. A* 2020, 124, 8040–8049 Read Online

ACCESS |

 Metrics & More Article Recommendations Supporting Information

ABSTRACT: The current work showcases general principles at play in systems consisting of cations present inside molecular cages. Such systems, relevant to chemistry and biology, have been carefully investigated by computational methods. The important Ge(II)-encapsulating cage systems have been studied first. The very fact that such compounds exist appears highly unlikely, given the highly reactive nature of the Ge(II) dication. Our studies reveal what really occurs in solution when such complexes are formed: the Ge(II) dications are actually present as $[\text{Ge}-\text{X}]^+$ (where X is the “non-coordinating” counterion employed in such systems) during entry and subsequent existence at the center of the cage. Hence, what is actually present is a “pseudomonocation”. Interestingly, such pseudomonocation-encapsulated cages are seen to be equally relevant in systems of biological importance, such as for dicationic s block-based ionophores. In explaining such cases, the concept of “isoionicity” is introduced, demonstrating that the counterion-coordinated dications are isoionic with a monocation, such as Li(I), isolated in the same ionophore.



1. INTRODUCTION

A model that deserves a closer look is that of a cation inside an enclosing molecular-caged structure. This chemical system is of relevance to several important areas of chemistry, biology, and surface science. For instance, pendant molecular cage structures in polymer electrolyte membranes (PEMs) serve to transport protons from the anode to the cathode in state-of-the-art fuel cells;¹ a crown ether is seen to flit from one cationic polypeptide site to the next, serving as a relevant model for understanding the dynamics in biology² and the progress of a cation through an ion channel can be visualized as its passage through a successive series of molecular cages linked together. The current theoretical and computational investigation is the first to carefully look at this “cation in a cage” model across different disciplines and finds surprising insights with it (i) in chemistry: in cages containing group 14 dications,³ the understanding of which helps to explain phenomena (ii) in biology: for the behavior of dications of groups 1 and 2 encased in ionophores.

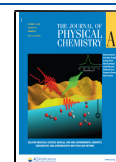
In chemistry, low oxidation state cations and dications of heavier group 13 and 14 elements have received a significant amount of attention in recent years.⁴ Of these, the most interesting family consists of single, isolated, and charged species surrounded by a cage, with no covalent interactions between the central cation and the surrounding cage. The genesis of this field lies in the discovery of the Ge(II)-cryptand system by Baines and co-workers in 2008.⁵ The Ge(II) center is encapsulated within the cryptand and assumed to be stabilized by numerous weak donor-acceptor interactions because of the presence of six oxygen and two nitrogen atoms in the cavity. Following their discovery, many more such complexes have been reported, with various ligands

acting as support to the central Ge(II) cation and possessing the same property as described before (complexes 1–4, Figure 1). These include [12]-crown-4 and [18]-crown-6.^{6,7} Related compounds with 1,4,7-triazacyclononane (TACN) and 1,4,8,11-tetramethyl-1,4,8,11-tetraazacyclotetradecane (cyclam) ligands have also been reported (Figure 1).⁷ Moreover, the field has further expanded to include other group 13 and 14 elements.⁴ In these systems (1–4), the primary interaction between the Ge(II) center and donor atoms (N and O) is primarily noncovalently electrostatic, as had been pointed out in the original report by Baines and co-workers,⁵ and also experimentally confirmed by the same group.⁸ This is quite interesting, as the central germanium has a single-filled orbital and three empty orbitals, thereby making it a highly reactive species. Therefore, why does it stay isolated at the center of the cage, interacting only through electrostatic means with the atoms of the cage and forgoing almost any covalent interactions altogether? An even more interesting question pertains to the general expectation that had been observed about these systems when they were first reported nearly 12 years back: if they could be employed as the starting point for various synthetic routes because of the ready availability of a highly reactive naked germanium dication that could be subjected to remote bond activation reactions on a variety of

Received: July 31, 2020

Revised: September 7, 2020

Published: September 7, 2020



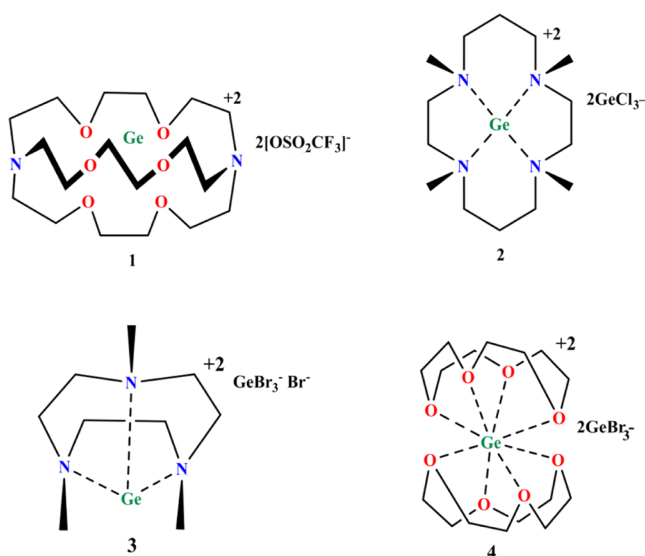


Figure 1. Cryptand- and crown ether-stabilized Ge(II) with their counteranions, as isolated in the crystal structure.

substrates.⁹ Such an expectation has not been realized. This is not because of steric constraints because the encapsulating cage provides ample space for the approach and departure of substrates. The absence of such chemistry for these set of compounds may point to the possibility that the germanium dication may not be as readily available as has been considered.

A further question that indeed needs asking is the apparent ease by which such compounds have been reported to have formed. Most reports state a very high yield for these complexes.^{5–7} How does this come about? If the germanium dication were to enter unassisted into the cage, it would come into close proximity with the cage atoms while doing so, and this would lead to chemical interactions between the highly unsaturated germanium center and the cage atoms, which should result in the destruction of the cage. Indeed, as we will demonstrate in the **Results and Discussion** section, room-temperature *ab initio* molecular dynamics (AIMD) simulations indicate that such decomposition reactions would occur in a matter of picoseconds. In other words, systems that show a naked germanium cation sitting unassisted in the center of a cage (complexes 1–4, **Figure 1**) should have been difficult to synthesize and should have only been formed in low yields, if at all. However, they are formed in very high yields. What accounts for this?

The current computational study, with high-level static density functional theory (DFT), as well as AIMD simulations, seeks to address these issues, focusing on compounds 1–4. What is revealed is the hidden role played by the counterions: it is seen that the counterions facilitate the entry of such caged dications inside their encapsulating cages and ensure their subsequent stability. This insight is useful because it then allows us to understand how one could employ strategies to make the group 14 dications exist in isolation at the center of the cage, thereby opening up the possibility of further synthetic transformation of potential substrates at the cationic centers.

Furthermore, we have taken the insights gained from the studies of these group 14 complexes and looked across the periodic table into other systems, such as the biologically relevant dicationic group 2 ionophores: Mg–ionophore VII and calcimycin, and shown that factors similar to group 14

dications are in play in these systems as well. What is especially important in these studies is the realization that the counterion-coordinated dication systems {such as [Mg–Cl]⁺} have a net charge at the center that matches almost exactly the charge of a lithium monocation: Li(I) at the center of the same cage. The counterion-coordinated dication is, therefore, like a “pseudomonocation”, or, in other words, it is isoionic with a monocation. This isoionic analogy has relevance because it provides a possible explanation for the unusual similarity that has been observed in the behavior of Mg(II) and Li(I) cations in biology.¹⁰ A further important consequence is that the isoionic analogy allows us to postulate that two monocations inside the same cage represent a stable configuration, by looking at an experimentally identified structure where two counterion-coordinated dications (*i.e.* two “pseudomonocations”) were present together in a valinomycin cage.¹¹

Hence, the current computational exploration of cation encapsulated cage systems reveals the hidden role of counterions, introduces the isoionic analogy, and exploits them to shed light on the behavior of important caged systems in chemistry, as well as in biology.

2. METHODS

All the DFT calculations were carried out using the Gaussian 09 suite of quantum-chemical programs.¹² All Ge(II) complex geometries were optimized at the M06-2X/6-311G(d,p) level of theory.¹³ All the ionophore complex geometries were optimized at the M06-2X/6-31G(d)//M06-2X/6-311G(d,p) level of theory. This was done keeping the computational expense in mind because of the larger size of the ionophore complexes. Frequency calculations on all the stationary points were carried out to characterize the nature of each stationary point and also to evaluate the respective molecular entropic terms. The solvent effect was added through the conductor-like polarization continuum model using the actual solvent, as used for all the Ge(II) complex geometries considered, and using water as a solvent for the described ionophore complexes.^{14,15} Natural bond orbital (NBO) charges have been used to calculate the net electrostatic force on the dicationic germanium center.¹⁶ All the Wiberg bond indices (WBIs) reported are the maximum values reported between Ge(II) and the heteroatoms (N, O, and S), that is, if there are four Ge(II)–O interactions, for instance, in a particular cage, the WBI indicating the greatest interaction has been reported.

The binding energies of the all the Ge(II) complexes described in this work were calculated as follows

$$\Delta G(\text{binding}) = G_{\text{Ge(II) cage}} - G_{\text{cage}} - G_{\text{Ge(II)}}$$

The net force on Ge(II) was calculated using Coulomb’s law, where the electrostatic force is given by

$$F_{\text{electrostatic}} = (1/4\pi\epsilon) \times (q_{\text{Ge(II)}}q_{\text{atom}})/(r_{\text{Ge(II)-atom distance}})^2$$

where $q_{\text{Ge(II)}}$ is the charge on the Ge(II) atom, q_{atom} is the charge on other atoms, $r_{\text{Ge(II)-atom distance}}$ is the distance, and ϵ is the dielectric constant for the respective solvents between Ge(II) and other atoms. The charge was assigned from the NBO charge analysis. A vector summation was done at the Ge(II) center in order to determine the net electrostatic force at Ge(II) because of the presence of cage atoms. Likewise, the electrostatic energy was calculated from

$$E_{\text{electrostatic}} = (1/4\pi\epsilon) \times (q_{\text{Ge(II)}}q_{\text{atom}})/(r_{\text{Ge(II)-atom distance}})$$

The code to calculate the force and the energy was written in the Python language.

Isotropic NMR shielding tensors were calculated at the M06-2X/6-311G(d,p) level of theory in Gaussian 09 using the gauge-independent atomic orbital method.¹⁷ The AIMD simulations were performed with the TeraChem 1.9 quantum chemistry and AIMD software packages^{18–24} using the B3LYP density functional^{25–33} and the def2-SVP basis set to calculate the Born–Oppenheimer potential energy surface. A different functional is employed when using TeraChem software because the M06-2X functional has not been implemented in this suite of software. A slightly lower quality basis set has been employed in this case keeping the computational expense of the full quantum chemical molecular dynamics simulations in mind. The equations of motion were integrated numerically using Langevin dynamics with an equilibrium temperature of 300 K (also the starting temperature). The electronic state of the germanium dication was considered to be a singlet, or a closed shell configuration, in the AIMD simulations. Also, all our static DFT calculations have been done considering the singlet germanium dication as the ground state. The triplet state requires the excitation of one electron from the 4s orbital to the 4p orbital. As the energy gap between 4s and 4p is considerably large, the former phenomenon should be highly unfeasible. Hence, this should make any involvement of triplet electronic state highly unfavorable.

In order to further ascertain the predominantly noncovalent electrostatic interaction present in the systems described in this report, noncovalent interaction (NCI) regions have been plotted (Figures S15 and S16, Supporting Information) using the nciplot-3.0 suite of programs.³⁴

3. RESULTS AND DISCUSSION

3.1. Group 14 Chemistry. As discussed in the Introduction, it is expected that there exist only noncovalent electrostatic interactions between the Ge(II) dication and the encapsulating cage in the considered cases 1–4 (see Figure 1). This has been verified as follows: for cases 1–4, an almost 100.0% 4s orbital with minimal orbital mixing was obtained by NBO analysis (Table S1, Supporting Information), and the plotting of NCI for these systems (1–4) exemplifies (Figure S15, Supporting Information) the fact that the electrostatic interaction is the primary factor between the molecular cages and their cationic hosts. Hence, as discussed in the Introduction, we have first attempted to understand whether the germanium dication could enter unassisted into the cages (1–4) and stay stabilized. To this end, we have employed AIMD simulations. What was first investigated were AIMD simulations where the bare Ge(II) dication was kept on the outside of the cage and a counterion was located on the opposite side. The simulations were done for the cases 1–4 discussed in the Introduction. For every case, a boundary radius of 9.0 Å was employed, in order to ensure that the Ge(II) dication did not fly away from the cage altogether during the AIMD simulations, a phenomenon known as the “evaporation” event. Figure 2 shows snapshots of the results for case 1, which are very revealing. It is seen that in the absence of coordination to the counterion, the Ge(II) dication begins interacting with the cage, extracting a hydrogen (as hydride) from it and thus initiating the process of destroying it (see Figure 2). The fact that the H-abstraction happens as a hydride

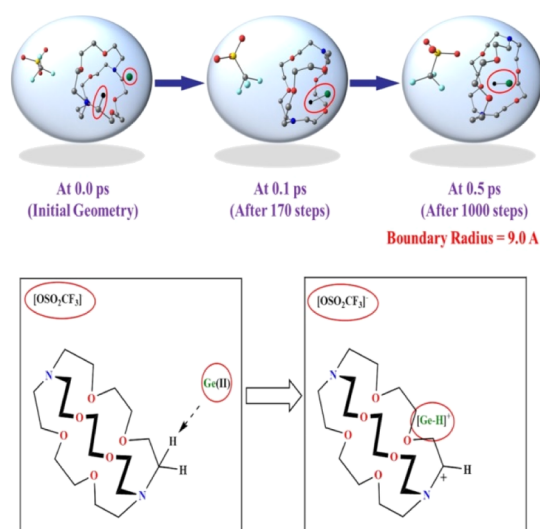


Figure 2. Snapshots depicting the trajectory of AIMD simulations done for case 1, where the Ge(II) and the counteranion, $[\text{OSO}_2\text{CF}_3]^-$, remain unattached. A red circle encloses Ge(II) as well as the H atom abstracted by it during the course of the simulation. Color scheme: germanium = deep green, oxygen = red, carbon = gray, hydrogen = black, nitrogen = blue, sulfur = yellow, and fluorine = sky blue. Hydrogen atoms not pertinent to the reaction have been removed for clarity.

anion and not as a H-radical is proved by the net NPA charge of the $[\text{Ge}-\text{H}]^+$ moiety. A net NPA charge of 0.69 in the complex proves that the $[\text{Ge}-\text{H}]^+$ moiety is a monocationic species. This occurs after only a short time has elapsed in the course of the AIMD simulations. A movie file, labeled **Movie S1**, is provided in the Supporting Information, which captures the decomposition of the cage by the dication, a phenomenon that occurs in a matter of picoseconds. Though Figure 2 shows this decomposition process for the original Baines system, Ge(II) with triflate ($\text{C}_{20}\text{H}_{36}\text{F}_6\text{GeN}_2\text{O}_{12}\text{S}_2$) and the cryptand cage, and the same was seen to occur for all the other cases 2–4 as well. The corresponding figures for cases 2–4 are shown in Figures S1, S3, and S5 in the Supporting Information. The AIMD simulations therefore make clear that if the Ge(II) dication were to enter the cage in a naked, unassisted fashion, its reactive nature, as evidenced by its three empty orbitals and unsaturation, would lead to unwanted side reactions and cage decomposition. However, as mentioned earlier, very high yields have been reported for the formation of the encapsulated Ge(II) systems, which suggests that such side reactions are completely absent during the formation of the caged Ge(II) compounds.

In order to explain this apparent contradiction, we hypothesized that the reactive behavior of the Ge(II) dication could be reduced if it were to be coordinated with one of the counterions present in solution when it approached the cage. In order to test this hypothesis, AIMD simulations were done for all the cases (1–4), with the Ge(II) dication associated with the corresponding counterion in each case, and kept as before in the vicinity of the cage. The results are shown for case 1 in Figure 3 and in Figures S2, S4, and S6 for cases 2–4, respectively, in the Supporting Information. Interestingly, what was seen now is that, for every case, the Ge(II)-counterion entered without interacting with the cage and settled at the center. A movie file, labeled **M2**, is provided in the Supporting Information capturing the entry of the dication into the cage.

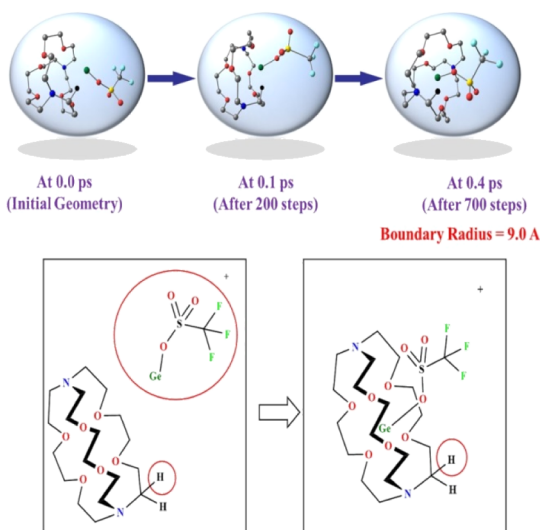


Figure 3. Snapshots depicting the trajectory of AIMD simulations for case 1, where Ge(II) and the counteranion (${}^{-}\text{OSO}_2\text{CF}_3$) remain attached. Color scheme: germanium = deep green, oxygen = red, carbon = gray, hydrogen = black, nitrogen = blue, sulfur = yellow, and fluorine = sky blue. Hydrogen atoms not pertinent to the reaction have been removed for clarity.

Hence, what the results indicate is that the reactivity of the Ge(II) dication is tamed by the presence of a counterion, and this not only stops unwanted side reactions from taking place but also ensures that the Ge(II) dication enters into the cage and settles at its center.

For case 4, an interesting deviation was observed. The counteranion (GeBr_3^{-} in this case) ferries the dicationic germanium into the sandwich crown ether cage during the course of the simulations, as was done by the other counterions for the other cases. However, the counteranion does not itself enter the cage in this case. What happens instead is that one of the two crown ether moieties that makes up the cage reorients itself to accommodate the Ge(II) (see Figure S6 in the Supporting Information). This is an exception for the other cases where the counteranion enters into the cage along with Ge(II).

For all the other three cases (1–3), AIMD simulations show that the counteranion remains coordinated to the Ge(II) even after its entry into the cage. The reason for this becomes clear from static DFT calculations, which show that the $[\text{Ge(II)-counteranion}]^{+}$ species inside the cage represents a stable structure. Indeed, it is seen that this complex is more stable than the corresponding system where the counteranion is stationed as a noncoordinating species at a much greater distance (see Table 1 and Figure S11 in the Supporting Information). This was observed for all the cases considered, with the exception of case 4, where the counteranion (GeBr_3^{-})

Table 1. Thermodynamic Parameters of Counterion Binding of the Respective Counteranions in Solution at the M06-2X/6-311G(d,p)//M06-2X/6-311G(d,p) Level of Theory

molecule	solvent	ΔG (kcal/mol)	counterion (C.I)
1	tetrahydrofuran	−8.8	OTf^{-}
2	dichloromethane	−4.2	GeCl_3^{-}
3	acetonitrile	−7.9	Br^{-}

left the Ge(II) dication center during the optimization process (Figure S12 in the Supporting Information). (For case 2, the Ge(II)-counteranion distance is ~ 3.70 Å, but this still represents a much closer distance than in the crystal structure.) This result thus explains why the counteranion remains with the dication for cases 1–3 in the AIMD simulations and also why the counteranion completely detaches from the Ge(II) cation after thrusting it into the molecular cage in case 4. Therefore, in almost all the cases considered, the calculations indicate that the counterion stays in the proximity of the Ge(II) dication in solution. This is significant because it reveals that the reality in solution is far removed from what is observed from the reported crystal structures. This also helps to explain perhaps why the systems are so stable and have been reported in high yields.

Furthermore, we have examined whether a similar phenomenon occurs when the Ge(II) dication is attached to the heteroatom of their respective solvents in which they were synthesized (similar to the case described earlier when the counteranion was attached to the dicationic germanium center). AIMD calculations have been carried out on each of the complexes (1–4). For every case, a similar boundary radius of 9.0 Å as imposed earlier was employed and the respective counteranions were placed unattached at a large distance apart from the Ge(II)-explicit solvent adduct centers (see Figures S7–S10, Supporting Information). Simulations illustrate that Ge(II) destroys the cage by abstracting a hydride from the cage in all the complexes (see Figures S7–S9, Supporting Information), except in 4, where, earlier we had shown that the dication was unattached to the counteranion. For 4, though the dication does not destroy the cage as in previous cases (1–3), it forms a distorted structure which is geometrically different from the experimentally isolated structure (Figure S10, Supporting Information). Hence, the presence of an explicit solvent molecule does not play a beneficial role that the counteranions display in stabilizing the dications inside the cages.

A further important point that needs to be made here pertains to the ${}^{19}\text{F}$ NMR data that have been reported by Baines and co-workers for case 1.⁵ When ${}^{19}\text{F}$ NMR was done for this system, a single resonance signal akin to a triflate anion was obtained.² This would suggest that the triflate anion remains in a dissociated form outside the cage away from the Ge(II) dication, thus reinforcing the crystal structure orientation of the counterion and contradicting our current results. In order to investigate this seeming discrepancy, we have done ${}^{19}\text{F}$ NMR DFT calculations to determine the shifts with the counterion (i) bound as well as (ii) not bound to the Ge(II) dication center. What we found was that the simulated ${}^{19}\text{F}$ NMR shift patterns were almost the same whether the triflate anion was bound to the Ge(II) center or stayed outside the cage. Hence, the experimental ${}^{19}\text{F}$ NMR data obtained for the Baines system (case 1) in solution do not contradict the computational results and allows for the likelihood of the counterion binding to the Ge(II) center inside the cage, when the caged system is present in solution. Moreover, the crystal structure for a crown ether complex of Ge(II) shows that one of the counteranions is attached to the central dication.⁶ Also, certain other Sn(II), In(I), and Ga(I) crown ether and cryptand complexes show at least some interaction between the counterion and the cationic center.^{35–39}

Hence, for cases 1–4, the counterion is seen to play an important role in keeping the Ge(II) inside the cage and

Table 2. Force at the Ge(II) Center for Reported Ge(II) Complexes (1–4)^a

compound	solvent	net force on Ge(II) (pN)/NBO	relative values of the force on Ge(II) for each case, compared to case 4	relative values of the energy at the Ge(II) center for each case, compared to case 1
1	tetrahydrofuran	611.7	10.9	1.0
2	dichloromethane	769.0	13.7	1.9
3	acetonitrile	235.8	4.2	10.8
4	acetonitrile	56.1	1.0	4.7

^aReported values are for the cationic fragment of the complex.

reducing its propensity for unwanted side reactions. Another factor that makes it favorable for a charged species to be at the center of the cage is the energetic favorability of this configuration. In other words, once a monocation (or a dication) settles at the center of the cage, it is likely to remain there because that is seen to be the most favored configuration energetically. We have determined this through differential calculus (shown in the [Supporting Information](#)) for a model system taking a symmetrical cage: what we have found is that the most favorable configuration would have the Ge(II) dication situated at the exact center of the cage. This is due to the fact that the primary interactions are electrostatic in nature (see the [Supporting Information](#)).

Another important conclusion is that only one counterion out of the two binds to the dication at the center: when optimizations were done for case 1 keeping both triflate counterions in the germanium center, the second triflate anion returned to the uncoordinated geometry during the optimization cycle (Figure S14 in the [Supporting Information](#)). This is because the reduced charge on the Ge(II) center after one counteranion binding makes it less favorable to bind another negatively charged counterion at the same center. Other inhibiting factors such as steric effects could further reduce this favorability. The lower charge on Ge(II) also serves to reduce its reactivity inside the cage. These observations can be extended to other cases where counteranion coordination was seen to be important (cases 2 and 3).

A further point worth considering is the strength of the dication–counteranion interaction when the two are encapsulated inside the cage. For this, we have looked into the interaction of Ge(II) with Br[−] in case 3. We have observed that in the optimized structure, there is an elongation of the bond length in [Ge–Br]⁺ (bond length = 2.79 Å), as compared to an unconfined and isolated [Ge–Br]⁺ ion (bond length = 2.25 Å). The bond order in the encapsulated [Ge–Br]⁺ is also seen to be significantly lower (see Table S2 in the [Supporting Information](#)). In other words, there is a confinement, “cage effect”, on the interaction between Ge(II) and Br[−] in case 3, and this leads to the weakening of the interaction of the cation and the anion inside the cage. Why this occurs is due to the favorable electrostatic interactions between the two ions and the partial charges of the cage atoms. This cage effect perhaps helps explain why the counteranion dissociates during the crystallization process and is observed to be found outside the cage in the experimentally observed crystal structures in cases 1–4.

Hence, the current computational investigations show that in almost all the cases investigated, it is likely that the counterion would bind to Ge(II) at the center of the cage in solution, a situation very different from that envisaged from the obtained crystal structures, which show the two counterions to be present outside the cage. This is also significant in a different sense. In a commentary on the results obtained by

Baines and co-workers, Lambert and Müller had suggested that these unusual compounds could be employed as the starting point for new synthetic strategies:^{9,40} as the Ge(II) dication lay uncoordinated and accessible at the center of the cage with plenty of space for substrates to enter, they could be approached by a range of substrates and new products could therefore be made from the subsequent interaction between the Ge(II) dication and the different substrates. However, no reports of such synthetic strategies have been reported to date. Only loosely coordinated adducts with water and ammonia molecules have been reported so far.⁴¹ The current results help explain why this is so: the Ge(II) dicationic center is not present in an accessible form in solution but is coordinated to a counterion. Hence, an incoming substrate would first have to remove the counterion from the Ge(II) dication in order for new chemistry to take place, and this would be difficult in the sterically constrained area in the caged structures. This hypothesis is further exemplified by the fact that a NHC-stabilized Ge(O^tBu)₂ synthesized from the cryptand complex 1 required a strong nucleophile such as potassium *tert*-butoxide.⁵ Hence, the current work serves to explain the difficulties in exploiting such systems for new chemistry. However, now that the explanation has been provided, can we also suggest means by which this problem could be overcome? The answer is a “yes”: case 4 provides the clue. Though the Ge(II) dication was seen to enter the cage with the assistance from the counterion in case 4, the counteranion did not remain with Ge(II), as was discussed earlier. If the reasons why this happens could be understood, then this would serve as a means of designing new cages in future where the counterion would not be necessary for stabilizing the Ge(II) dication inside the cage in solution.

In order to understand why Ge(II) in case 4 is stabilized without any attachment to the counterion, we have employed a new computational approach that we have recently developed, which determines the force and energy experienced by the Ge(II) dication when at the center of the cage. This is because the main interactions between Ge(II) and the cage atoms are electrostatic in nature. If the force pulling the Ge(II) away from its preferred position at the center of the cage is higher in some cases than in others, it would explain why the germanium dication needs a counterion to stay at the center of the cage in some cases and not in others. The computational strategy that we employed has been explained in detail in the [Methods](#) section. We had previously shown that force can be employed to determine the strength of hydrogen bonding interactions.⁴² Here, we have developed a strategy where we have (i) considered dicationic cases, where the cages were optimized with the Ge(II) dication at the center without any counterion, (ii) obtained the charges on the different atoms of the cage, as well as on the Ge(II) center (NPA charges were employed for this purpose), and (iii) determined the electrostatic force between the Ge(II) center and each atom, by using Coulomb’s

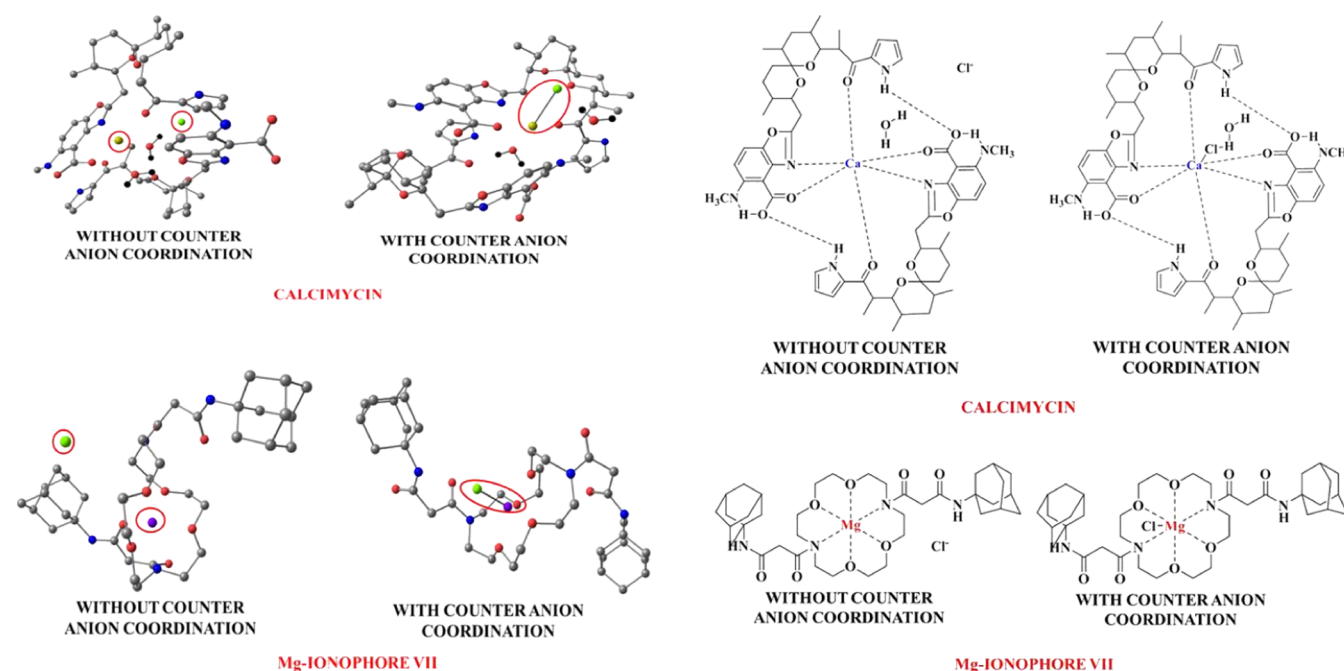


Figure 4. Optimized geometries of free and counteranion-bound ionophore complexes of Mg(II) and Ca(II), with Cl^- considered as the counteranion. Color scheme: magnesium = violet, calcium = yellow, oxygen = red, carbon = gray, nitrogen = blue, and chlorine = green. Hydrogen atoms on the ionophore cages are not shown for the purpose of clarity.

law, and (iv) then obtained the net force acting at the Ge(II) center by vectorially adding up all the individual force values. This is a simple strategy, and its effectiveness lies in the fact that the absolute values of the forces are not as significant as the relative values obtained for the different cases considered. Column 4 in Table 2 shows the results obtained for the cases 1–4. For all the cases, the net electrostatic force was seen to be repulsive. Case 4 was seen to have the lowest repulsive force at the Ge(II) center, while the Ge(II) in case 2 was seen to be experiencing the highest repulsive force. Indeed, the force was 13.7 times higher in case 2 than in case 4 (Table 2). This is largely due to the fact that, for case 4, the Coulombic interactions between the heteroatom oxygens and the almost oppositely placed Ge(II), which are the primary interactions, largely cancel each other out due to the orientation of the cage (Figure S13 in the Supporting Information), and this leads to a reduced repulsive force at the Ge(II) center. This analysis indicates that the nature of the cage is very relevant in determining how favorably Ge(II) would sit inside the cage without support from the counterion, and indeed, as we had seen, the counterion is not necessary for case 4 and is present outside the cage in this case.

A similar computational strategy also allows us to calculate the electrostatic energy of the interaction of Ge(II) with the cage atoms (see column 5 in Table 2). A perusal of the values shows that it does not explain why the counteranion does not stay coordinated to Ge(II) in case 4 but does so in the other three cases. Indeed, here, case 1 is seen to show the most favorable electrostatic interactions between Ge(II) and the atoms of the enclosing cage. These results serve to show that the electrostatic force is a better parameter to understand cation–cage interactions than the electrostatic energy of interactions because when charged species are present in close proximity, the distance between them becomes a crucial factor. This is because the energy of interaction varies as the inverse of the distance, while the force varies as the square of

the inverse, and therefore, the force becomes a more dominant entity. This result underlines the value of developing strategies to evaluate the force of electrostatic interaction between charged species that are present close together.

The value of the insights gained from this analysis is that it shows that the principal quality a cage should have to keep a naked cation at its center is to reduce repulsive electrostatic interactions with the cationic center as much as possible *via* efficient design of the cage. Hence, our work (i) reveals the hidden role played by the counterion in stabilizing the Ge(II) dication inside caged structures and (ii) shows the principal factor necessary to have naked Ge(II) cations in cages. This has relevance for the development of synthetic strategies beginning from accessing naked cations in caged structures.

3.2. Alkali and Alkaline-Earth Metal Cations Relevant to Biology.

The previous section detailed the insights into group 14 chemistry, specifically showing how Ge(II) dications are stabilized by the presence of a counteranion inside the enclosing cage in solution. What is important to note in this is that the interactions that had to be considered were primarily electrostatic in nature. This points to a significant fact that the insights gained from the study of group 14 systems might be equally relevant across the periodic table. This is because, for instance, alkali and alkaline-earth metal cations interact primarily through electrostatic interactions, and if one were to investigate cages encapsulating such cations, the principal interaction between the cage and the cations would also be electrostatic in nature. Specifically, one could consider the important area of ionophores enclosing dicationic group 2 ions, which are of significant interest in biology.

Ionophores are molecules that catalyze the transport of ions across hydrophobic cell membranes.⁴³ The role of the ionophore is to reversibly and selectively coordinate to a cation and shield it from the cell membrane, hence facilitating the diffusion of the cation into the ion channel. In other words, the ionophore serves to insulate the charge of the cation from

the hydrophobic cell membrane, therefore their function is even more significant when the charge on the cation is +2, that is, for dicationic systems. These dications are usually Mg(II) or Ca(II). Hence, we have chosen two molecular cages that specifically bind to dication magnesium (Mg–ionophore VII) and calcium (calcimycin), respectively. Such encapsulated dicationic ionophore systems such as Mg–ionophore VII and calcimycin (see Figure 4) have a lot in common with the encapsulated group 14 dications that have been discussed in the previous section. As they have an octet configuration, it is likely that they would have negligible covalent interactions with the heteroatoms of the ionophore cage after coordination (see Table S3, Supporting Information). NCI plots also illustrate the large noncovalent electrostatic interaction present within these systems (see Figure S16, Supporting Information).

The results with the group 14 systems had indicated the significance of the coordination of one counteranion to the dicationic center. The purpose of looking at the ionophores encapsulating Mg(II) and Ca(II) dications was to check whether the same holds true for group 2 systems as well. In biological systems, phosphate (PO_4^{3-}) and chloride (Cl^-) are the principal counteranions, and there is at least one previous report that has indicated the presence of a counterion (chlorate, ClO_4^- , in that case) that was present inside the valinomycin ionophore cage, coordinated to a Ba(II) dication, with two such Ba(II)– ClO_4^- ions being present together inside the cage.¹² In the current investigation, we have focused on the possibility of coordinating a Cl^- counteranion to the dicationic center in the Mg–ionophore VII and Ca–calcimycin ionophore systems.

The free energy of chloride binding was seen to be favorable for the Mg(II) case by 3.7 kcal/mol and feasible in the Ca(II) case (marginally unfavorable by 0.1 kcal/mol). In other words, for the Mg(II) case, the equilibrium would strongly favor counteranion binding to the Mg(II) center, while in the case of Ca(II), there would be an equal probability of the counteranion existing inside or outside the ionophore cage. Ionophores function as a shield to the charged dication from the hydrophobic membranes of the channel and thus help in the smooth transfer of the cations. Hence, this counteranion binding to the dication (that reduces the formal charge on the cation) serves as a secondary layer of insulation of the charge from the membrane layer.

At this point, it is worth noting that the counteranion coordination in group 14, as well as group 2, dications inside molecular cages effectively reduces the formal charge on the dication from +2 to +1. In other words, coordination of a counterion to the dication results in the formation of a net “pseudomonocation” at the center of the cage. As monocationic alkali-metal systems encapsulated by cryptands and crown ethers have been widely reported and discussed in the literature,^{44,45} these stable pseudomonocationic systems situated at the center of the cryptand and crown ether cages appear strikingly similar. Hence, one could consider the pseudomonocationic systems to be “isoionic” to an alkali metal encapsulated inside the same molecular cage.

One begins to understand the significance of the isoionic analogy when considering and comparing dicationic magnesium and monocationic lithium ions. Recent experimental results suggest that Mg(II) can interact with the ATP triphosphate side chain and Li(I) can cobind with the native Mg(II) to form ATP–Mg–Li, and hence modulate the

receptor response.⁴⁶ The net charge has been demonstrated to play a pivotal role in the competition between Li(I) and Mg(II) for metal-binding sites and the subsequent inhibition of key enzymes involved in specific neurotransmission pathways.⁴⁷ Dudev and Lim had demonstrated, *via* computational studies, that Mg(II) binds in a tridentate fashion to the phosphate groups of ATP and Li(I) binds to the same anionic phosphate groups in a bidentate fashion.⁴⁸ Hence, there is evidence to suggest that dicationic magnesium and monocationic lithium act on a specific site by modulation of counteranion coordination, so that they become isoionic with each other during the interaction. That, coupled with the similarity of their radii due to their diagonal relationship in the periodic table, might explain the similarity of their observed biological behavior. In order to investigate whether the isoionic analogy holds for Mg(II) and Li(I) in caged structures, we decided to replace $[\text{Mg(II)}-\text{Cl}]^+$ in the Mg–ionophore VII with an Li(I). A comparison of the NPA charges revealed that Li(I) and $[\text{Mg}-\text{Cl}]^+$ have almost the same partial charges (0.61 and 0.66, respectively) and are therefore isoionic to each other (Figure 5).

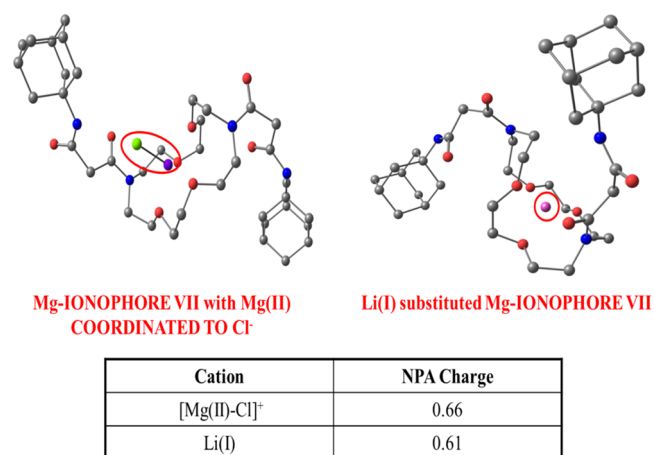


Figure 5. Illustration of the isoionic phenomenon. Color scheme: magnesium = violet, lithium = pink, oxygen = red, carbon = gray, nitrogen = blue, and chlorine = green. Hydrogen atoms on the ionophore cages are not shown for the purpose of clarity.

One conclusion from this is that Li(I) can compete and replace an $[\text{Mg(II)}-\text{counteranion}]^+$ ion inside ionophores such as Mg–ionophore VII, which provides a fresh new insight into the competition between alkali and alkaline-earth metal systems in biology. However, there is a larger point that can be made here. The isoionic analogy also allows us to consider the interesting case of the valinomycin-encapsulated Ba(II) chlorate system that had been mentioned previously.¹² Spectroscopic studies revealed that there were two Ba(II) chlorate ions present inside the valinomycin ionophore. In the context of the current work, this indicates the presence of two pseudomonocations inside the caged structure. This was made possible because of the flexible valinomycin cage undergoing a conformational change, thereby adopting a novel conformation different from the uncomplexed valinomycin ionophore,¹¹ which allowed it to successfully stabilize the two pseudomonocations inside the cage. Now, with the insights that we have developed in the current work on pseudomonocations, as well as of the isoionic analogy, this experimental result makes it clear that it should be possible to stabilize two monocations

that are isoionic with the counteranion-coordinated dication inside similar flexible molecular cages.

In order to drive home this point, we have looked at Mg-ionophore VII and encapsulated two Li(I) monocations inside the cage, instead of one, as done earlier. We considered two cases here, one where the two Li(I) ions were allowed to relax into a stable configuration inside the cage and one where the distance between the two Li(I) ions was kept fixed inside the cage (Figure S17 in the Supporting Information). What is interesting is that the energy difference between the two optimized structures was only 6.1 kcal/mol. This is due to the fact that the flexible ionophore ligand was able to reorient itself to stabilize the two mutually repelling Li(I) cations inside the ionophore cavity *via* interactions with the negatively charged heteroatoms of the molecular cage, even when the distance between the two positive ions was kept fixed. Hence, molecular cages possessing a flexible, electron-rich, and large cavity size possess the ability to stabilize not only the dications in the form of pseudomonocations but also the two monocations located inside its periphery.

4. CONCLUSIONS

The current work provides a comprehensive computational exploration of an interesting class of compounds: cations encapsulated in molecular rings. Such compounds are of significance in many diverse and important areas of science, including inorganic chemistry and biology. Discussed first are molecular cages containing group 14 dications. It is shown that the reality of their existence in solution is very different from what their crystal structures look like. The current work demonstrates that this family of compounds exists as “pseudomonocations” inside their cages. Next, the insights inferred from the earlier case are applied to group 2 systems important to biology: to dicationic Ca(II)- and Mg(II)-binding ionophores, and the same pseudomonocation model is found to fit perfectly in these cases as well. Furthermore, for the Mg(II)-binding ionophore, we show that $[\text{Mg}(\text{II})-\text{Cl}]^+$ can be replaced by a Li(I) inside the same ionophore, and the two systems—one a pseudomonocation and the other a monocation—would possess the same charge inside the cage. This leads to the formulation of the “isoionic analogy” and indicates that Li(I) can compete with Mg(II) for the same ionophore center, which has implications for the biochemistry of ionophores. The isoionic analogy also leads to the realization that two monocations can be stabilized inside a sufficiently flexible and polarizable cage, which provides a means of analyzing similar systems in future.

Our current work therefore provides insights into the behavior of cations enclosed in molecular cages and explains a wide range of experimentally observed phenomena in such systems. It is easy to see that the insights gained from the current studies would have implications for other phenomena observed for caged systems. For example, in PEMs, low proton-transfer barriers are coveted for the efficient transfer of protons through the membrane. The tendency of the cation to stabilize itself at the center of molecular cages can aid in understanding the mechanism of hopping of the proton through pendant cages in certain PEMs.¹ Furthermore, the potential stabilization of two monocations inside the same molecular cage could justify the stability of similar molecular rings on various surfaces, as in the case of the recently reported isolation of a rare C_{18} ring on a NaCl surface.⁴⁹

In summary, the current theoretical and computational study delves into the interplay between cations, anions, and molecular cages in a wide range of structures important to different areas of science and leads to a significant understanding of the hidden factors at play in such systems.

■ ASSOCIATED CONTENT

Supporting Information

The Supporting Information is available free of charge at <https://pubs.acs.org/doi/10.1021/acs.jpca.0c06995>.

Different parameters associated with the reported Ge(II) complexes (1–4), snapshots depicting the trajectory of AIMD simulations of complexes 1–4 when Ge(II) and the counteranions remain unattached/attached, snapshots depicting the trajectory of AIMD simulations of complexes 1–4 when Ge(II) and the solvent remain attached, geometries of free and counteranion-bound crown ether and cryptand complexes (1–3) of Ge(II) optimized at the M06-2X/6-311G (d, p) level of theory, geometry optimization trajectory of counteranion binding in Case 4, illustration of cancellation of Coulombic interactions between the Ge(II) center and the oxygen heteroatoms in Case 4, DFT optimization trajectory for Case 1 keeping both triflate counterions at the germanium center, different parameters comparing the case of $[\text{Ge}-\text{Br}]^+$ in a bare state with the $[\text{Ge}-\text{Br}]^+$ encapsulated inside the cage in Case 3 in solution, NCI plots for complexes 1–4 and for Mg/Ca/Li-based ionophores, NMR calculation output with Gaussian09, mechanism for the dication staying at the center of the cage, highest WBIs of the ionophore cation and a heteroatom in the ionophore cage in all the ionophores reported, thermodynamic parameters for reported ionophores at different levels of theory, optimized geometries of two Li(I) cations encompassed by Mg-ionophore VII (the two lithium unfixed and fixed) at the M06-2X/6-31G* level of theory, and Cartesian coordinates (PDF)

Decomposition of the cage by the dication (MP4)

Entry of the dication into the cage (MP4)

■ AUTHOR INFORMATION

Corresponding Author

Kumar Vanka – Physical and Materials Chemistry Division, CSIR-National Chemical Laboratory, Pune 411008, India; Academy of Scientific and Innovative Research (AcSIR), Ghaziabad 201002, India; orcid.org/0000-0001-7301-7573; Email: k.vanka@ncl.res.in

Authors

Anagh Mukherjee – Physical and Materials Chemistry Division, CSIR-National Chemical Laboratory, Pune 411008, India; Academy of Scientific and Innovative Research (AcSIR), Ghaziabad 201002, India

Siddharth Ghule – Physical and Materials Chemistry Division, CSIR-National Chemical Laboratory, Pune 411008, India; Academy of Scientific and Innovative Research (AcSIR), Ghaziabad 201002, India

Mrityunjay K. Tiwari – Department of Chemistry, Indian Institute of Science Education and Research, Bhopal 462066, India

Complete contact information is available at:

<https://pubs.acs.org/10.1021/acs.jpca.0c06995>

Author Contributions

The manuscript was written through contributions of all authors. All authors have given approval to the final version of the manuscript.

Notes

The authors declare no competing financial interest.

ACKNOWLEDGMENTS

The authors thank Dr. V. Sitaramam, Dr. Sakya. S. Sen, and Mr. Tamal Das for fruitful discussions. The authors would also like to thank the reviewers for their valuable comments and suggestion to improve the standard of the manuscript. K.V. is grateful to the Department of Science and Technology (DST) (EMR/2014/000013) for providing financial assistance. A.M. and S.G. acknowledge UGC-New Delhi and CSIR-New Delhi, respectively, for research fellowships.

REFERENCES

- (1) Mane, M. V.; Vanka, K. Proposing efficient new pendant group polymer electrolyte membranes for fuel cells: a computational study. *J. Phys. Chem. C* **2014**, *118*, 784–795.
- (2) Weimann, D. P.; Winkler, H. D. F.; Falenski, J. A.; Kokschi, B.; Schalley, C. A. Highly dynamic motion of crown ether along oligolysine peptide chain. *Nat. Chem.* **2009**, *1*, 573–577.
- (3) Swidan, A.; Macdonald, C. L. B. Polyether complexes of group 13 and 14. *Chem. Soc. Rev.* **2016**, *45*, 3883–3915.
- (4) Swamy, V. S. V. S. N.; Pal, S.; Khan, S.; Sen, S. S. Cations and dications of heavier group 14 elements in low oxidation states. *Dalton Trans.* **2015**, *44*, 12903–12923.
- (5) Rupar, P. A.; Staroverov, V. N.; Baines, K. M. A cryptand-encapsulated germanium (II) dication. *Science* **2008**, *322*, 1360–1362.
- (6) Rupar, P. A.; Bandyopadhyay, R.; Cooper, B. F. T.; Stinchcombe, M. R.; Ragnogna, P. J.; Macdonald, C. L. B.; Baines, K. M. Cationic crown ether complexes of germanium (II). *Angew. Chem., Int. Ed.* **2009**, *121*, 5257–5260.
- (7) Cheng, F.; Hector, A. L.; Levason, W.; Reid, G.; Webster, M.; Zhang, W. Germanium (II) dications stabilized by azamacrocycles and crown ethers. *Angew. Chem., Int. Ed.* **2009**, *48*, 5152–5154.
- (8) Ward, M. J.; Rupar, P. A.; Murphy, M. W.; Yiu, Y.-M.; Baines, K. M.; Sham, T. K. Ionic nature of Ge (II)-centered dications: a germanium K-edge X-ray absorption near edge structures study. *Chem. Commun.* **2010**, *46*, 7016–7018.
- (9) Lambert, J. B. CHEMISTRY: A Tamed Reactive Intermediate. *Science* **2008**, *322*, 1333–1334.
- (10) Jakobsson, E.; Argüello-Miranda, O.; Chiu, S.-W.; Fazal, Z.; Kruczek, J.; Nunez-Corales, S.; Pandit, S.; Pritchett, L. Towards a unified understanding of lithium action in basic biology and its significance for applied biology. *J. Membr. Biol.* **2017**, *250*, 587–604.
- (11) Devarajan, S.; Nair, C. M. K.; Easwaran, K. R. K.; Vijayan, M. A novel conformation of valinomycin in its barium complex. *Nature* **1980**, *286*, 640–641.
- (12) Frisch, M. J.; Trucks, G. W.; Schlegel, H. B.; Scuseria, G. E.; Robb, M. A.; Cheeseman, J. R.; Scalmani, G.; Barone, V.; Mennucci, B.; Petersson, G. A.; et al. *Gaussian 09*, Revision B.01; Gaussian, Inc.: Wallingford, CT, 2009.
- (13) Zhao, Y.; Truhlar, D. G. The M06 suite of density functionals for main group thermochemistry, chemical kinetics, noncovalent interactions, excited states, and transition elements: two new functionals and systematic testing of four M06-class functionals and 12 other functionals. *Theor. Chem. Acc.* **2008**, *120*, 215–241.
- (14) Barone, V.; Cossi, M. Quantum calculation of molecular energies and energy gradients in solution by a conductor solvent model. *J. Phys. Chem. A* **1998**, *102*, 1995–2001.
- (15) Cossi, M.; Rega, N.; Scalmani, G.; Barone, V. Energies, structures, and electronic properties of molecules in solution with the C-PCM solvation model. *J. Comput. Chem.* **2003**, *24*, 669–681.
- (16) Reed, A. E.; Weinstock, R. B.; Weinhold, F. Natural population analysis. *J. Chem. Phys.* **1985**, *83*, 735–746.
- (17) Wolinski, K.; Hinton, J. F.; Pulay, P. Efficient implementation of the gauge-independent atomic orbital method for NMR chemical shift calculations. *J. Am. Chem. Soc.* **1990**, *112*, 8251–8260.
- (18) Ufimtsev, I. S.; Martinez, T. J. Quantum chemistry on graphical processing units. 3. Analytical energy gradients, geometry optimization, and first principles molecular dynamics. *J. Chem. Theory Comput.* **2009**, *5*, 2619–2628.
- (19) Ufimtsev, I. S.; Luehr, N.; Martinez, T. J. Charge transfer and polarization in solvated proteins from ab initio molecular dynamics. *J. Phys. Chem. Lett.* **2011**, *2*, 1789–1793.
- (20) Isborn, C. M.; Luehr, N.; Ufimtsev, I. S.; Martinez, T. J. Excited-state electronic structure with configuration interaction singles and Tamm–Dancoff time-dependent density functional theory on graphical processing units. *J. Chem. Theory Comput.* **2011**, *7*, 1814–1823.
- (21) Titov, A. V.; Ufimtsev, I. S.; Luehr, N.; Martinez, T. J. Generating efficient quantum chemistry codes for novel architectures. *J. Chem. Theory Comput.* **2013**, *9*, 213–221.
- (22) Ufimtsev, I. S.; Martínez, T. J. Graphical processing units for quantum chemistry. *Comput. Sci. Eng.* **2008**, *10*, 26–34.
- (23) Ufimtsev, I. S.; Martinez, T. J. Quantum chemistry on graphical processing units. 1. Strategies for two-electron integral evaluation. *J. Chem. Theory Comput.* **2008**, *4*, 222–231.
- (24) Ufimtsev, I. S.; Martinez, T. J. Quantum chemistry on graphical processing units. 2. Direct self-consistent-field implementation. *J. Chem. Theory Comput.* **2009**, *5*, 1004–1015.
- (25) Perdew, J. P.; Chevary, J. A.; Vosko, S. H.; Jackson, K. A.; Pederson, M. R.; Singh, D. J.; Fiolhais, C. Atoms, Molecules, Solids, and Surfaces: Applications of the Generalized Gradient Approximation for Exchange and Correlation. *Phys. Rev. B: Condens. Matter Mater. Phys.* **1992**, *46*, 6671–6687.
- (26) Perdew, J. P.; Chevary, J. A.; Vosko, S. H.; Jackson, K. A.; Pederson, M. R.; Singh, D. J.; Fiolhais, C. Erratum: Atoms, Molecules, Solids, and Surfaces: Applications of the Generalized Gradient Approximation for Exchange and Correlation. *Phys. Rev. B: Condens. Matter Mater. Phys.* **1993**, *48*, 4978.
- (27) Perdew, J. P.; Chevary, J. A.; Vosko, S. H.; Jackson, K. A.; Pederson, M. R.; Singh, D. J.; Fiolhais, C. Atoms, Molecules, Solids, and Surfaces: Applications of the Generalized Gradient Approximation for Exchange and Correlation. *Phys. Rev. B: Condens. Matter Mater. Phys.* **1992**, *46*, 6671.
- (28) Adamo, C.; Barone, V. Exchange functionals with improved long-range behaviour and adiabatic connection methods using adjustable parameters: The mPW and mPW1PW models. *J. Chem. Phys.* **1998**, *108*, 664.
- (29) Becke, A. D. Density-functional thermochemistry III. The role of exact exchange. *J. Chem. Phys.* **1993**, *98*, 5648.
- (30) Lee, C.; Yang, W.; Parr, R. G. Development of Colle-Salvetti correlation-energy formula into a functional of the electron density. *Phys. Rev. B: Condens. Matter Mater. Phys.* **1988**, *37*, 785.
- (31) Roothaan, C. C. J. Self-Consistent Field Theory for Open Shells of Electronic Systems. *Rev. Mod. Phys.* **1960**, *32*, 179.
- (32) McWeeny, R.; Diercksen, G. Self-Consistent Perturbation Theory. II. Extension to Open Shells. *Chem. Phys.* **1968**, *49*, 4852.
- (33) Pople, J. A.; Nesbet, R. K. Self-Consistent Orbitals for Radicals. *J. Chem. Phys.* **1954**, *22*, 571.
- (34) Johnson, E. R.; Keinan, S.; Mori-Sánchez, P.; Contreras-García, J.; Cohen, A. J.; Yang, W. Revealing Noncovalent Interactions. *J. Am. Chem. Soc.* **2010**, *132*, 6498–6506.
- (35) Bandyopadhyay, R.; Cooper, B. F. T.; Rossini, A. J.; Schurko, R. W.; Macdonald, C. L. B. Crown Ether complexes of tin (II) trifluoromethanesulfonate. *J. Organometal. Chem.* **2010**, *695*, 1012–1018.

- (36) Avery, J. C.; Hanson, M. A.; Herber, R. H.; Bladec, K. J.; Rugar, P. A.; Nowik, I.; Huang, Y.; Baines, K. M. Cationic cryptand complexes of tin (II). *Inorg. Chem.* **2012**, *51*, 7306–7316.
- (37) Cooper, B. F. T.; Macdonald, C. L. B. Synthesis and structure of an indium (I) “crown sandwich”. *J. Organomet. Chem.* **2008**, *693*, 1707–1711.
- (38) Andrews, C. G.; Macdonald, C. L. B. Crown ether ligation: an approach to low-oxidation-state indium compounds. *Angew. Chem., Int. Ed.* **2005**, *117*, 7619–7622.
- (39) Bourque, J. L.; Boyle, P. D.; Baines, K. M. Synthesis and characterization of cationic low-valent gallium complexes of cryptand [2,2,2]. *Chem.—Eur. J.* **2015**, *21*, 9790–9796.
- (40) Müller, T. Splendid isolation for a nonmetallic dication. *Angew. Chem., Int. Ed.* **2009**, *48*, 3740–3743.
- (41) Bandyopadhyay, R.; Nguyen, J. H.; Swidan, A. a.; Macdonald, C. L. B. Water and Ammonia Complexes of Germanium(II) Dications. *Angew. Chem.* **2013**, *125*, 3553–3556.
- (42) Tiwari, M. K.; Vanka, K. Exploiting directional long range secondary forces for regulating electrostatics dominated non-covalent interactions. *Chem. Sci.* **2017**, *8*, 1378–1390.
- (43) Bakker, E.; Bühlmann, P.; Pretsch, E. Carrier-based ion-selective electrodes and bulk optodes. 1. General Characteristics. *Chem. Rev.* **1997**, *97*, 3083–3132.
- (44) Buschmann, H.-J. The complexation of alkali metal ions by crown ethers, aza crown ethers, and cryptands in propylene carbonate. *J. Inclusion Phenom. Mol. Recognit. Chem.* **1989**, *7*, 581–588.
- (45) Haymore, B. L.; Lamb, J. D.; Izatt, R. M.; Christensen, J. J. Thermodynamic origin of the macrocyclic effect in crown ether complexes of sodium (1+), potassium (+1) and barium (2+). *Inorg. Chem.* **1982**, *21*, 1598–1602.
- (46) Briggs, K. T.; Giulian, G. G.; Li, G.; Kao, J. P. Y.; Marino, J. P. A molecular model for lithium’s bioactive form. *Biophys. J.* **2016**, *111*, 294–300.
- (47) Dudev, T.; Lim, C. Competition between Li⁺ and Mg²⁺ metalloproteins. Implication for lithium therapy. *J. Am. Chem. Soc.* **2011**, *133*, 9506–9515.
- (48) Dudev, T.; Grauffel, C.; Lim, C. How native and alien metal cations bind ATP: implication for lithium as a therapeutic agent. *Sci. Rep.* **2017**, *7*, 42377.
- (49) Kaiser, K.; Scriven, L. M.; Schulz, F.; Gawel, P.; Gross, L.; Anderson, H. L. An sp-hybridized molecular carbon allotrope, cyclo [18] carbon. *Science* **2019**, *365*, 1299–1301.